On memfractance of plants and fungi

Alexander E Beasley, Mohammed-Salah Abdelouahab, René Lozi, Anna L Powell, Andrew Adamatzky

Submitted to PLOS ONE

On memfractance of plants and fungi

Alexander E. Beasley[1,*], Mohammed-Salah Abdelouahab[3], René Lozi[2], Anna L. Powell[1], and Andrew Adamatzky[1]

[1] *Unconventional Computing Laboratory, UWE, Bristol, UK*
[*] *Corresponding author: Alexander Beasley, alex.beasley@uwe.ac.uk*
[2] *Laboratory of Mathematics and their interactions, University Centre Abdelhafid Boussouf, Mila 43000, Algeria*
[3] *Université Côte d'Azur, CNRS, LJAD, Nice, France*

May 22, 2020

Abstract

The key feature of a memristor is that the resistance is a function of its previous resistance, thereby the behaviour of the device is influenced by changing the way in which potential is applied across it. Ultimately, information can be encoded on memristors, which can then be used to implement a number of circuit topologies.Biological substrates have already been shown to exhibit some memristive properties.It is, therefore, logical that all biological media will follow this trend to some degree. In this paper we demonstrate that a range of yet untested specimens exhibit memristive properties, including mediums such as water and dampened wood shavings on which we can cultivate biological specimens. We propose that memristance is not a binary property $\{0, 1\}$, but rather a continuum on the scale [0,1]. The results imply that there is great potential for hybrid electronic systems that combine traditional electronic typologies with naturally occurring specimens.

*K*eywords: memristor, fungi, fuits, memfractance

1 Introduction

Originally proposed by Leon Chua in 1971 [6], the memristor poses an fourth basic circuit element, whose characteristics differ from that of R, L and C elements. The model of an optimal memristor (Fig. 1) shows a number of key features: (1) lobes in the positive and negative half of the cycle, and (2) a 'pinch' (or crossing) point at 0V.

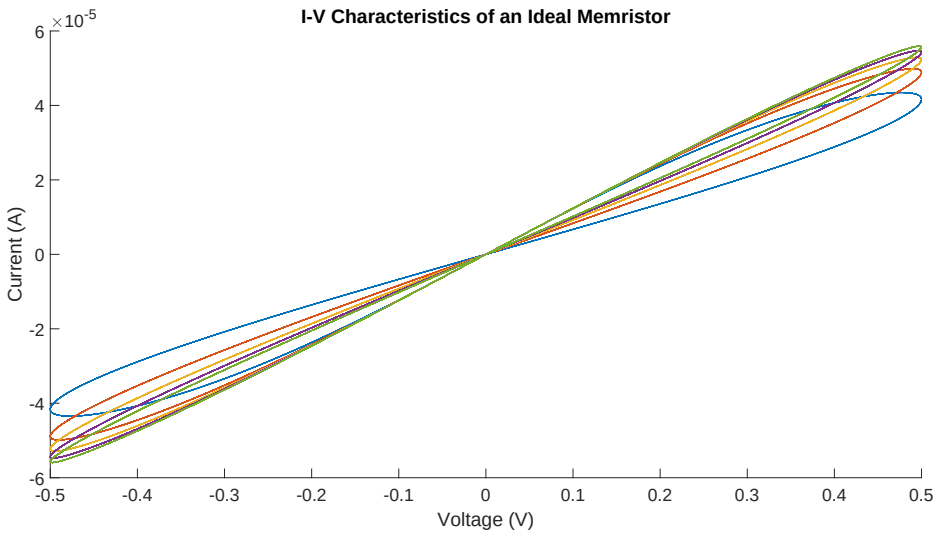

Figure 1: I-V characteristics from a model of an ideal memristor [15].

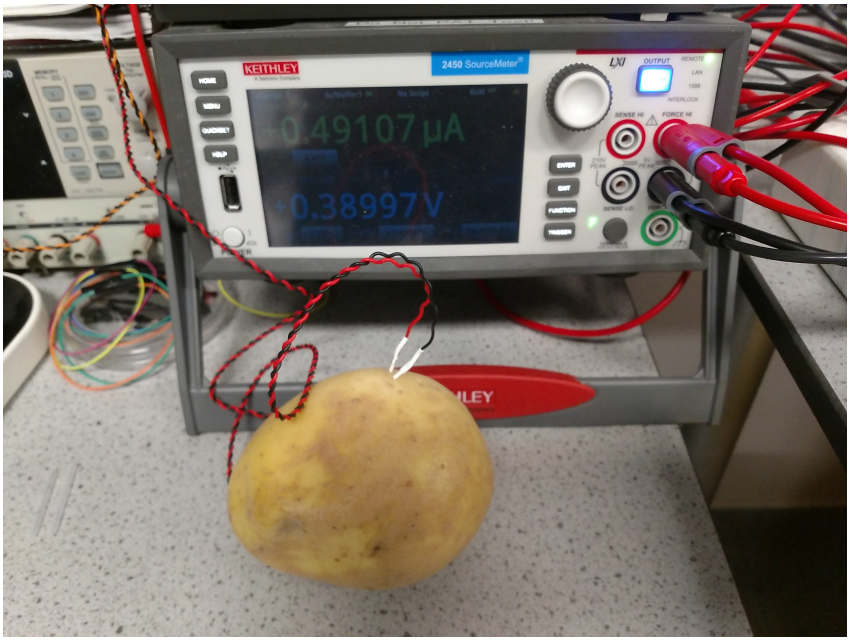

Figure 2: Sample specimen under test using Keithley SMU.

Memristance has been seen in nano-scale devices, where solid-state electronic and ionic transport are coupled under an external bias voltage [28]. Strukov *et al.* posit that the hysteric I-V characteristics observed in thin-film, two-terminal devices can be understood as memristive. However, this is observed behaviour of devices that already have other, large signal behaviours.

Finding a true memristor is by no means an easy task, however, a number of studies have turned to nature to provide the answer, with varying success. Memristive properties of organic polymers have been studied since 2005 [9] in experiments with hybrid electronic devices based on polyaniline-polyethylenoxide junction [9]. Memristive properties of living creatures and their organs and fluids have been demonstrated in skin [23], blood [18], plants [30] (including fruits [29]), slime mould [11], tubulin microtubules [8, 5].

From a more global point of view, mem-fractance which involves fractional calculus, is a general paradigm for unifying and enlarging the family of memristive, mem-capacitive and mem-inductive elements.

This paper presents a study of the I-V characteristics of a number of specimens of plants, fungi, and cultivation mediums. Why choose specimens from nature? Previous work has demonstrated significant potential for the use of naturally occurring substances as memristors. Taking these studies as a basis, it is proposed that any substance taken from nature — that has once been living — will exhibit the same memristive properties.

Why we are looking for memristive properties? A memristor is a material implication [4, 20]. Therefore, memristors can be used for constructing other logical circuits, statefull logic operations [4], logic operations in passive crossbar arrays of memristos [22], memory aided logic circuits [19], self-programmable logic circuits [3], and, indeed, memory devices [14]. If the substances show memristive properties then we can implement a large variety of memory and computing devices embedded directly into hybrid electronic circuits that utilise naturally occurring resources.

The rest of this paper is organised as follows. Section 2 details the experimental set up used to examine the I-V characteristics of fungal fruit bodies. Section 3 presents the results from the experimentation. A mathematical modelling onion mem-fractance is presented in Sect. 4. A discussion of the results is given in Sect. 5 and finally conclusions are given in Sect. 5.

2 Experimental method

A number of subjects were identified for the purposes of testing the I-V characteristics of biological medium. Samples fall under the following categories: fruiting bodies, flora, fungi and water. In addition, a number of control samples were also subject to test (dry wood shavings and de-ionised water).

Fruits and vegetables used in experiments are large garlic (origin Spain, Tesco Stores Ltd.), aubergine (origin Spain, Aldi UK), onion (origin UK, Aldi UK), potato (origin UK, Aldi UK), banana (Aldi UK), cucumber (origin Spain, Aldi UK), mango (origin Peru, Aldi UK), and bell pepper (origin Spain, Aldi UK). Plants used in experiments are *Echeveria pulidonis* and *Senecio ficoides*. Fungi used in experiments grey oyster fungi *Pleurotus ostreatus* (Ann Miller's Speciality Mushrooms Ltd, UK) cultivated on wood shavings.

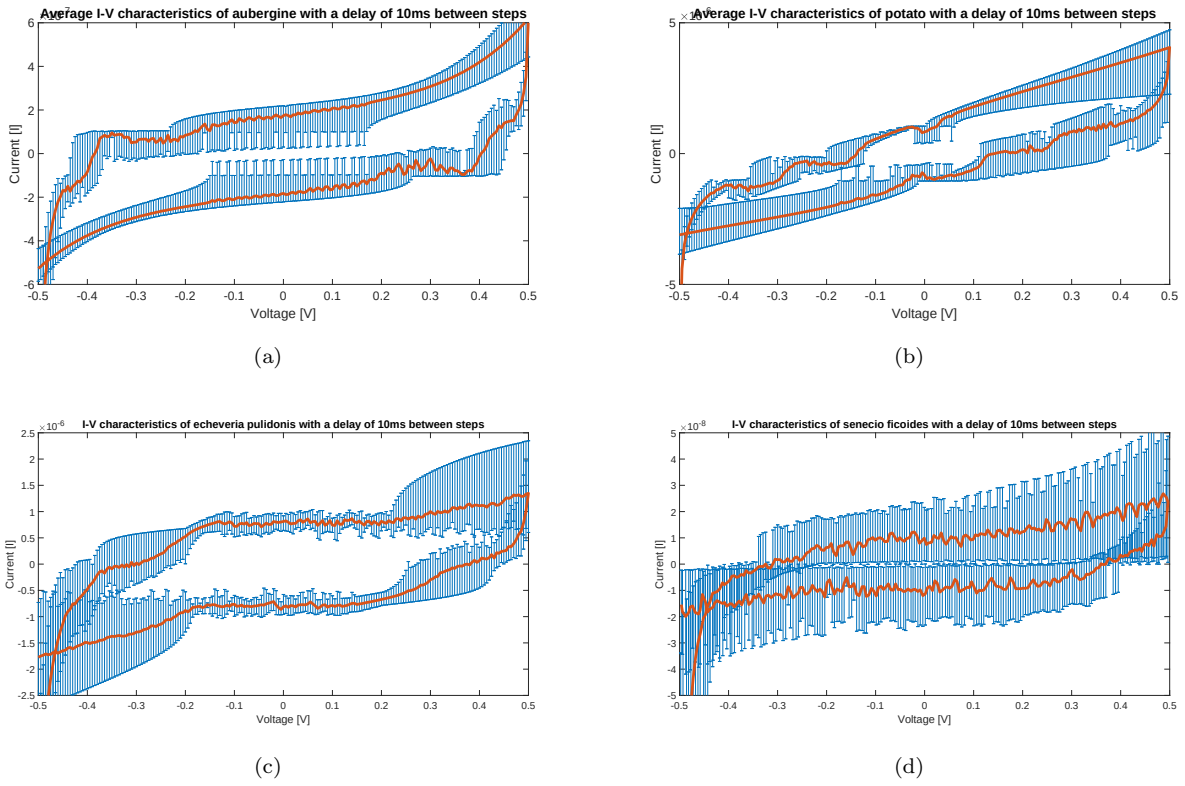

Figure 3: I-V characteristics of specimens, error bars shown. Cyclic voltammetry performed over -0.5V to 0.5V, with a step delay of 10ms. (a) aubergine, (b) potato, (c) *Echeveria pulidonis*, (d) *Senecio ficoides*.

Iridium-coated stainless steel sub-dermal needles with twisted cables (Spes Medica SRL, Italy) were inserted approximately 10 mm apart in each of the samples under test, such as in the example in Fig. 2. I-V sweeps were performed on the each of the samples using a Keithley Source Measure Unit (SMU) 2450 (Keithley Instruments, USA) under a range of conditions:

- Cyclic voltammetry performed from -0V5 to 0V5 and -1V to 1V. The voltage limits of the cyclic voltammetry are limited as to not exceed the electrolysis of water.
- Delay between consecutive voltage settings: 0.01s, 0.1s and 1s.

The composition of tap water is measured to be the following: conductivity 573 micro Siemens (measured at 22.7°C with Eutch Instruments, Model CONDG+), pH 6.86 (measured at 22.5°C with VWR pH 10), pH 7.0 standardised at 25°C, total dissolved solids 393 ppm, salinity: 0.3 ppm. All conditions were repeated a number of times and the resulting I-V curves processed using MATLAB.

3 Results

A number of key findings have been drawn from the tests that support the assertion that any biological object exhibits memristance. This section present a subset of the results from I-V characterisation of the specimens. All raw data plots for I-V characteristics may be found in the appendices (section 6).

3.1 Vegetables and plants

From the species tested in this study, it is seen that the I-V sweeps that the resistance of the subject is varied depending not only on the previously applied voltage but also on the frequency with which the voltage is changed. As a general rule, the faster the voltage is changed the greater the divergence in conducted current between the positive and negative phases of the cyclic voltammetry. Additionally, increasing the frequency of the voltage will yield a larger conducted current. Figure 3 shows the average I-V response for a selection of the test specimens.

Test substrates were subjected to cyclic voltammetry over two voltage ranges. Naturally, for the larger voltage range, the maximum conducted current is also far greater. The greater the applied voltage, the closer the test subject is to a

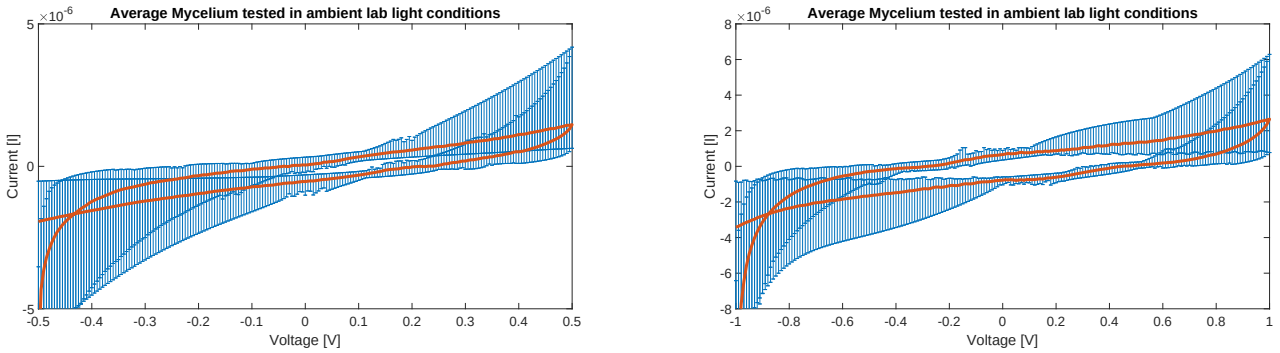

(a) (b)

Figure 4: Average mycelium I-V characteristics. (a) cyclic voltammetry performed from -0.5V to 0.5V. (b) cyclic voltammetry performed from -1V to 1V.

breakdown voltage where larger current flow can be expected, similar behaviour to a p-n-p junction in a traditional silicon semi-conductor.

3.2 Mycelium

This study also covered the use of mycelium as a memristor, Fig. 4. The mycelium exhibits the same memristive properties as the other fruiting bodies and flora. However, the mycelium is cultivated on dampened wood shavings. Therefore, cyclic voltammetry was conducted on both dampened wood shavings and tap water, Fig. 5, to explore the potential memristance of the growth medium. The I-V sweeps demonstrate that the control samples also exhibit memristive properties, albeit with a lower conducted current than the mycelium. This is something that is not seen in dry wood shavings (Fig. 5(c)). The dry shavings respond in a similar way as an open circuit for the test set-up. It is therefore concluded that the addition of water to the growth medium provides a transport mechanism that allows the conduction of current. Tap water has a number of impurities dissolved in it that act as charge carriers, combining this with the wood shavings in a thin layer increases the conducted current compared to the tap water alone in volume.

3.3 Spiking

The cyclic voltammetry of the subject matter illustrates that periods of 'spiking' (oscillations) occur in their I-V characteristics. The spiking behaviour is important as it is a classic component of devices that exhibit memristive properties [12, 26, 27]. By way of example, MATLAB was used to detect the occurrence of the spikes in I-V traces from some of the samples that were tested and the results are shown below.

Figure 6 shows the spiking density from the aubergine and Fig. 7 shows the spiking density from the plant *Echeveria pulidonis*. It is clear that spiking tends to occur over sections of the I-V curve, for a number of periods of the oscillation (also shown in figures of I-V sweeps from Sect. 3). However, there are instances where individual spikes can occur over the waveform. These are characterised by having a larger voltage interval from other occurrences of spikes. The number of spikes, or length of an oscillation period, will vary from between different samples. The important note is that these spikes are exhibited, thereby reinforcing the the resistance of the substance is a function of the previous voltage state and frequency of the voltage swing.

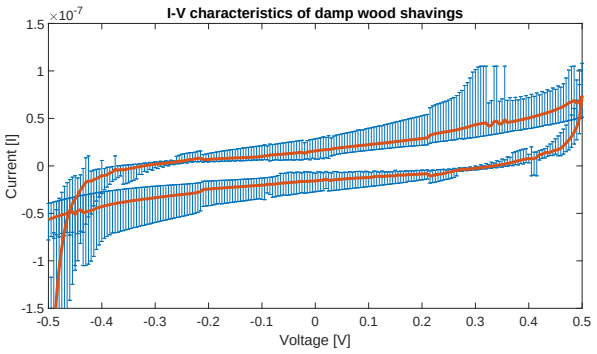

(a)

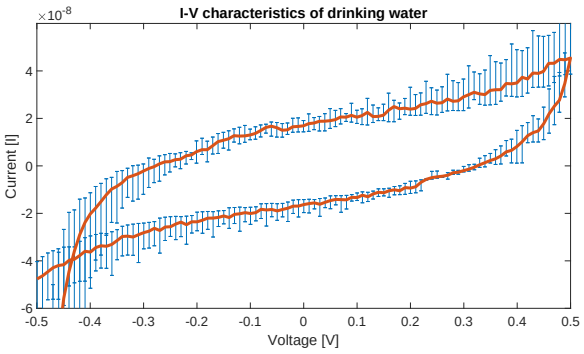

(b)

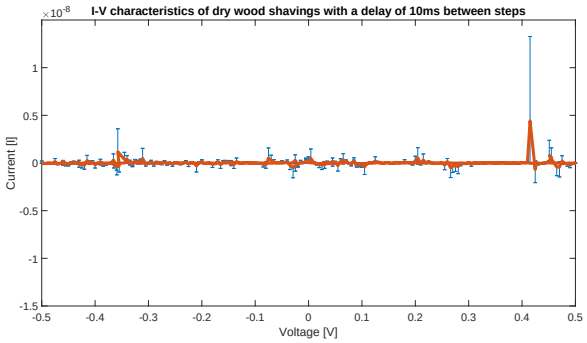

(c)

Figure 5: Average I-V characterisation of control mediums. Cyclic voltammetry performed over -0.5V to 0.5V. (a) damp wood shavings. (b) Bristol tap water sample. (c) dry wood shavings

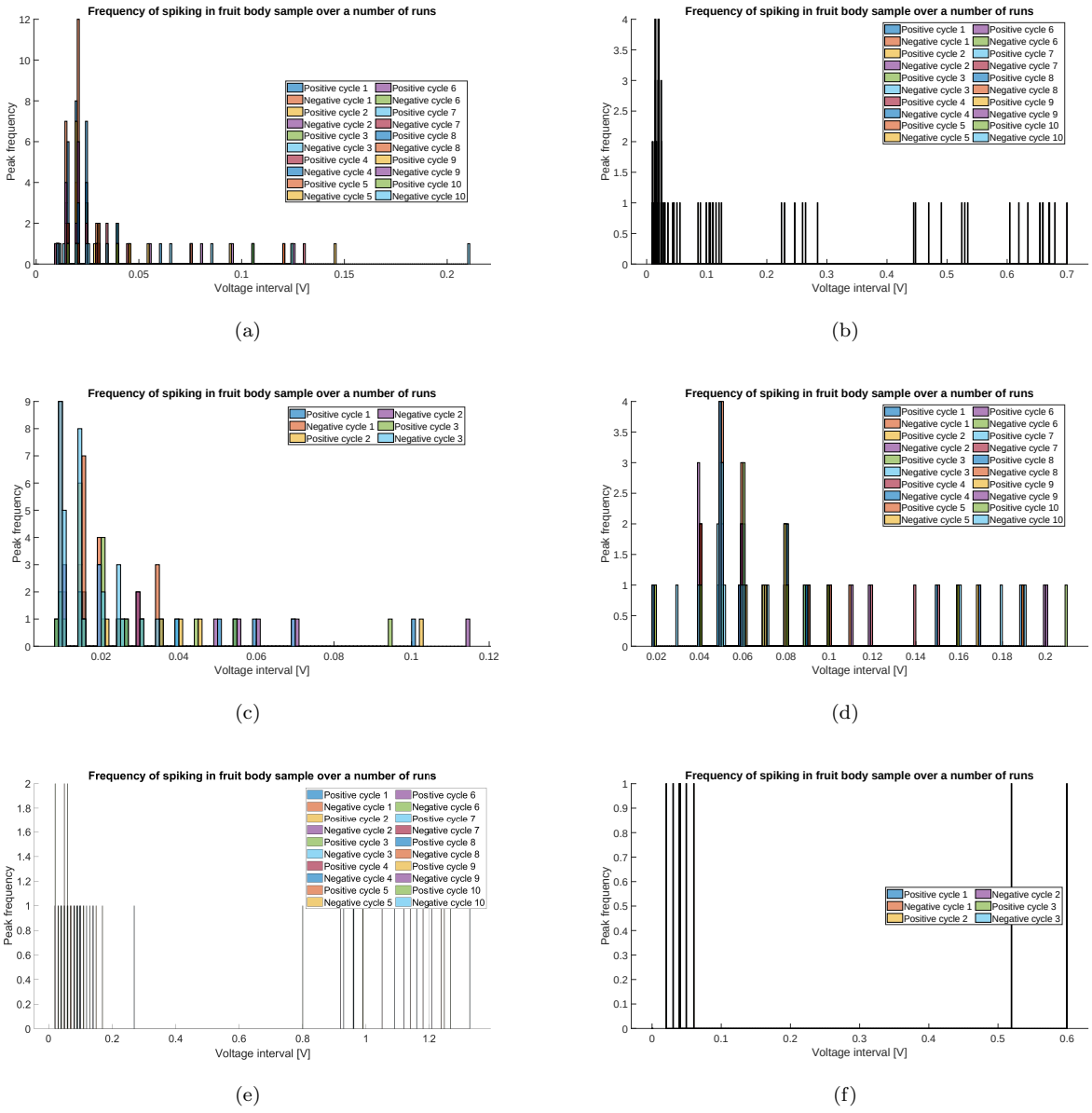

Figure 6: Frequency of voltage interval between spikes for cyclic voltammetry of aubergine under the following conditions: (a) -0.5V to 0.5V, sample delay 10ms, (b) -0.5V to 0.5V, sample delay 100ms, (c) -0.5V to 0.5V, sample delay 1000ms, (d) -1V to 1V, sample delay 10ms, (e) -1V to 1V, sample delay 100ms, (f) -1V to 1V, sample delay 1000ms.

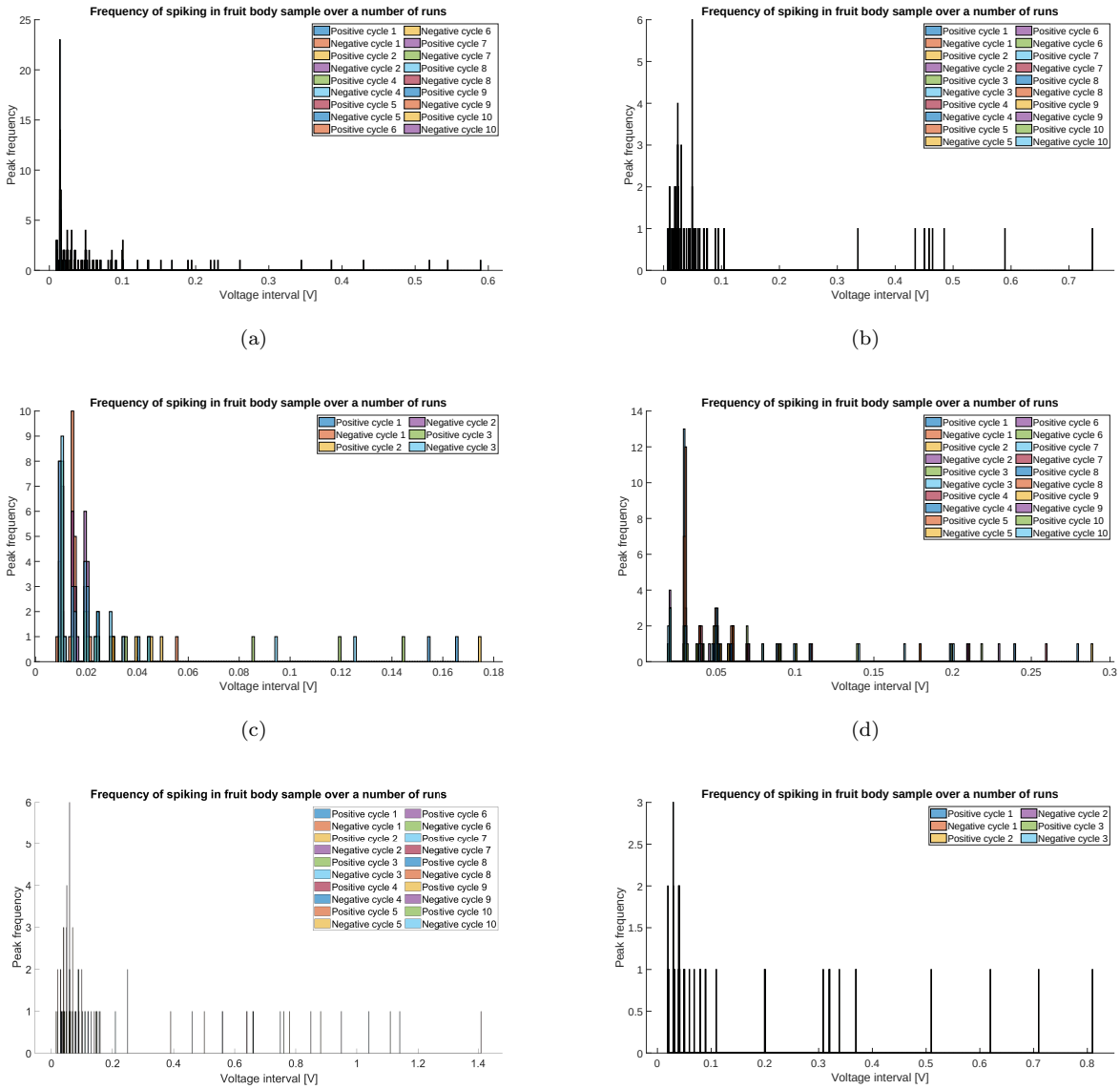

Figure 7: Frequency of voltage interval between spikes for cyclic voltammetry of *Echeveria pulidonis* under the following conditions: (a) -0.5V to 0.5V, sample delay 10ms, (b) -0.5V to 0.5V, sample delay 100ms, (c) -0.5V to 0.5V, sample delay 1000ms, (d) -1V to 1V, sample delay 10ms, (e) -1V to 1V, sample delay 100ms, (f) -1V to 1V, sample delay 1000ms

Table 1: Coefficient of P(t)

a_0	-1.94717918941007e-37	a_{16}	2.12544609190968e-10
a_1	7.05370777962793e-35	a_{17}	-7.02417186413251e-09
a_2	-1.09608654138843e-32	a_{18}	1.49798679659499e-07
a_3	9.17166664784253e-31	a_{19}	-2.25915349408741e-06
a_4	-3.96814860043400e-29	a_{20}	2.4811118088567 7e-05
a_5	2.72250233614171e-28	a_{21}	-0.000198753598325262
a_6	6.27868812867892e-26	a_{22}	0.00113701417453570
a_7	-3.22386131288943e-24	a_{23}	-0.00438858300276266
a_8	5.35491902163618e-23	a_{24}	0.00970067769202458
a_9	5.67150904115691e-22	a_{25}	-0.00277217499616736
a_{10}	-2.10303480491708e-20	a_{26}	-0.0499326832665322
a_{11}	-1.15343437980144e-19	a_{27}	0.145011436255266
a_{12}	-3.79360135264957e-17	a_{28}	-0.184313854027240
a_{13}	3.22192992558703e-15	a_{29}	0.131713253328233
a_{14}	-6.04224119899083e-14	a_{30}	-0.517083007531048
a_{15}	-2.79837373009902e-12		

4 Modelling Onion Memfractance

Here we report the I-V characteristics of onion (-0V5 to 0V5) with a delay of 10ms between steps (Fig. 18). It is evident from the results that onion displays memristive behaviour. Although this vegetable typically does not demonstrate the 'pinching' property of an ideal memristor [7], it can be clearly seen that the biological matter exhibits memory properties when the electrical potential across the substrate is swept. A positive sweep yields a higher magnitude current when the applied voltage is positive; and a smaller magnitude current when the applied voltage is negative.

Fractional Order Memory Elements (FOME) are proposed as a combination of Fractional Order Mem-Capacitors (FOMC) and Fractional Order Mem-Inductors (FOMI) [1]. The FOME (1) is based on the generalised Ohm's law and parameterised as follows: α_1, α_2 are arbitrary real numbers which satisfy $0 \leq \alpha_1, \alpha_2 \leq 2$ and models the solution space by [2], $F_M^{\alpha_1,\alpha_2}$ is the memfractance, $q(t)$ is the time dependent charge, $\varphi(t)$ is the time dependent flux. Therefore, the memfractance ($F_M^{\alpha_1,\alpha_2}$ is an interpolation between four points: MC — memcapacitance, R_M - memristor, MI — meminductance, and R_{2M} - the second order memristor. Full derivations for the generalised FOME model are given by [1, 2]. The definition of memfractance can be straightforward generalised to any value of α_1, α_2 (see [1, Fig. 27]).

$$D_t^{\alpha_1}\varphi(t) = F_M^{\alpha_1,\alpha_2}(t) D_t^{\alpha_2} q(t) \tag{1}$$

The appearance of characteristics from various memory elements in the onion I-V curves supports the assertion that the onion is a memfractor where α_1 and α_2 are both greater than 0 and less than 2.

There is no biological reason for memfractance of onion, be a usual closed formula. Therefore, one can get only a mathematical approximation of this function. In this section, we propose two alternatives to obtain the best approximation for memfractance in the case of onion I-V characteristics for averaged cyclic voltammetry of Fig. 18.

4.1 Single Polynomial Approximation on the whole interval

Raw data include the time, voltage and intensity of each reading characteristics of onion with a delay of 10 ms between steps. There are 401 readings for each run. The process of these data, in order to obtain a mathematical approximation of memfractance, in the first alternative, takes 4 steps as follows. First step: approximate $v(t)$ by a thirty-degree polynomial.

First step: approximate v(t) by a thirty-degree polynomial (Fig. 8) whose coefficients are given in table 1.

$$v(t) \approx P(t) = \sum_{j=0}^{j=30} a_j t^j \tag{2}$$

The polynomial fits very well the experimental voltage curve, as the statistical indexes show in table 2.

Step 2: in the same way approximate the current $i(t)$ using a thirty-degree polynomial (Fig. 9) whose coefficients are given in Tab. 3.

$$i(t) \approx Q(t) = \sum_{j=0}^{j=30} b_j t^j \tag{3}$$

Table 2: Quality of fitness.

Sum of squared estimate of errors	$SSE = \sum_{j=1}^{j=n}(v_j - \hat{v_j})^2$	0.00433091975307024
Sum of squared residuals	$SSR = \sum_{j=1}^{j=n}(\hat{v_j} - \bar{v})^2$	33.3245185894048
Sum of square total	$SST = SSE + SSR$	33.3288495091578
Coefficient of determination	$R - square = \frac{SSR}{SST}$	0.999870054927882

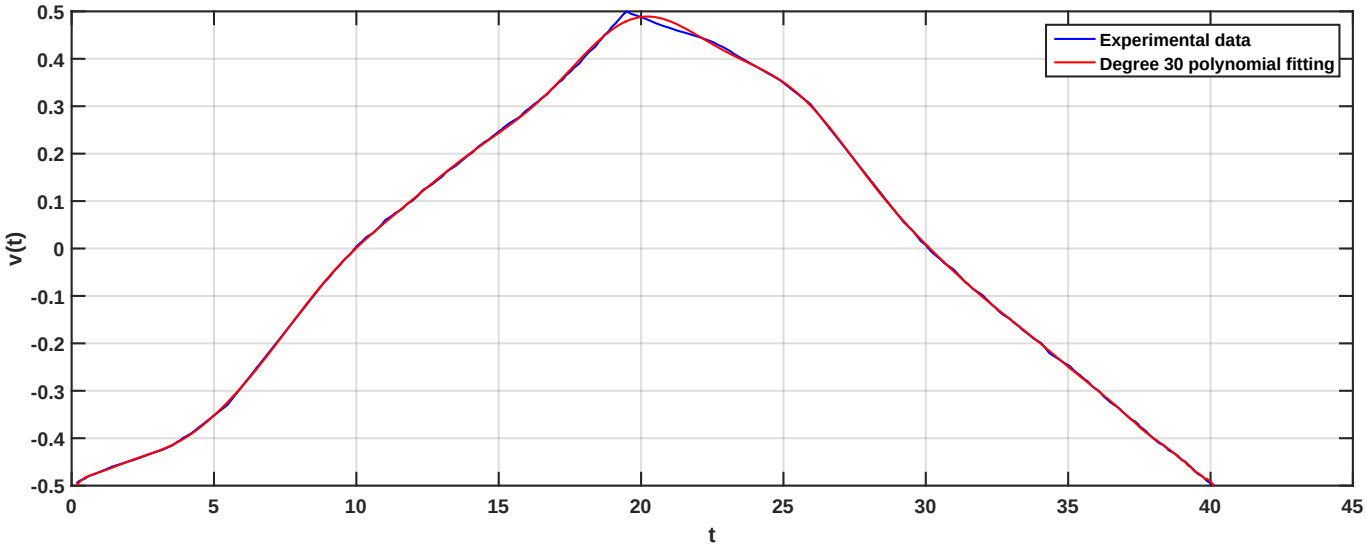

Figure 8: Voltage versus time and its approximation by a 30-degree polynomial.

Table 3: Coefficient of Q(t)

b_0	6.68985942609987e-43	b_{16}	-6.07388014701807e-15
b_1	-2.71853051938565e-40	b_{17}	2.25277616546114e-13
b_2	4.74482538144499e-38	b_{18}	-5.52975396257029e-12
b_3	-4.51931699470006e-36	b_{19}	9.83125923574317e-11
b_4	2.37196020005930e-34	b_{20}	-1.31005323328773e-09
b_5	-4.77095462655549e-33	b_{21}	1.32446639560140e-08
b_6	-1.72460618050188e-31	b_{22}	-1.01592865082809e-07
b_7	1.31453124268333e-29	b_{23}	5.86034919766866e-07
b_8	-3.41852207771790e-28	b_{24}	-2.50008266407625e-06
b_9	1.33534616806178e-26	b_{25}	7.69320497766088e-06
b_{10}	-1.05754298813303e-24	b_{26}	-1.65013726134833e-05
b_{11}	4.06179631752752e-23	b_{27}	2.35982843687423e-05
b_{12}	5.95988497909884e-23	b_{28}	-2.12898753184482e-05
b_{13}	-5.64419454512205e-20	b_{29}	1.14379593758435e-05
b_{14}	1.13468538605641e-18	b_{30}	-3.40155939059945e-06
b_{15}	7.60350529110369e-17		

Table 4: Quality of fitness.

Sum of squared estimate of errors SSE	2.97429625769270e-12
Sum of squared residuals SSR	3.15876438461950e-10
Sum of square total SST	3.18850734719642e-10
Coefficient of determination R-square	0.990671822474212

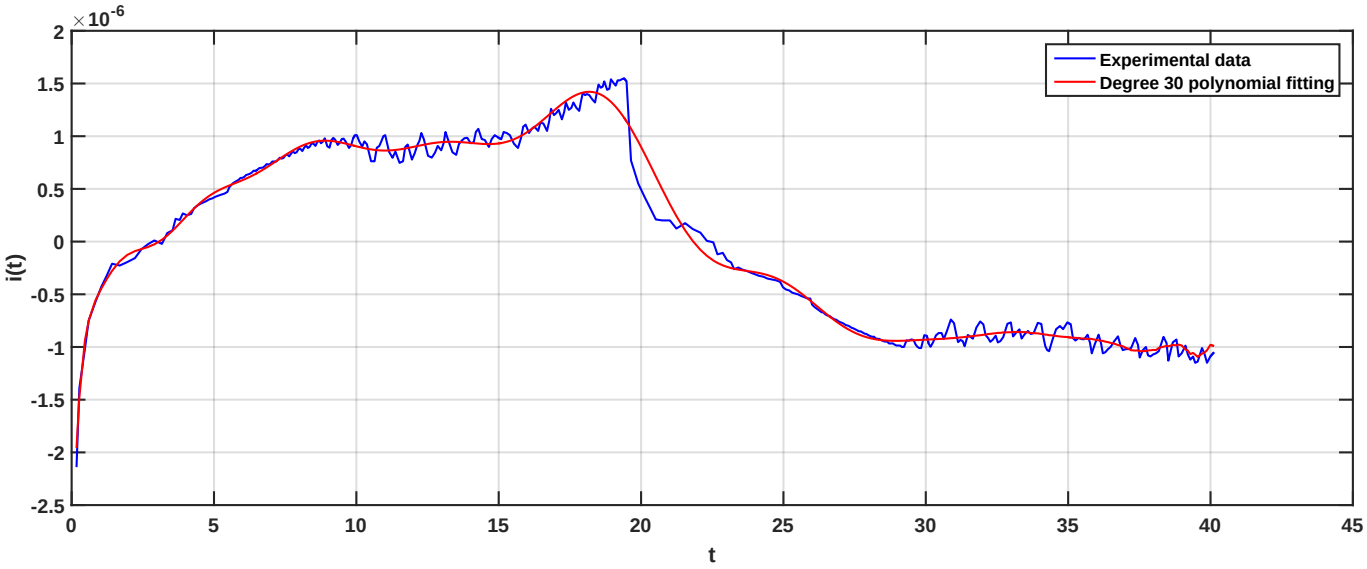

Figure 9: Current versus time and its approximation by a 30-degree polynomial.

Again, the polynomial fits well the experimental intensity curve, as displayed in Tab. 4.

Step 3: From (1) used under the following form when $D_t^{\alpha_2} q(t) \neq 0$.

$$F_M^{\alpha_1,\alpha_2}(t) = \frac{D_t^{\alpha_1}\varphi(t)}{D_t^{\alpha_2} q(t)} \tag{4}$$

and the Rieman-Liouville fractional derivative defined by [25].

$${}_0^{RL}D_t^{\alpha} f(t) = \frac{1}{\Gamma(m-\alpha)}\frac{d^m}{dt^m}\int_0^t (t-s)^{m-\alpha-1} f(s)ds, \text{ m - } 1 < \alpha < m \tag{5}$$

together with the formula for the power function

$${}_0^{RL}D_t^{\alpha}\left(at^{\beta}\right) = \frac{a\Gamma(\beta+1)}{\Gamma(\beta-\alpha+1)}t^{\beta-\alpha},\ \beta > -1, \alpha > 0, \tag{6}$$

we obtain the closed formula of $F_M^{\alpha_1,\alpha_2}(t)$, approximation of the true biological memfractance of onions.

$$F_M^{\alpha_1,\alpha_2}(t) = \frac{D_t^{\alpha_1}\varphi(t)}{D_t^{\alpha_2}\varphi(t)} = \frac{{}_0^{RL}D_t^{\alpha_1}\sum_{j=0}^{j=30}\frac{a_j}{j+1}t^{j+1}}{{}_0^{RL}D_t^{\alpha_2}\sum_{j=0}^{j=30}\frac{b_j}{j+1}t^{j+1}} = \frac{\sum_{j=0}^{j=30}\frac{a_j\Gamma(j+1)}{\Gamma(j+2-\alpha_1)}t^{j+1-\alpha_1}}{\sum_{j=0}^{j=30}\frac{b_j\Gamma(j+1)}{\Gamma(j+2-\alpha_2)}t^{j+1-\alpha_2}} \tag{7}$$

Step 4 choice of parameter α_1 and α_2: We are looking for the best value of these parameters in the range $(\alpha_1, \alpha_2) \in [0,2]^2$. In this goal, we are considering first the singularities of $F_M^{\alpha_1,\alpha_2}(t)$ in order to avoid their existence, using suitable values of the parameters. Secondly, we will choose the most regular approximation.

We compute numerically, the values $t^*(\alpha_2)$ which vanish the denominator of $F_M^{\alpha_1,\alpha_2}(t)$ (Fig. 10).

We observe one, two or three coexisting solutions depending on the value of α_2. Moreover, there is no value of α_2 without zero of the denominator. Therefore, in order to eliminate the singularities, we need to determine the couples $(\alpha_1, \alpha_2) \in [0,2]^2$, vanishing simultaneously denominator and numerator of $F_M^{\alpha_1,\alpha_2}(t)$ (Figs. 11 and 12).

In the second part of step 4, we choose the most regular approximation. We consider that the most regular approximation is the one for which the function range $(F_M^{\alpha_1,\alpha_2}(t))$ is minimal (Fig. 13).

$$\text{range}\left(F_M^{\alpha_1,\alpha_2}(t)\right) = \max_{t\in[0,41]}\left(F_M^{\alpha_1,\alpha_2}(t)\right) - \min_{t\in[0,41]}\left(F_M^{\alpha_1,\alpha_2}(t)\right) \tag{8}$$

From the numerical results, the best couple (α_1, α_2) and the minimum range of $F_M^{\alpha_1,\alpha_2}(t)$ are given in table 5, and the corresponding Memfractance is displayed in Fig. 14.

The value of (α_1, α_2) given in Table 5 belongs to the triangle T_1 of Fig. 15, whose vertices are memcapacitor, capacitor and negative-resistor, which means that Onion is like a mix of such basic electronic devices.

As a counter-example of our method for choosing the best possible memfractance, Fig. 16 displays, the memfractance for a non-optimal couple $(\alpha_1, \alpha_2) = (1.2, 0.5)$ which presents two singularities.

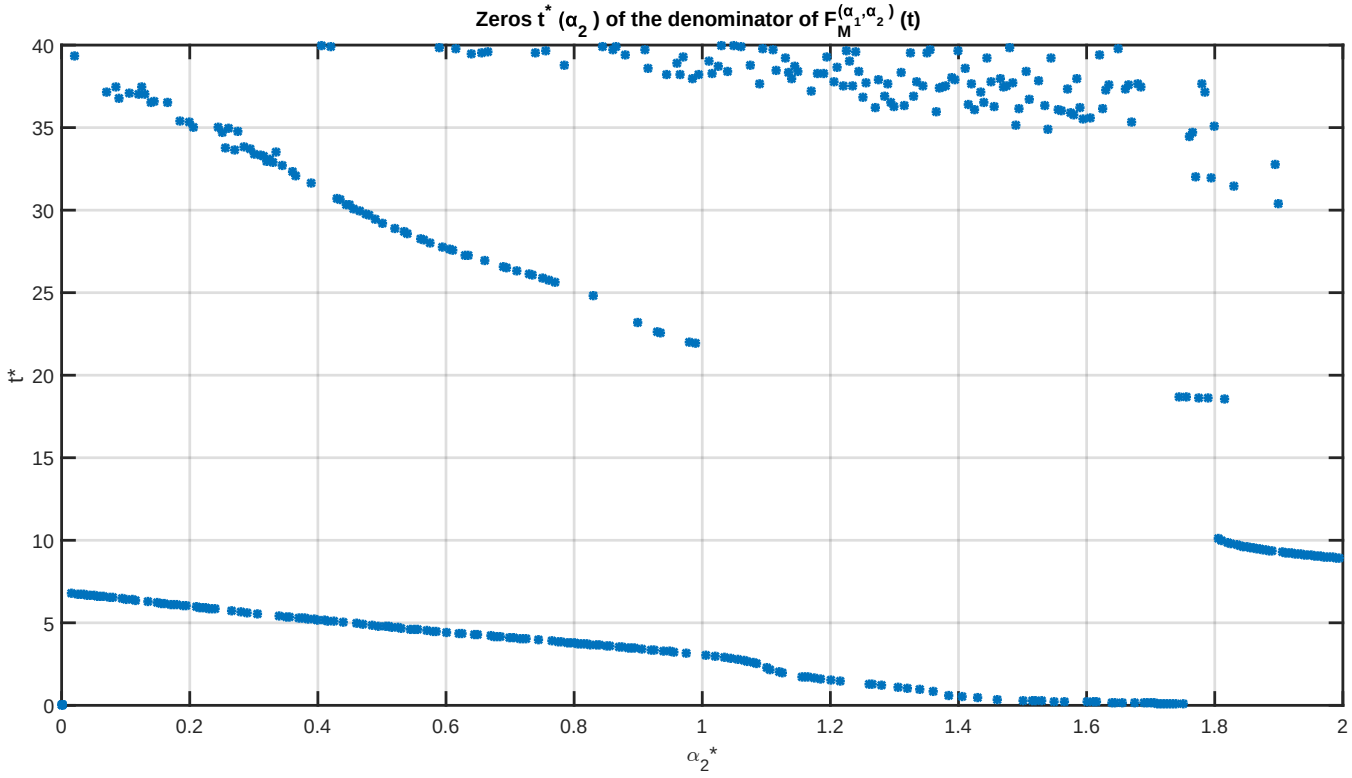

Figure 10: Zeros $t^*(\alpha_2)$ of the denominator of $F_M^{\alpha_1,\alpha_2}(t)$.

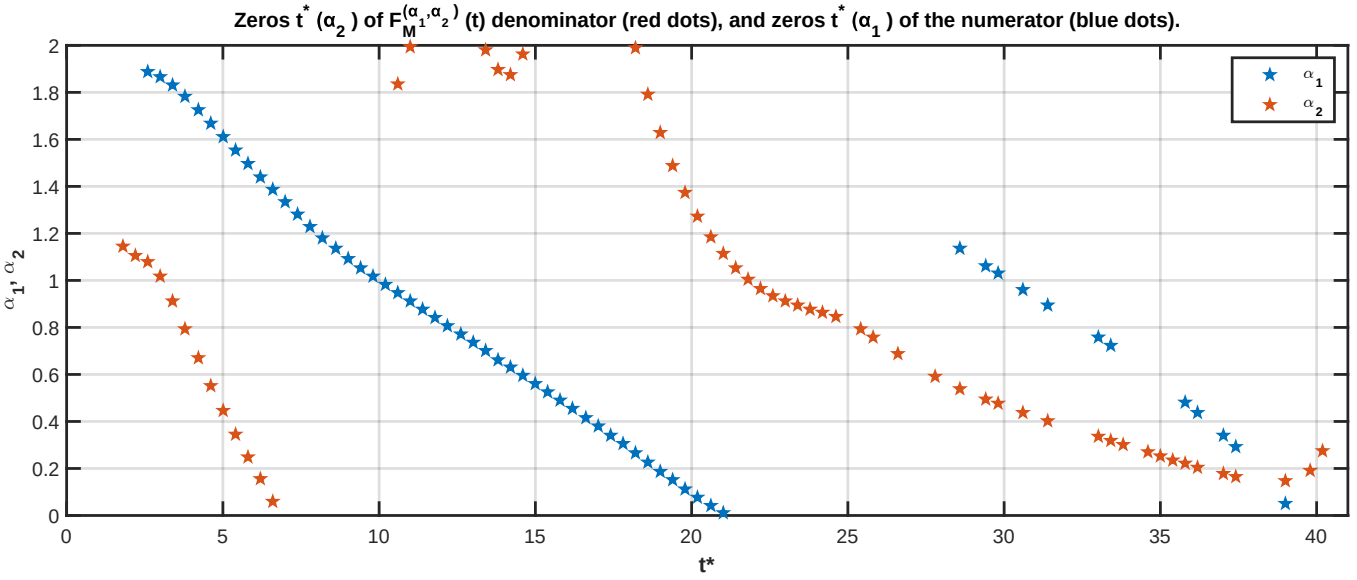

Figure 11: Zeros $t^*(\alpha_2)$ of $F_M^{\alpha_1,\alpha_2}(t)$ denominator (red dots), and zeros $t^*(\alpha_1)$ of the numerator (blue dots).

Table 5: Minimum values of α

α_1	α_2	Minimum range of $F_M^{\alpha_1,\alpha_2}(t)$
1.441224116	0.154232123	1085076.46348631

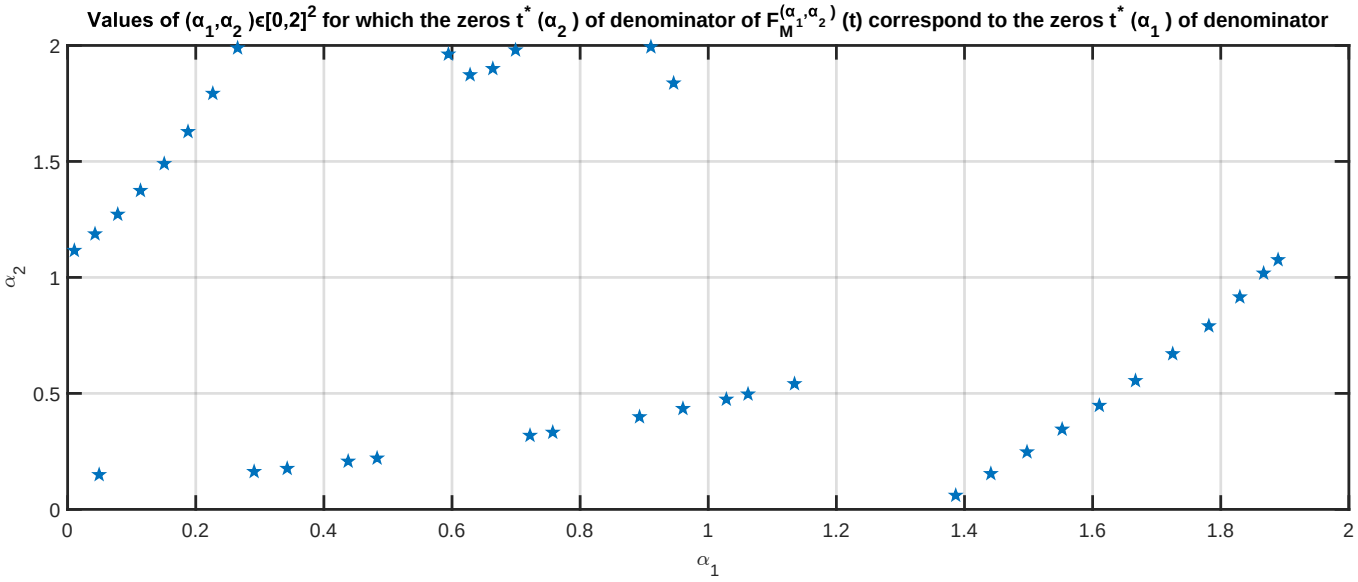

Figure 12: Values of $(\alpha_1, \alpha_2) \in [0,2]^2$ for which the zeros $t^*(\alpha_2)$ of denominator of $F_M^{\alpha_1,\alpha_2}(t)$ correspond to the zeros $t^*(\alpha_1)$ of denominator.

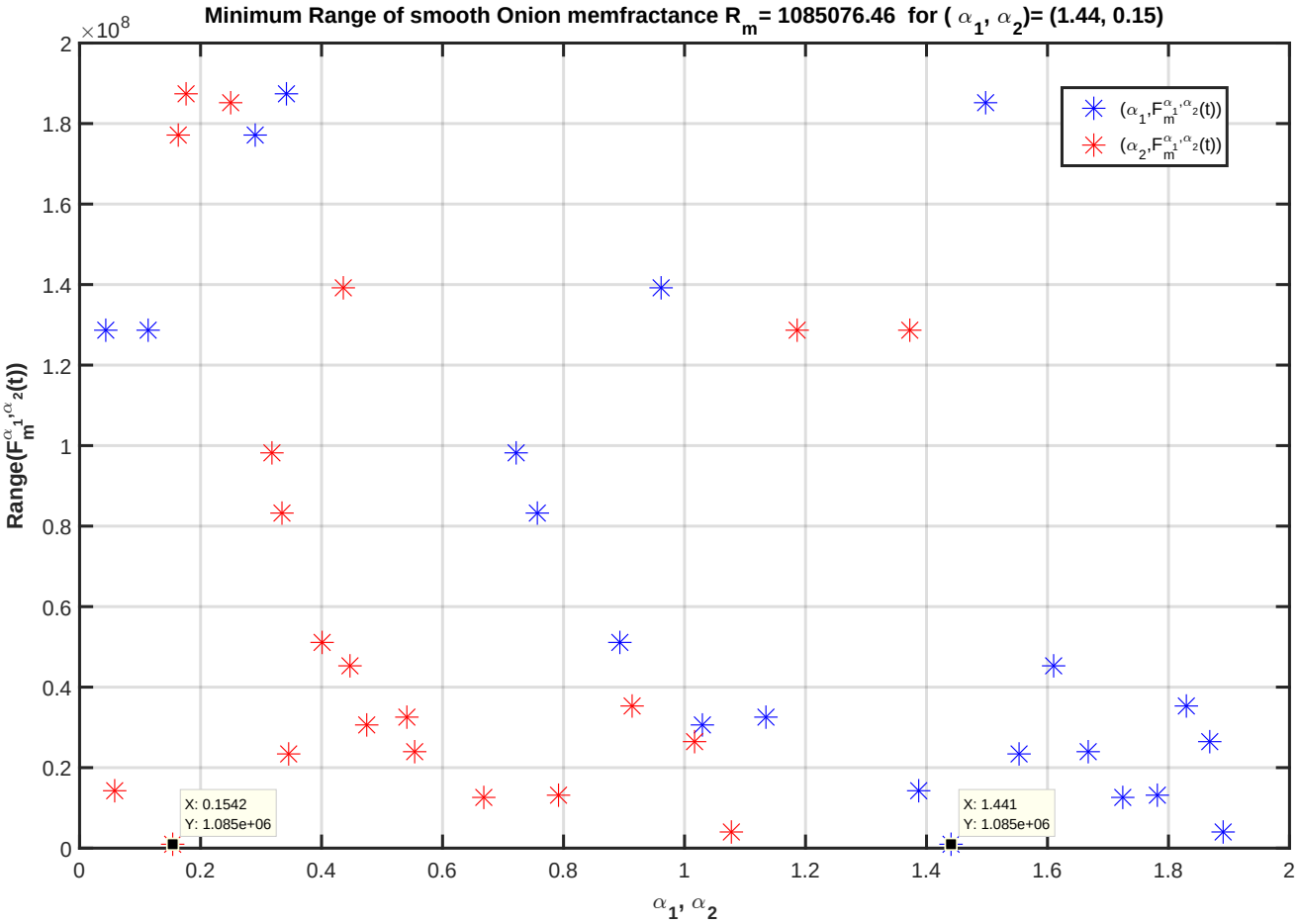

Figure 13: Values of range $(F_M^{\alpha_1,\alpha_2}(t))$ for $(\alpha_1, \alpha_2) \in [0,2]^2$.

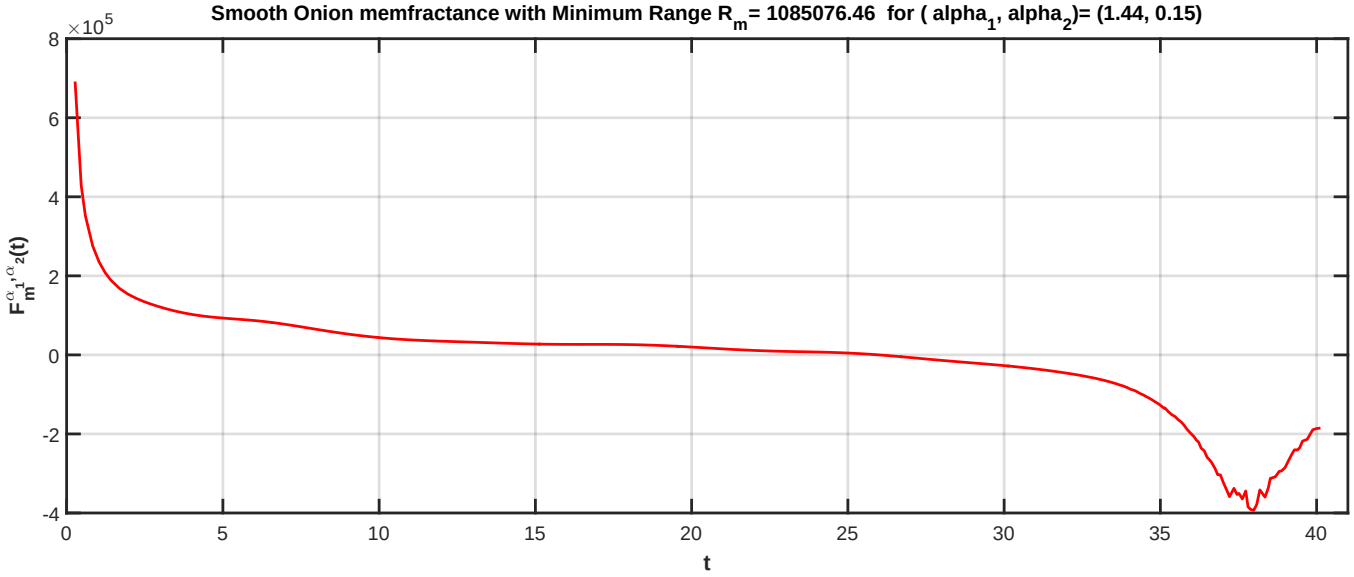

Figure 14: Memfractance for (α_1, α_2) given in Tab. 5.

Table 6: Coefficients of a and a'

Coefficient	Value for $0 \leq t \leq T$	Coefficient	Value for $T < t < T_{\max}$
a_0	-5.51E-11	a'_0	6.87E-11
a_1	4.46E-09	a'_1	-2.02E-08
a_2	-1.39E-07	a'_2	2.64E-06
a_3	1.90E-06	a'_3	-0.000202629
a_4	-5.30E-06	a'_4	0.010116533
a_5	-0.000154541	a'_5	-0.342890106
a_6	0.001735895	a'_6	7.988613675
a_7	-0.006015086	a'_7	-126.3046069
a_8	0.00583923	a'_8	1296.836674
a_9	0.025851171	a'_9	-7808.105752
a_{10}	-0.497985462	a'_{10}	20935.49797

The comparison of average experimental data of cyclic voltammetry performed over -0.5 V to 0.5 V, and closed approximate formula is displayed in Fig. 17, showing a very good agreement between both curves except near the maximum value of $v(t)$ and $i(t)$.

Figure 18 shows that the curve computed from closed approximate formula belongs to the histogram of data of all runs.

4.2 Alternative approximation of the cycling voltammetry

Due to the way of conducting the experiments, the voltage curve presents a vertex, that means that the function $v(t)$ is non-differentiable for $T = 19.4897504$ (Fig. 8). In fact, the value of T is the average value of the non-differentiable points for the 10 runs. The value $T_{\max} = 40.12276457$ is the maximum time of the experimentation, $0 \leq t \leq T_{\max}$.

In this alternative approximation, we follow the same 4 steps as in 4.1, changing the approximation by a thirty-degree polynomial to an approximation by a 2-piecewise D-degree-polynomial, for both $v(t)$ and $i(t)$. Here $D = 10$.

First step: approximation of $v(t)$ by a 2-piecewise tenth-degree-polynomial (Fig. 19) whose coefficients are given in table 6.

$$v(t) = \begin{cases} P_1(t) = \sum_{j=0}^{j=D} a_j t^j, \text{ for } 0 \leq t \leq T \\ P_2(t) = \sum_{j=0}^{j=D} a'_j t^j, \text{ for } t \leq t < T_{\max} \end{cases} \tag{9}$$

The flux is obtained integrating $v(t)$ versus time.

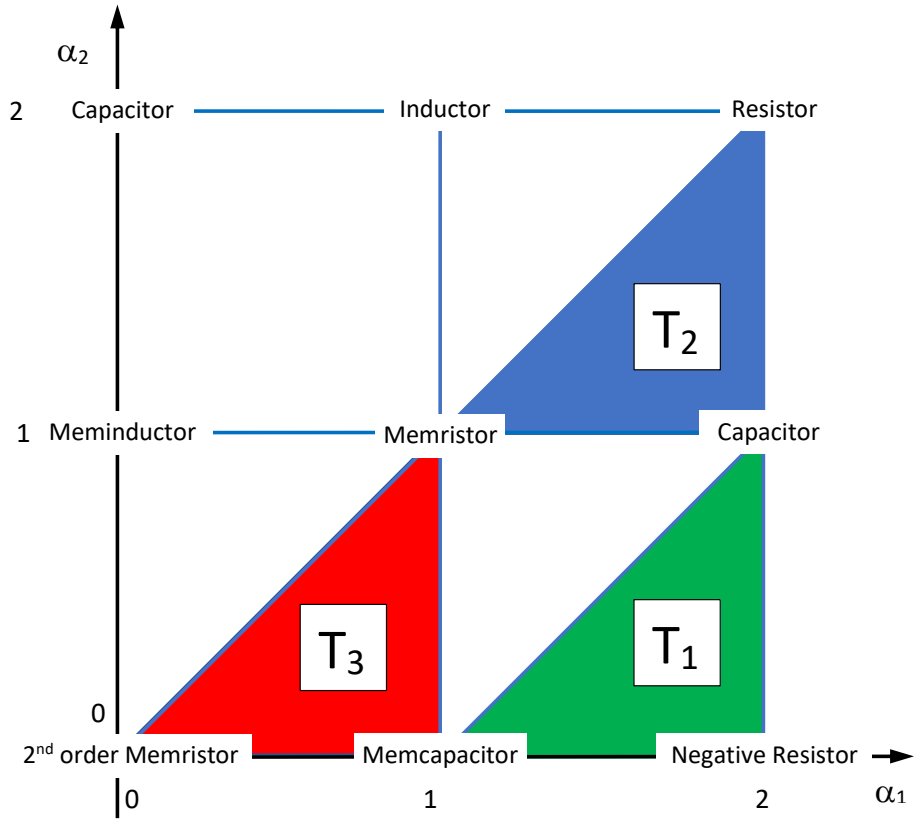
α2
2
Capacitor
Inductor
Resistor
T2
1
Meminductor
Memristor
Capacitor
T3
T1
0
2nd order Memristor
Memcapacitor
Negative Resistor
α1
0
1
2

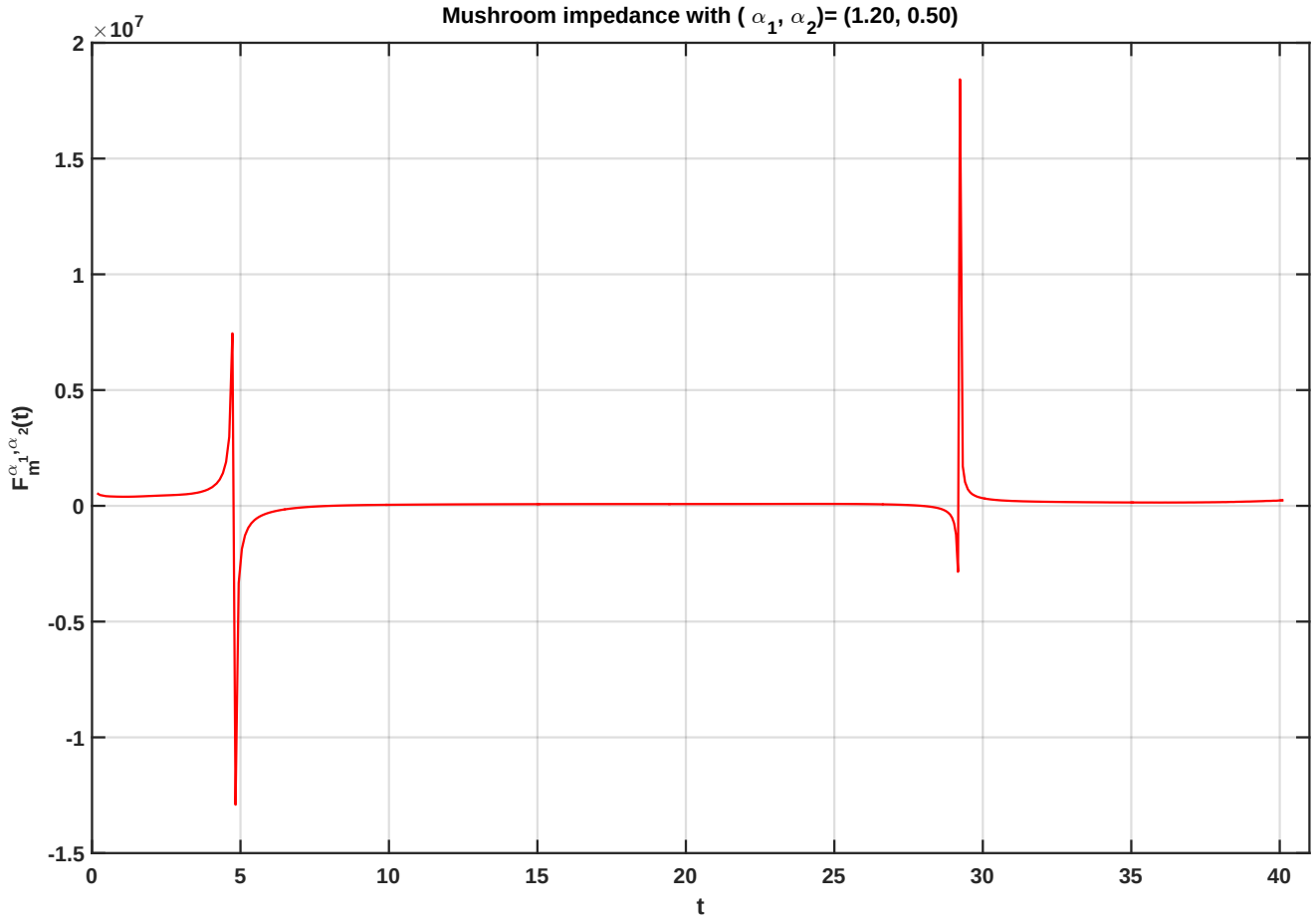

Figure 16: Memfractance with two singularities for $(\alpha_1, \alpha_2) = (1.2, 0.5)$.

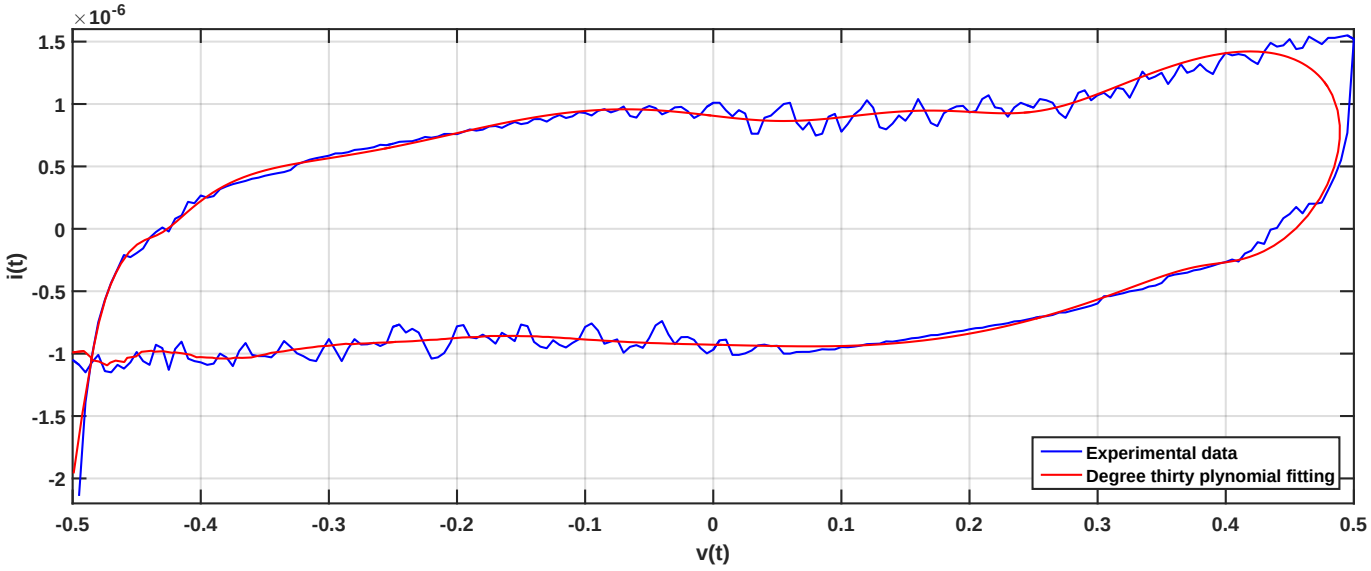

Figure 17: Comparison between average experimental data of cyclic voltammetry performed over -0.5 V to 0.5 V, placement, and approximate values of $v(t)$ and $i(t)$.

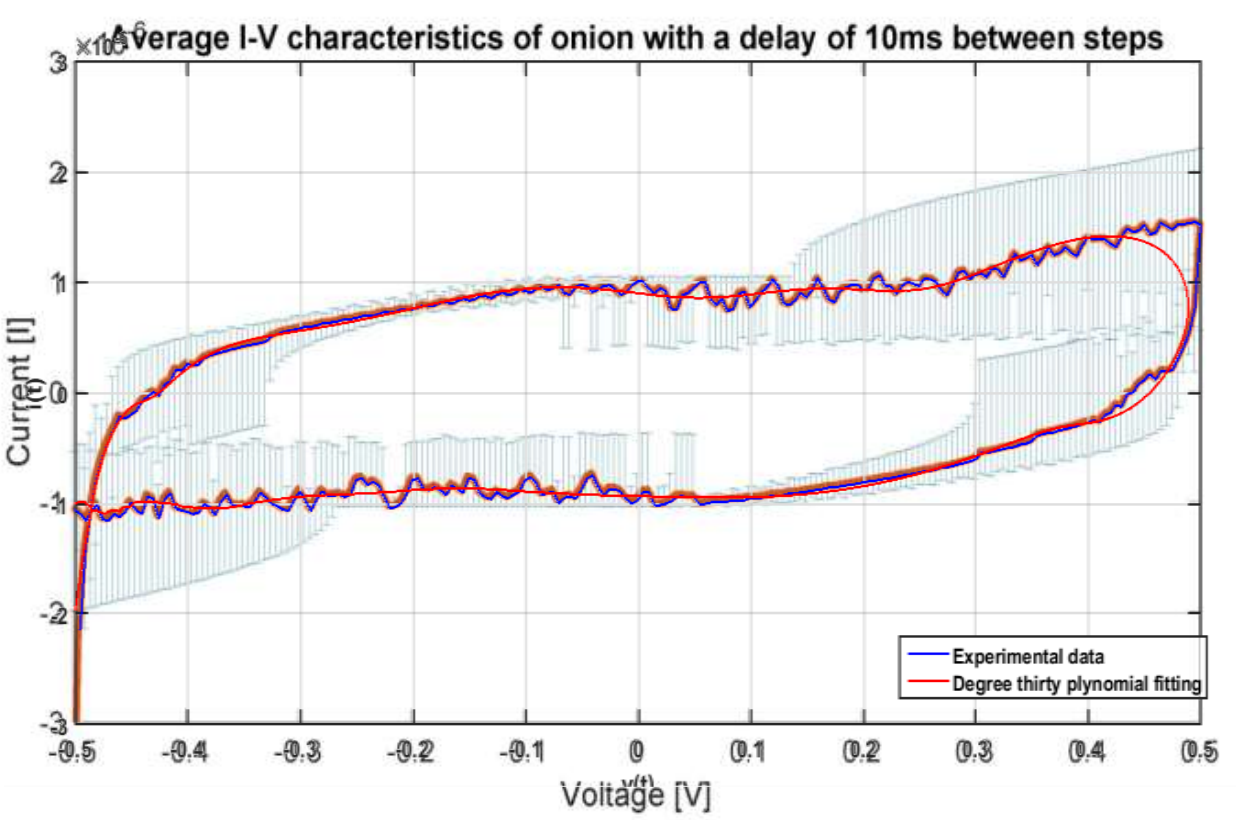

Figure 18: Both average experimental data curve and the curve computed from closed approximate formula are nested into the histogram of data of all runs.

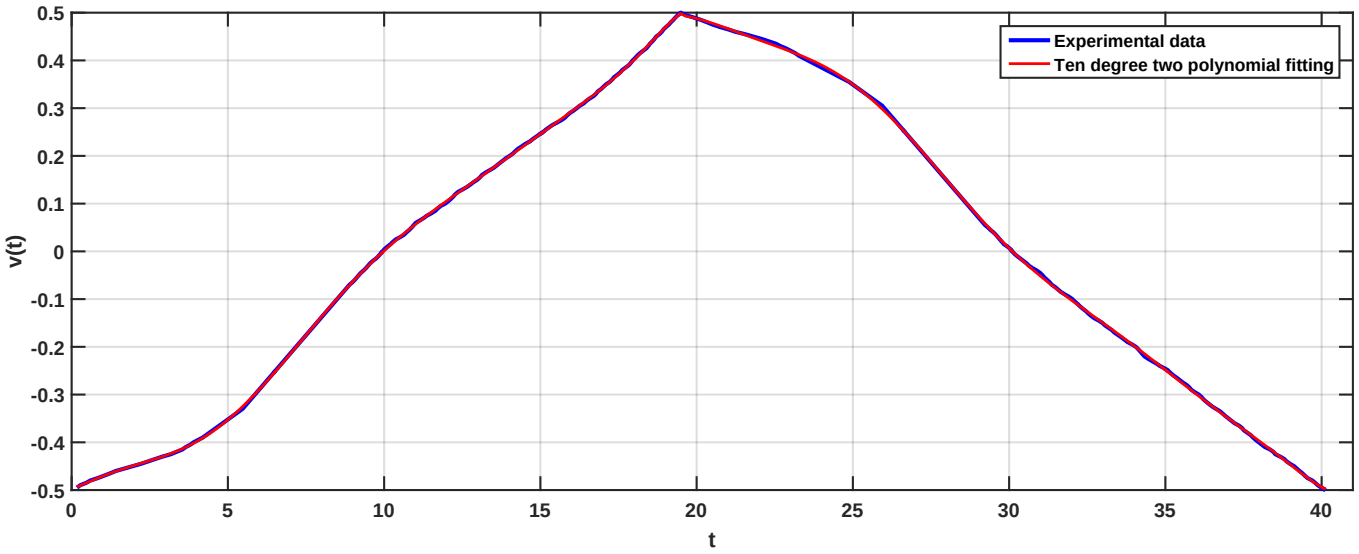

Figure 19: Voltage versus time and its approximation by 2-piecewise tenth degree polynomial.

Table 7: Goodness of fit

Approximation interval	$t < T$	$t > T$
Sum of squared estimate of errors SSE	0.000390862	0.001120834
Sum of squared residuals SSR	16.66147438	16.66067277
Sum of square total SST	16.66186524	16.66179361
Coefficient of determination R-square	0.999976541518186	0.999932730288331

Table 8: Coefficients of b and b'.

Coefficient	Value for $0 \leq t \leq T$	Coefficient	Value for $T < t < T_{\max}$
b_0	3.13E-10	b'_0	-2.13E-09
b_1	-4.86E-09	b'_1	1.09E-07
b_2	4.88E-08	b'_2	-3.78E-06
b_3	-3.18E-07	b'_3	9.07E-05
b_4	1.31E-06	b'_4	-0.001481936
b_5	-3.20E-06	b'_5	0.015797711
b_6	4.26E-06	b'_6	-0.099223872
b_7	-2.52E-06	b'_7	0.278895403
b_8	3.13E-10	b'_8	-2.13E-09
b_9	-4.86E-09	b'_9	1.09E-07
b_{10}	4.88E-08	b'_{10}	-3.78E-06

$$\varphi(t) = \begin{cases} IP_1(t) = \sum_{j=0}^{j=D} \frac{a_j}{j+1} t^{j+1}, \text{ for } 0 \leq t \leq T \\ IP_2(t) = \sum_{j=0}^{j=D} \frac{a'_j}{j+1} t^{j+1}, \text{ for } T \leq t < T_{\max} \end{cases} \tag{10}$$

The polynomial fits very well the experimental voltage curve, as the statistical indexes show in Tab. 7.

Step 2: in the same way, one approximates the current $i(t)$ using a 2-piecewise tenth degree polynomial (Fig. 20) whose coefficients are given in Tab. 8.

$$i(t) = \begin{cases} P_3(t) = \sum_{j=0}^{j=D} b_j t^j, \text{ for } 0 \leq t \leq T \\ P_4(t) = \sum_{j=0}^{j=D} b'_j t^j, \text{ for } T \leq t < T_{\max} \end{cases} \tag{11}$$

Again, the polynomial fits very well the experimental voltage curve, as the statistical indexes show in Tab. 9.

Therefore, the charge is given by

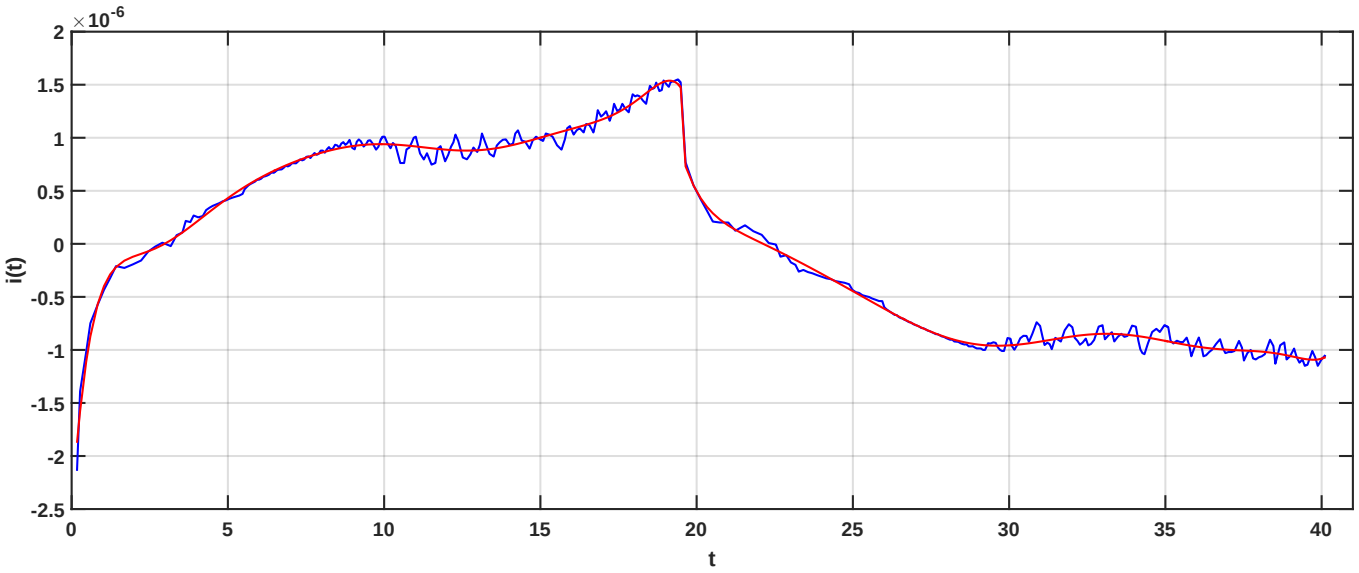

Figure 20: Current versus time and its approximation by 2-piecewise tenth degree polynomial.

Table 9: Quality of fitness.

Approximation interval	$t < T$	$t > T$
Sum of squared estimate of errors SSE	6.63E-13	5.92E-13
Sum of squared residuals SSR	4.97E-11	2.36E-11
Sum of square total SST	5.04E-11	2.41E-11
Coefficient of determination R-square	0.986832207	0.97550029

$$q(t) = \begin{cases} IP_3(t) = \sum_{j=0}^{j=D} \frac{b_j}{j+1} t^{j+1}, \text{ for } 0 \le t \le T \\ IP_4(t) = \sum_{j=0}^{j=D} \frac{b'_j}{j+1} t^{j+1}, \text{ for } T \le t < T_{\max} \end{cases} \tag{12}$$

Step 3: Following the same calculus as before with (4), one obtains

$$\text{for } 0 \le t \le T,\ F_M^{\alpha_1,\alpha_2}(t) = \frac{{}_0^{RL}D_t^{\alpha_1}\varphi(t)}{{}_0^{RL}D_t^{\alpha_2}q(t)} = \frac{{}_0^{RL}D_t^{\alpha_1}[IP_1(t)]}{{}_0^{RL}D_t^{\alpha_2}[IP_3(t)]} = \frac{\sum_{j=1}^{j=D} \frac{a_j\Gamma(j+1)}{\Gamma(j+2-\alpha_1)} t^{j+1-\alpha_1}}{\sum_{j=0}^{j=D} \frac{b_j\Gamma(j+1)}{\Gamma(j+2-\alpha_2)} t^{j+1-\alpha_2}} \tag{13}$$

However, because fractional derivative has memory effect, for $T < t < T_{\max}$, the formula is slightly more complicated

$$\begin{aligned} F_M^{\alpha_1,\alpha_2}(t) &= \frac{{}_0^{RL}D_t^{\alpha_1}\varphi(t)}{{}_0^{RL}D_t^{\alpha_2}q(t)} = \frac{\frac{1}{\Gamma(m_1-\alpha_1)}\frac{d^{m_1}}{dt^{m_1}}\int_0^t (t-s)^{m_1-\alpha_1-1}\varphi(s)ds}{\frac{1}{\Gamma(m_2-\alpha_2)}\frac{d^{m_2}}{dt^{m_2}}\int_0^t (t-s)^{m_2-\alpha_2-1}q(s)ds}, \ m_1-1<\alpha_1<m_1 \text{ and } m_2-1<\alpha_2<m_2 \\ &= \frac{\frac{1}{\Gamma(m_1-\alpha_1)}\frac{d^{m_1}}{dt^{m_1}}\left[\int_0^T (t-s)^{m_1-\alpha_1-1}IP_1(s)ds + \int_T^t (t-s)^{m_1-\alpha_1-1}IP_2(s)ds\right]}{\frac{1}{\Gamma(m_2-\alpha_2)}\frac{d^{m_2}}{dt^{m_2}}\left[\int_0^T (t-s)^{m_2-\alpha_2-1}IP_3(s)ds + \int_T^t (t-s)^{m_2-\alpha_2-1}IP_4(s)ds\right]} \\ &= \frac{\frac{1}{\Gamma(m_1-\alpha_1)}\frac{d^{m_1}}{dt^{m_1}}\sum_{j=0}^{j=D}\left[\frac{a_j}{j+1}\int_0^T (t-s)^{m_1-\alpha_1-1}s^{j+1}ds + \frac{a'_j}{j+1}\int_T^t (t-s)^{m_1-\alpha_1-1}s^{j+1}ds\right]}{\frac{1}{\Gamma(m_2-\alpha_2)}\frac{d^{m_2}}{dt^{m_2}}\sum_{j=0}^{j=D}\left[\frac{b_j}{j+1}\int_0^T (t-s)^{m_2-\alpha_2-1}s^{j+1}ds + \frac{b'_j}{j+1}\int_T^t (t-s)^{m_2-\alpha_2-1}s^{j+1}ds\right]} \end{aligned} \tag{14}$$

Using integration by part repeatedly $D+1$ times we obtain

$$
\begin{aligned}
&F_M^{\alpha_1,\alpha_2}(t)\\
&= \frac{\frac{1}{\Gamma(m_1-\alpha_1)}\frac{d^{m_1}}{dt^{m_1}}\sum_{j=0}^{j=D}\left[\frac{a_j}{j+1}\left[\sum_{k=0}^{k=j+1}\left[\frac{-(j+1)!\Gamma(m_1-\alpha_1)(t_T)^{m_1+k-\alpha_1}T^{j+1-k}}{(j+1-k)!\Gamma(m_1+k+1-\alpha_1}\right]+\frac{(j+1)!\Gamma(m_1-\alpha_1)t^{m_1+k-\alpha_1}}{\Gamma(m_1+j+1-\alpha_1)}\right]+\frac{a'_j}{j+1}\left[\sum_{k=0}^{k=j+1}\frac{(j+1)!\Gamma(m_1-\alpha_1)(t-T)^{m_1+k-\alpha_1}T^{j+1-k}}{(j+1-k)!\Gamma(m_1+k+1-\alpha_1)}\right]\right]}{\frac{1}{\Gamma(m_2-\alpha_2)}\frac{d^{m_2}}{dt^{m_2}}\sum_{j=0}^{j=D}\left[\frac{b_j}{j+1}\left[\sum_{k=0}^{k=j+1}\left[\frac{-(j+1)!\Gamma(m_2-\alpha_2)(t-T)^{m_2+k-\alpha_2}T^{j+1-k}}{(j+1-k)!\Gamma(m_2+k+1-\alpha_2)}\right]+\frac{(j+1)!\Gamma(m_2-\alpha_2)t^{m_2+k-\alpha_2}}{\Gamma(m_2+j+1-\alpha_2)}\right]+\frac{b'_j}{j+1}\left[\sum_{k=0}^{k=j+1}\frac{(j+1)!\Gamma(m_2-\alpha_2)(t-T)^{m_2+k-\alpha_2}T^{j+1-k}}{(j+1-k)!\Gamma(m_2+k+1-\alpha_2)}\right]\right]}\\
&= \frac{\frac{1}{\Gamma(m_1-\alpha_1)}\frac{d^{m_1}}{dt^{m_1}}\sum_{j=0}^{j=D}\left[(a'_j-a_j)\sum_{k=0}^{k=j+1}\left[\frac{j!\Gamma(m_1-\alpha_1)(t-T)^{m_1+k-\alpha_1}T^{j+1-k}}{(j+1-k)!\Gamma(m_1+k+1-\alpha_1)}\right]+a_j\frac{j!\Gamma(m_1-\alpha_1)t^{m_1+j+1-\alpha_1}}{\Gamma(m_1+j+2-\alpha_1}\right]}{\frac{1}{\Gamma(m_2-\alpha_2)}\frac{d^{m_2}}{dt^{m_2}}\sum_{j=0}^{j=D}\left[(b'_j-b_j)\sum_{k=0}^{k=j+1}\left[\frac{j!\Gamma(m_2-\alpha_2)(t-T)^{m_2+k-\alpha_2}T^{j+1-k}}{(j+1-k)!\Gamma(m_2+k+1-\alpha_2)}\right]+b_j\frac{j!\Gamma(m_2-\alpha_2)t^{m_2+j+1-\alpha_2}}{\Gamma(m_2+j+2-\alpha_2)}\right]}\\
&= \frac{\sum_{j=0}^{j=D}\left[(a'_j-a_j)\sum_{k=0}^{k=j+1}\left[\frac{j!(t-T)^{k-\alpha_1}T^{j+1-k}}{(j+1-k)!\Gamma(k+1-\alpha_1)}\right]+a_j\frac{j!t^{j+1-\alpha_1}}{\Gamma(j+2-\alpha_1)}\right]}{\sum_{j=0}^{j=D}\left[(b'_j-b_j)\sum_{k=0}^{k=j+1}\left[\frac{j!(t-T)^{k-\alpha_2}T^{j+1-k}}{(j+1-k)!\Gamma(k+1-\alpha_2)}\right]+b_j\frac{j!t^{j+1-\alpha_2}}{\Gamma(j+2-\alpha_2)}\right]}
\end{aligned}
\tag{15}
$$

Table 10: Minimum values of α.

α_1	α_2	Minimum range of $F_M^{\alpha_1,\alpha_2}(t)$
1.971795208	1.483238482	743101.176733524

In this 2-piece wise approximation, the vertex is non-differentiable, this implies that (15) expression has a singularity at T (because $(t-T)^{-\alpha_{1,2}} \to \infty$).

It could be possible to avoid this singularity, using a 3-piece wise approximation, smoothing the vertex. However, the calculus are very tedious. We will explain, below, what our simpler choice implies.

$$\begin{aligned}\text{Then } F_M^{\alpha_1,\alpha_2}(t) &= \frac{(t-T)^{-\alpha_1}\left[\sum_{j=0}^{j=D}\left[(a'_j-a_j)\sum_{k=0}^{k=j+1}\left[\frac{j!(t-T)^k T^{j+1-k}}{(j+1-k)!\Gamma(k+1-\alpha_1}\right)\right]+a_j\frac{j!t^{j+1-\alpha_1}(t-T)^{\alpha_1}}{\Gamma(j+2-\alpha_1)}\right]\right]}{(t-T)^{-\alpha_2}\left[\sum_{j=0}^{j=D}\left[(b'_j-b_j)\sum_{k=0}^{k=j+1}\left[\frac{j!(t-T)^k T^{j+1-k}}{(j+1-k)!\Gamma(k+1-\alpha_2)}\right]+b_j\frac{j!t^{j+1-\alpha_2}(t-T)^{\alpha_2}}{\Gamma(j+2-\alpha_2)}\right]\right]} \\ &= \frac{\sum_{j=0}^{j=D}\left[(a'_j-a_j)\sum_{k=0}^{k=j+1}\left[\frac{j!(t-T)^k T^{j+1-k}}{(j+1-k)!\Gamma(k+1-\alpha_1)}\right]+a_j\frac{j!t^{j+1-\alpha_1}(t-T)^{\alpha_1}}{\Gamma(j+2-\alpha_1)}\right]}{(t-T)^{\alpha_1-\alpha_2}\sum_{j=0}^{j=D}\left[(b'_j-b_j)\sum_{k=0}^{k=j+1}\left[\frac{j!(t-T)^k T^{j+1-k}}{(j+1-k)!\Gamma(k+1-\alpha_2)}\right]+b_j\frac{j!t^{j+1-\alpha_2}(t-T)^{\alpha_2}}{\Gamma(j+2-\alpha_2)}\right]}\end{aligned} \tag{16}$$

Finally

$$F_M^{\alpha_1,\alpha_2}(t) = \begin{cases}\frac{\sum_{j=0}^{j=D}\frac{a_j\Gamma(j+1)}{\Gamma(j+2-\alpha_1)}t^{j+1-\alpha_1}}{\sum_{j=0}^{j=D}\frac{b_j\Gamma(j+1)}{\Gamma(j+2-\alpha_2)}t^{j+1-\alpha_2}}, & \text{for } 0\le t\le T \\ \frac{\sum_{j=0}^{j=D}\left[(a'_j-a_j)\sum_{k=0}^{k=j+1}\left[\frac{j!(t-T)^k T^{j+1-k}}{(j+1-k)!\Gamma(k+1-\alpha_1)}\right]+a_j\frac{j!t^{j+1-\alpha_1}(t-T)^{\alpha_1}}{\Gamma(j+2-\alpha_1)}\right]}{(t-T)^{\alpha_1-\alpha_2}\sum_{j=0}^{j=D}\left[(b'_j-b_j)\sum_{k=0}^{k=j+1}\left[\frac{j!(t-T)^k T^{j+1-k}}{(j+1-k)!\Gamma(k+1-\alpha_2)}\right]+b_j\frac{j!t^{j+1-\alpha_2}(t-T)^{\alpha_2}}{\Gamma(j+2-\alpha_2)}\right]}, & \text{for } T<t<T_{\max}\end{cases} \tag{17}$$

Step 4 choice of parameter α_1 and α_2: Following the same idea as for the first alternative, we try to avoid singularity for $F_M^{\alpha_1,\alpha_2}(t)$, except of course the singularity near T, which is of mathematical nature (non-differentiability of voltage and intensity at $t=T$). Figure 21 display zeros $t^*(\alpha_2)$, of the denominator of $F_M^{\alpha_1,\alpha_2}(t)$.

Figure 22 displays the curves of couples (α_1,α_2) for which the denominator and numerator of $F_M^{\alpha_1,\alpha_2}(t)$ are null simultaneously for $t<T$ and $t>T$. On this figure, the value of α_1 that corresponds to $\alpha_2 = 1.483238482$ is $\alpha_1 \approx 1.971795208$. The corresponding memfractance is displayed in Fig. 24.

The singularity observed in Figs. 24 is due to the non-differentiability of both voltage and intensity functions at point T.

The value of $(\alpha_1 = 1.971795208, \alpha_2 = 1.483238482)$ belongs to the triangle T_2 of Fig. 15, whose edges are resistor, memristor, and capacitor. Therefore the mem-fractance property of onion is a combination of those of these electric components.

The comparison of average experimental data of cyclic voltammetry performed over -0.5 V to 0.5 V and closed approximative formula is displayed in Fig. 25, showing a very good agreement between both curves.

4.3 Alternative approximation of the cycling voltammetry of onion with a delay of 1s between steps

Due to the way of conducting the experiments, the voltage curve presents a vertex, that means that the function $v(t)$ is non-differentiable for $T = 218.835146340667$. In fact, the value of T is the average value of the non-differentiable points for the 3 runs. On has $T_{\max} = 446.142389256667$, and $D = 15$.

We perform an approximation by a 2-piecewise D-degree-polynomial, for both $v(t)$ and $i(t)$.

First step: approximation of $v(t)$ by a 2-piecewise fifteen-degree-polynomial defined by (9), (Fig. 26) whose coefficients are given in table 11.

The flux is again obtained integrating $v(t)$ versus time (10).

The polynomial fits very well the experimental voltage curve, as the statistical indexes show in Tab. 12.

Step 2: in the same way, one approximates the current $i(t)$ using a 2-piecewise fifteenth degree polynomial defined by (11), (Fig. 27) whose coefficients are given in table 13.

Again, the polynomial fits very well the experimental voltage curve, as the statistical indexes show in Tab. 14.

Therefore, the charge is given by (12).

Step 3: Following the same calculus as before with (4), for $0 \le t \le T$, $F_M^{\alpha_1,\alpha_2}(t)$ is defined by (13).

However, because fractional derivative has memory effect, for $T < t < T_{\max}$, the formula is slightly more complicated. It is defined by (14), (15), (16) and (17).

In this 2-piecewise approximation, the vertex is non-differentiable, this implies that (15) expression has a singularity at T (because $(t-T)^{-\alpha_{1,}} \to \text{inf}$).

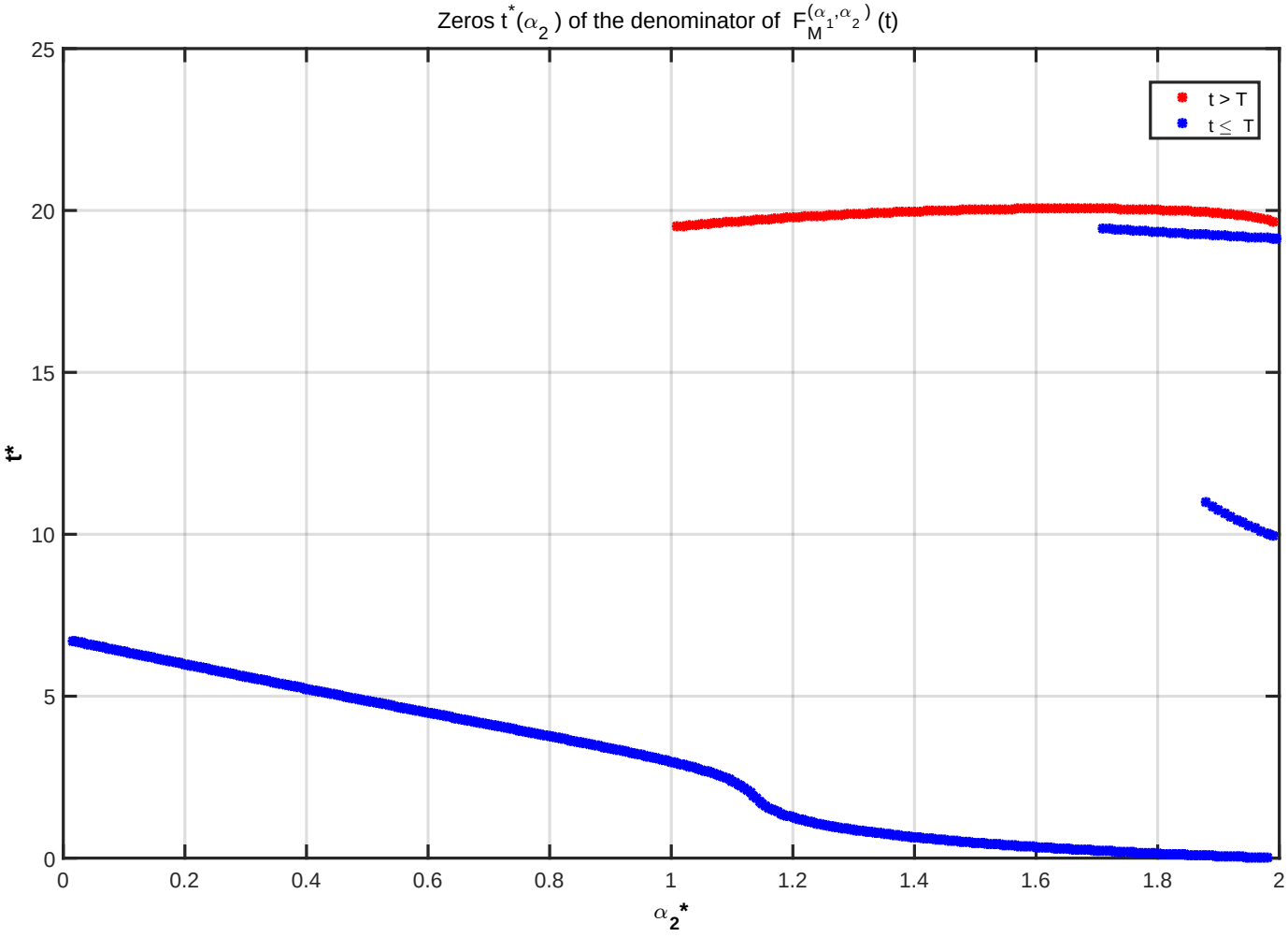

Figure 21: The zeros $t^*(\alpha_2)$, of the denominator of $F_M^{\alpha_1,\alpha_2}(t)$, as function of α_2.

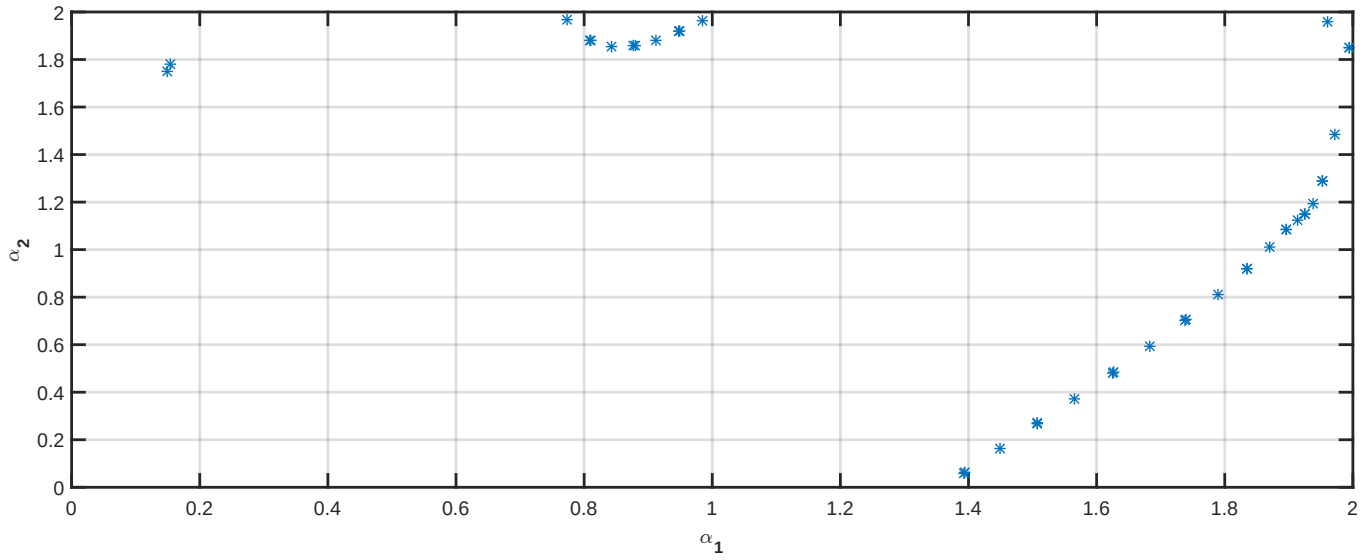

Figure 22: Couples (α_1, α_2) for which the denominator and numerator of $F_M^{\alpha_1,\alpha_2}(t)$ are null simultaneously.

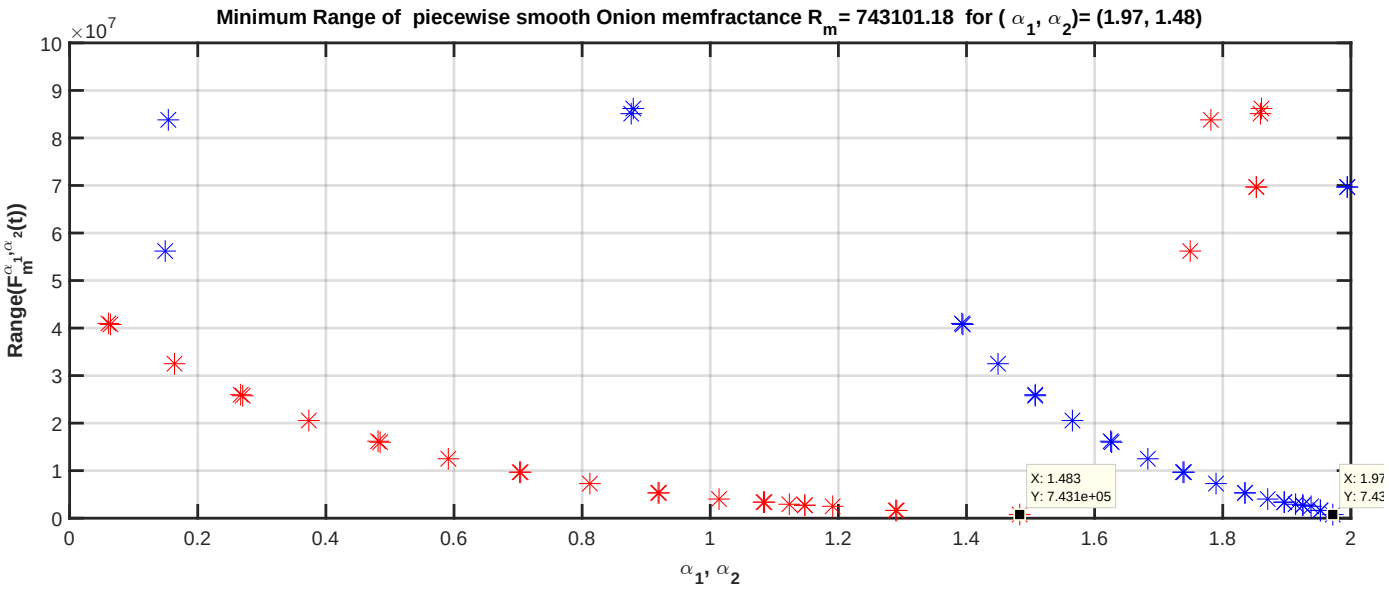

Figure 23: Values of range $(F_M^{\alpha_1,\alpha_2}(t))$ for $(\alpha_1, \alpha_2) \in [0, 2]^2$.

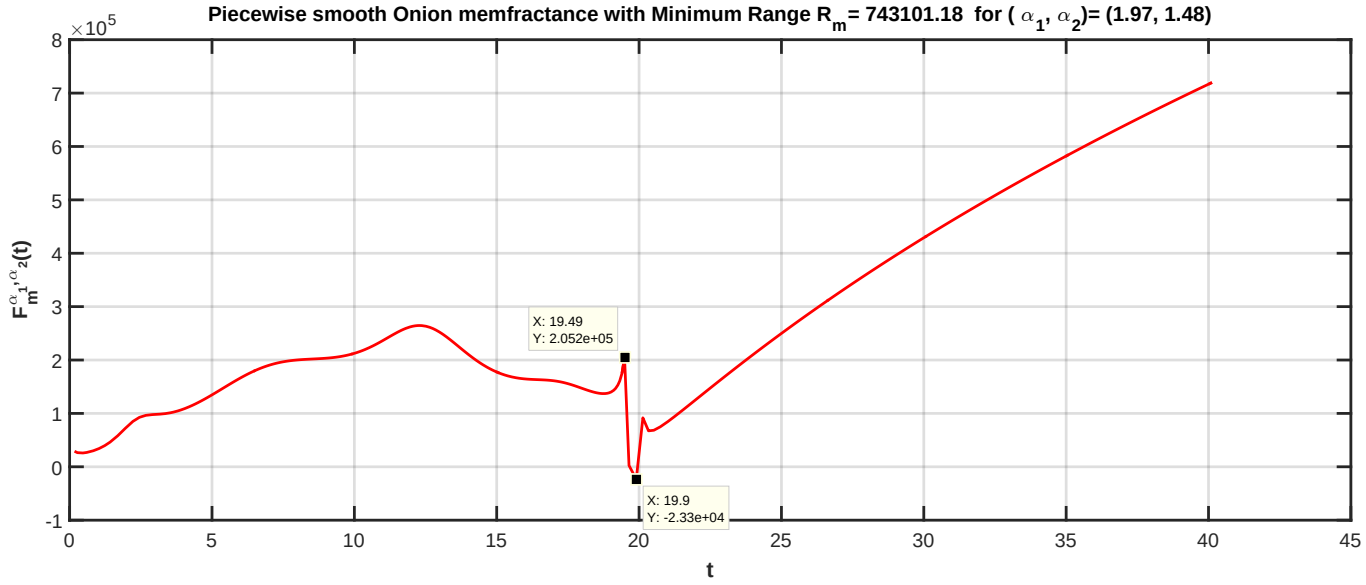

Figure 24: Memfractance for $(\alpha_1 = 1.971795208, \alpha_2 = 1.483238482)$ given in Tab. 10.

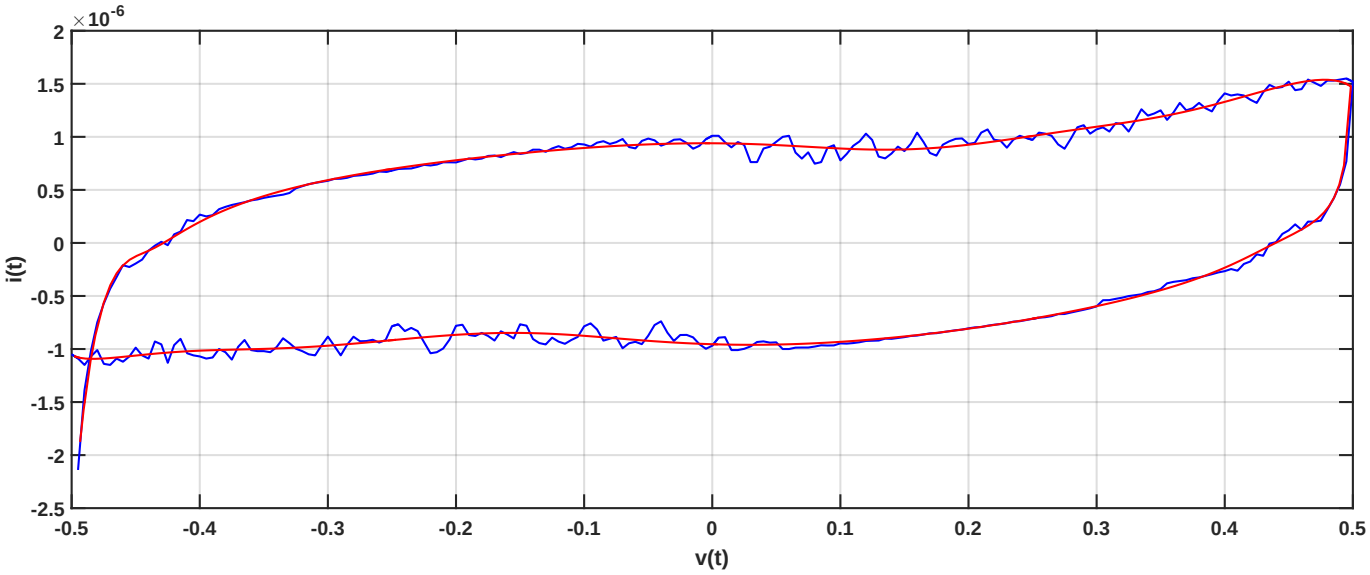

Figure 25: Comparison between average experimental data of cyclic voltammetry performed over -0.5 V to 0.5 V, Stem-to-cap electrode placement, and closed approximative formula.

Table 11: Coefficients of a and a'

Coefficient	Value for $0 \leq t \leq T$	Coefficient	Value for $T < t < 446.142389256667$
a_0	3.54420781829105e-30	a'_0	1.00427487680972e-30
a_1	-5.96398936924787e-27	a'_1	-5.20695580801111e-27
a_2	4.52630929682328e-24	a'_2	1.25279988942641e-23
a_3	-2.04721171726301e-21	a'_3	-1.85546677570461e-20
a_4	6.14198657142099e-19	a'_4	1.89174603354674e-17
a_5	-1.28714657924748e-16	a'_5	-1.40637895477368e-14
a_6	1.93189458719508e-14	a'_6	7.87564822151931e-12
a_7	-2.09391204258264e-12	a'_7	-3.38279075621789e-09
a_8	1.63042090512474e-10	a'_8	1.12362332993865e-06
a_9	-8.95113952596272e-09	a'_9	-0.000288613689878837
a_{10}	3.34546189613670e-07	a'_{10}	0.0568590592565226
a_{11}	-8.03669009474361e-06	a'_{11}	-8.43718319262010
a_{12}	0.000113493644607879	a'_{12}	912.822831960333
a_{13}	-0.000835676981290587	a'_{13}	-67977.9563028956
a_{14}	0.0122632177149911	a'_{14}	3115831.30623377
a_{15}	-1.00360065451426	a'_{15}	-66266900.3096982

Table 12: Quality of fitness.

Approximation interval	$t < T$	$t > T$
Sum of squared estimate of errors SSE	8.05206626404267e-05	0.000379119559037593
Sum of squared residuals SSR	66.6597470338760	66.7305863691811
Sum of square total SST	66.6598275545387	66.7309654887402
Coefficient of determination R-square	0.999998792066143	0.999994318686141

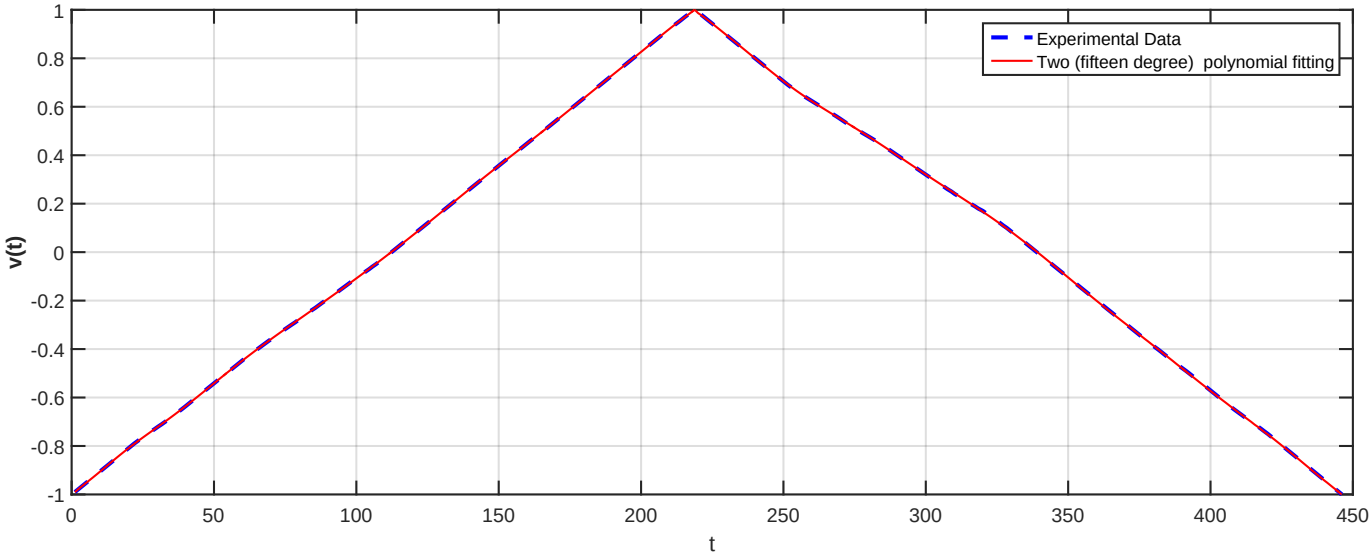

Figure 26: Voltage versus time and its approximation by 2-piecewise fifteenth degree polynomial.

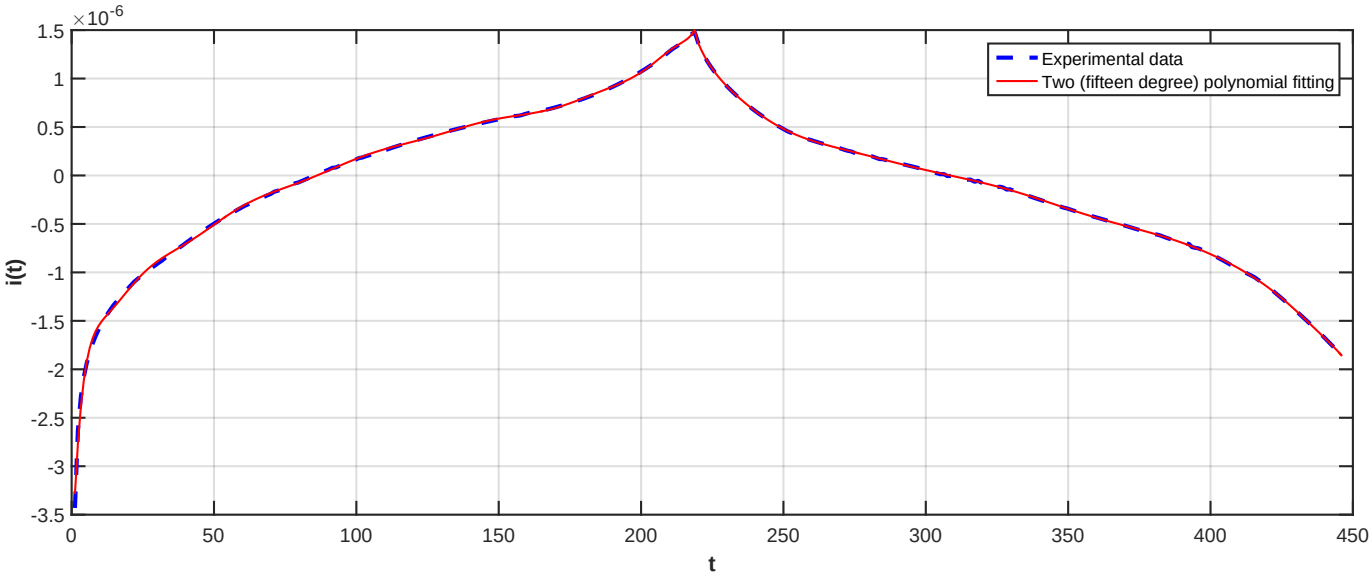

Figure 27: Current versus time and its approximation by 2-piecewise fifteenth degree polynomial.

Table 13: Coefficients of b and b'

Coefficient	Value for $0 \leq t \leq T$	Coefficient	Value for $T < t < 446.142389256667$
b_0	9.54254808462533e-35	b'_0	1.53300080630080e-38
b_1	-1.63161644309873e-31	b'_1	-2.89601182252080e-34
b_2	1.26206638752557e-28	b'_2	1.13996788975235e-30
b_3	-5.83981425666847e-26	b'_3	-2.25810438491826e-27
b_4	1.80113459097984e-23	b'_4	2.79988171542492e-24
b_5	-3.90531862314380e-21	b'_5	-2.39282614008484e-21
b_6	6.11858793928889e-19	b'_6	1.48305233409647e-18
b_7	-7.01109241829061e-17	b'_7	-6.85633253958774e-16
b_8	5.88169906789969e-15	b'_8	2.39797611614612e-13
b_9	-3.58165613133728e-13	b'_9	-6.36783612027411e-11
b_{10}	1.55442674717007e-11	b'_{10}	1.27624831718578e-08
b_{11}	-4.66705880467474e-10	b'_{11}	-1.89820925444517e-06
b_{12}	9.27058527759065e-09	b'_{12}	0.000202910655233761
b_{13}	-1.14142215596473e-07	b'_{13}	-0.0147140989613784
b_{14}	8.12388017501071e-07	$'_{14}$	0.646651137483905
b_{15}	-4.08952638018235e-06	b'_{15}	-12.9611877781724

Table 14: Goodness of fit

Approximation interval	$t < T$	$t > T$
Sum of squared estimate of errors SSE	7.99361696557309e-14	2.86502655937580e-15
Sum of squared residuals SSR	1.45875395884222e-10	1.02218430381697e-10
Sum of square total SST	1.45955332053877e-10	1.02221295408256e-10
Coefficient of determination R-square	0.999452324430147	0.999971972312150

Table 15: Values of α

α_1	α_2	Minimumg range of $F_M^{\alpha_1,\alpha_2}(t)$
0.171972381	0.054935584	12089427.7744264

Step 4 choice of parameter α_1 and α_2: Following the same idea as for the first alternative, we try to avoid singularity for $F_M^{\alpha_1,\alpha_2}(t)$, except of course the singularity near T, which is of mathematical nature (non-differentiability of voltage and intensity at $t = T$). Figure 28 display zeros$t^*(\alpha_2)$, of the denominator of $F_M^{\alpha_1,\alpha_2}(t)$.

Figure 29 displays the curves of couples (α_1, α_2) for which the denominator and numerator of $F_M^{\alpha_1,\alpha_2}(t)$ are null simultaneously for $t < T$ and $t > T$.

The singularity observed in Figs. 31 is due to the non-differentiability of both voltage and intensity functions at point T.

The value of $(\alpha_1 = 0.171972381, \alpha_2 = 0.054935584)$ belongs to the triangle T_3 of Fig. 15, whose extremities are 2nd memristor, memristor, and memcapacitor. In this experiment, onion has property related to these basic electric devices.

As a counter-example of our method for choosing the best possible memfractance, Fig. 32 displays, the memfractance for a non-optimal couple $(\alpha_1, \alpha_2) = (1.82, 1.6)$ which presents two singularities.

The comparison of average experimental data of cyclic voltammetry performed over -1 V to 1 V, Stem-to-cap electrode placement, and closed approxmating formula is displayed in Fig. 33, showing a very good agreement between both curves.

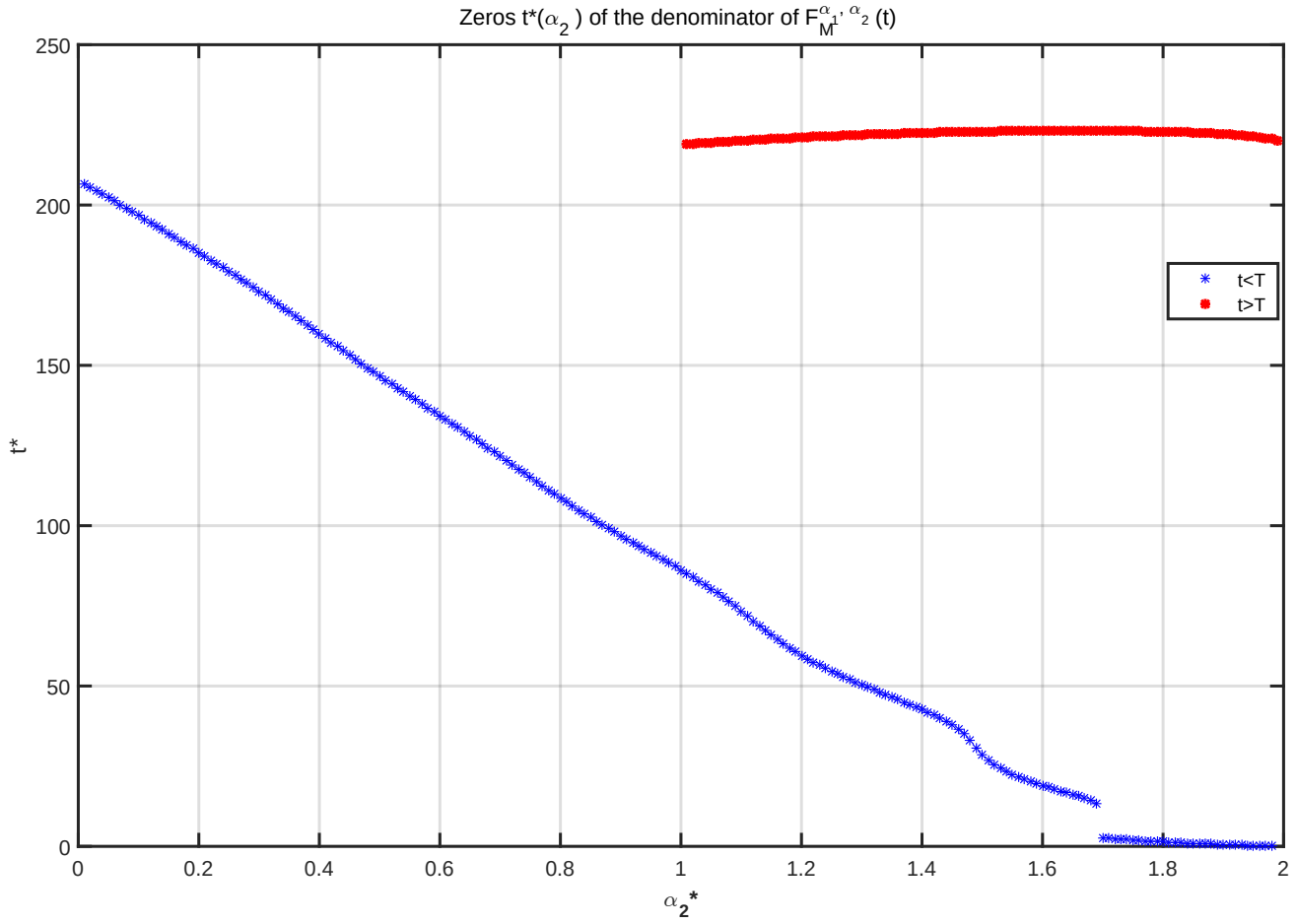

Figure 28: The zeros $t^*(\alpha_2)$, of the denominator of $F_M^{\alpha_1,\alpha_2}(t)$, as function of α_2.

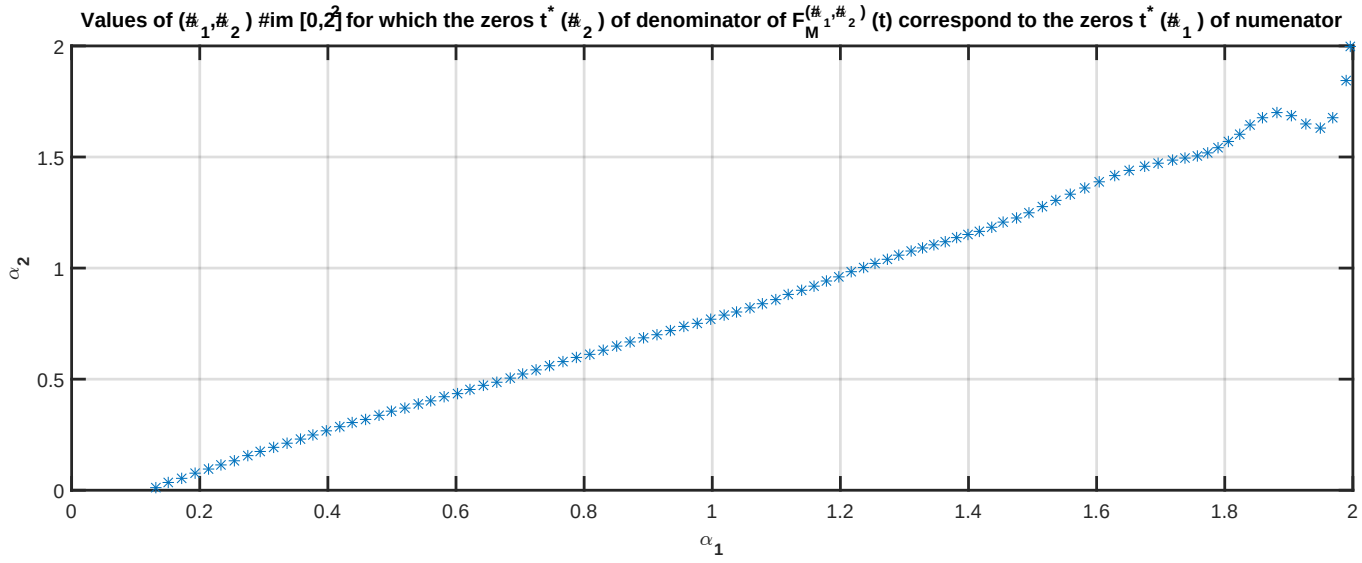

Figure 29: Couples (α_1, α_2) for which the denominator and numerator of $F_M^{\alpha_1,\alpha_2}(t)$ are null simultaneously.

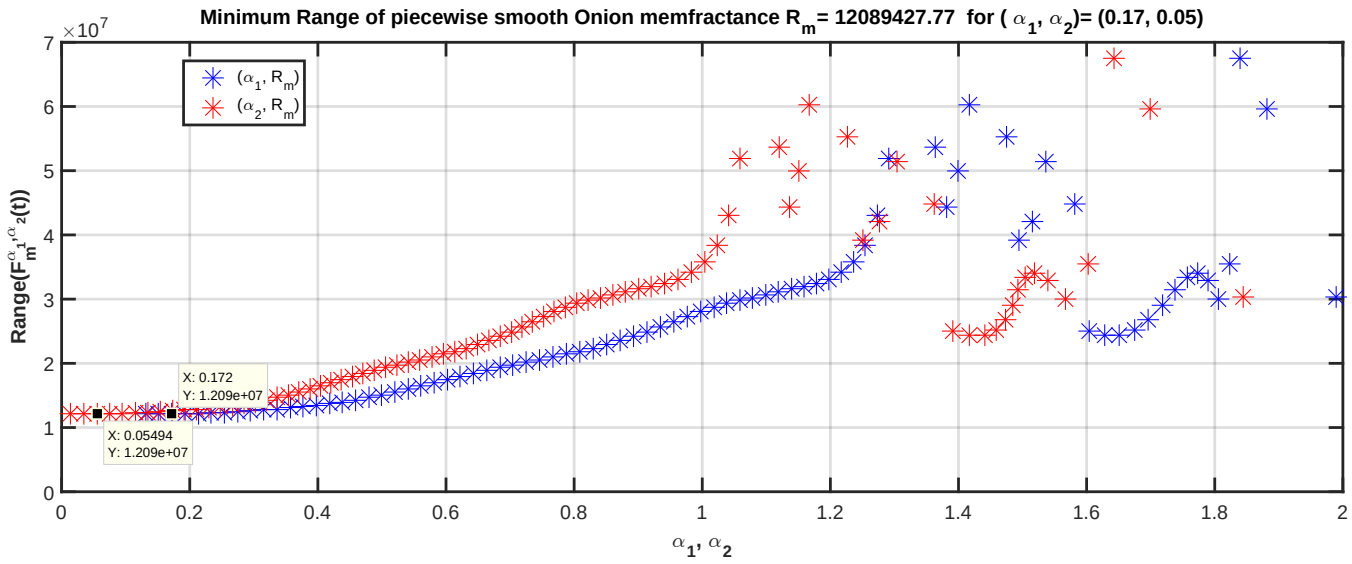

Figure 30: Values of range $(F_M^{\alpha_1,\alpha_2}(t))$ for $(\alpha_1, \alpha_2) \in [0,2]^2$.

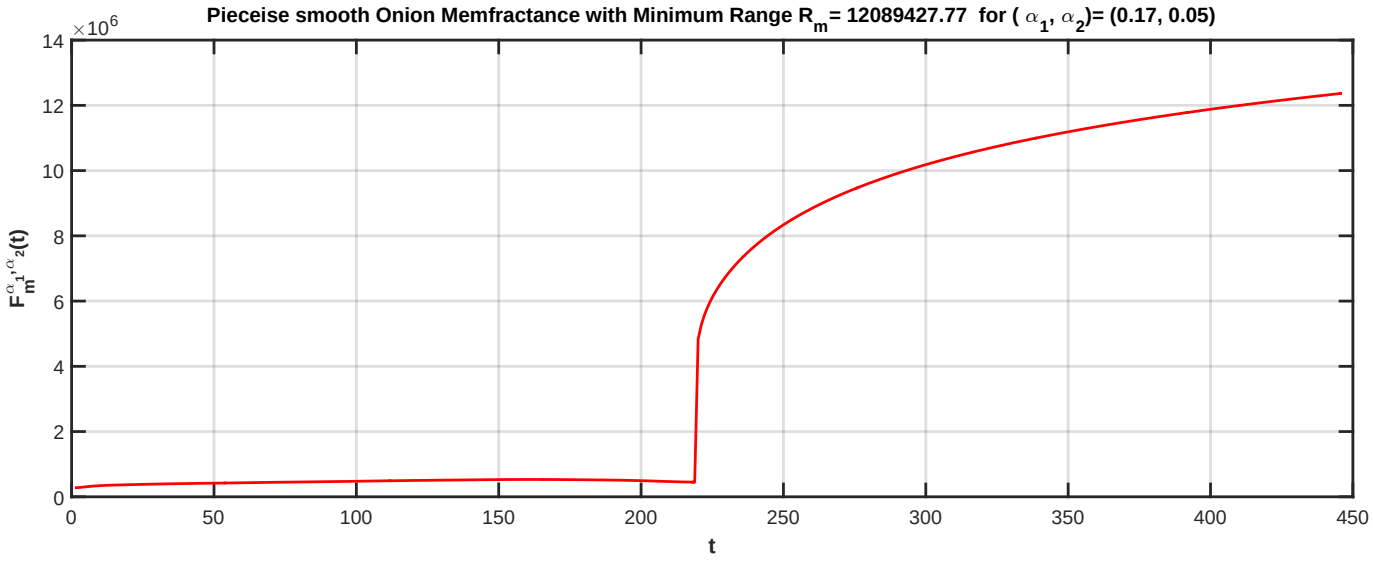

Figure 31: Memfractance for $(\alpha_1 = 0.171972381, \alpha_2 = 0.054935584)$ given in Tab. 15.

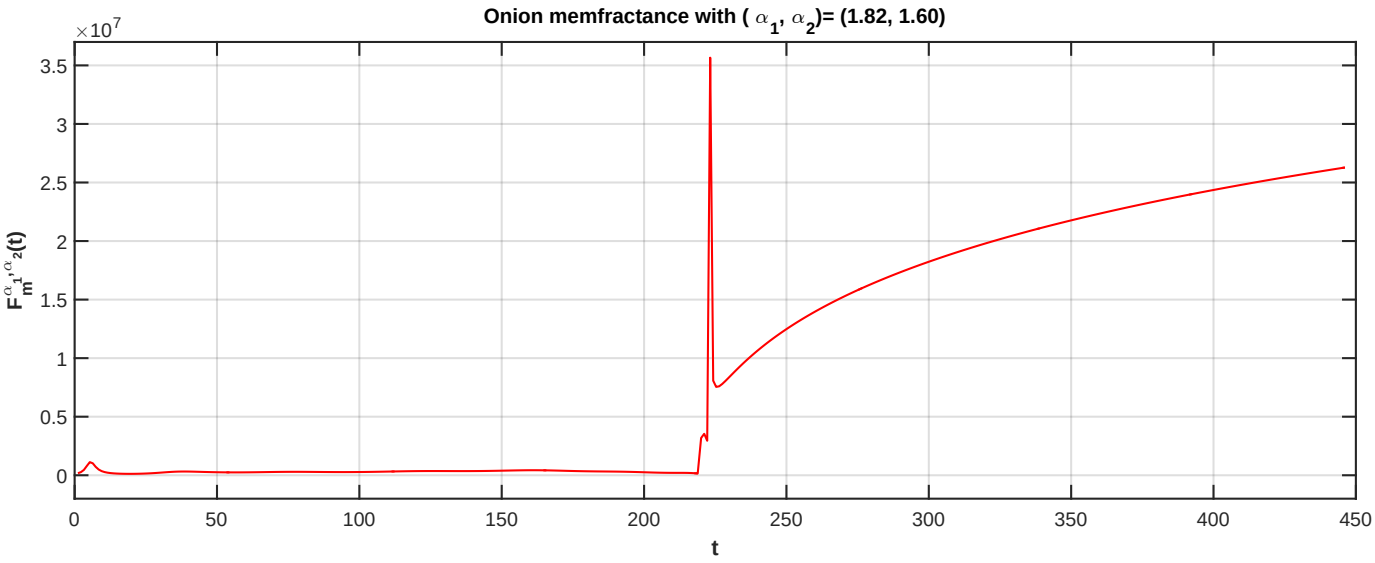

Figure 32: Memfractance with singularity for $(\alpha_1, \alpha_2) = (1.82, 1.6)$.

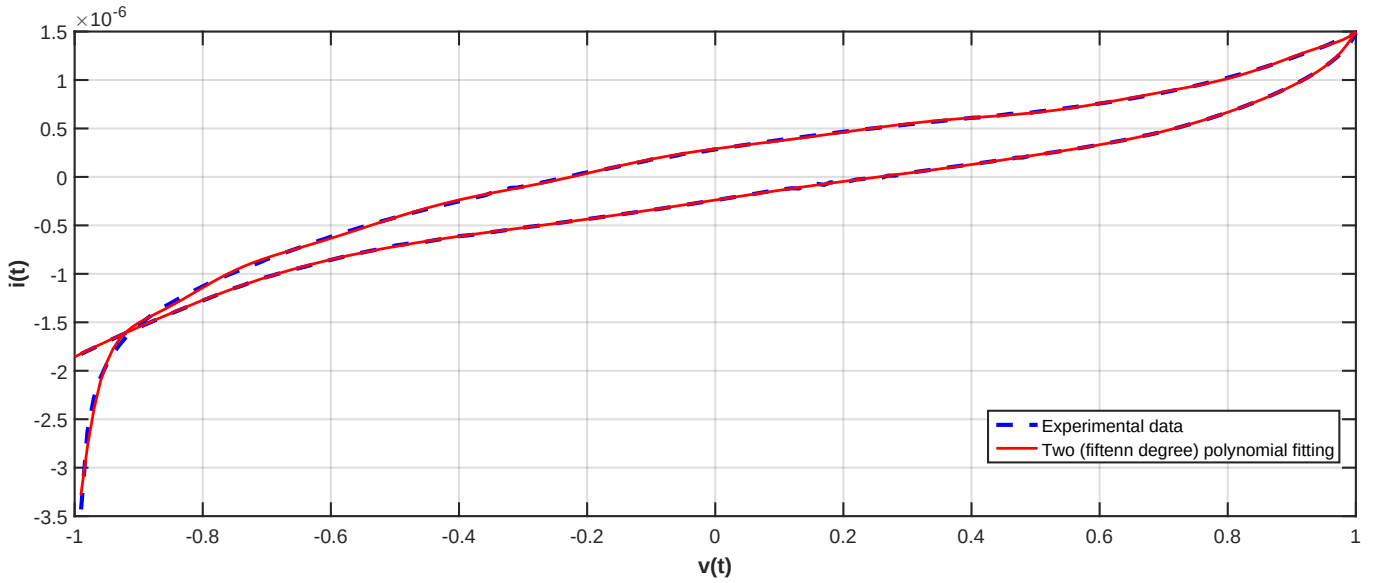

Figure 33: Comparison between average experimental data of cyclic voltammetry performed over -1 V to 1 V and closed approximative formula.

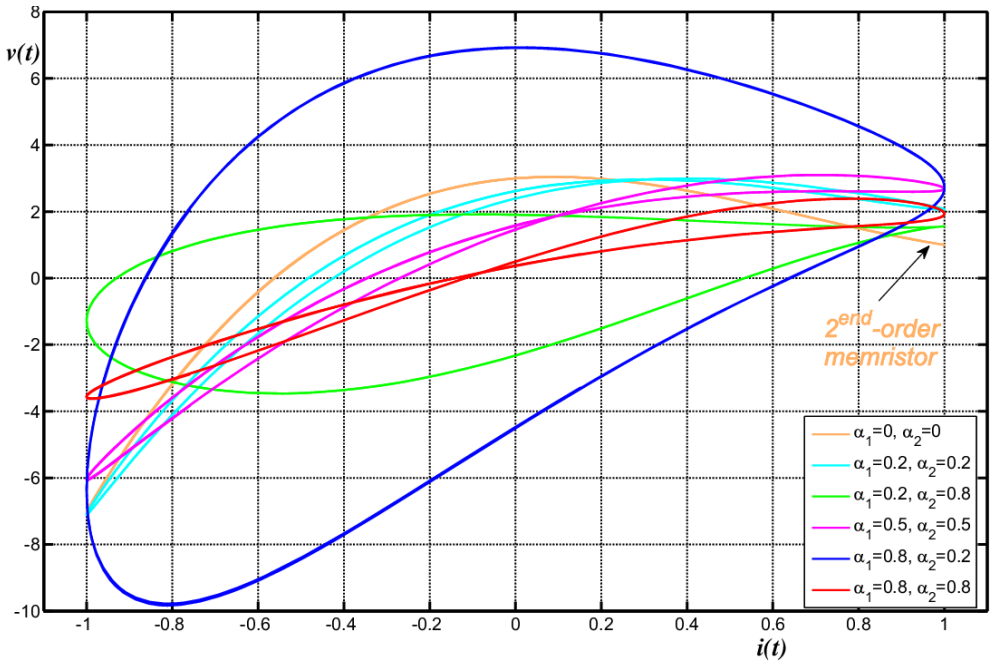

Figure 34: Ideal plots of mem-fractance

5 Discussions

It has been shown in this paper that items taken from nature all exhibit memristive properties wherein the conducted current from the positive half of a cyclic voltammetry sweep does not match the conducted current from the negative cycle. This is in line with previously published results on I-V characterisation of organic and biological substrates, which indicate memristive properties of organic polymers [9], skin [23], blood [18], slime mould *Physarum polycephalum* [11], plants [30], fruits [29], and tubulin microtubules [8, 5].

In addition, the level as to the divergence between the positive and negative cycles is also demonstrated to be a function of the sweep frequency (time). These memristive properties have also been observed in medium such as damp wood shavings and water. It is therefore proposed that any living system, a large proportion of which is water acting as a charge carrier, is able to exhibit memristive properties, the degree of which can be expressed on a continuous scale.

It is also observed that the crossing behaviour expected from an ideal, passive, memristor is not often seen from the naturally occurring specimens. A naturally occurring specimen is capable of generating its own potential, which has an associated conducted current, both of which have been measured as part of the cyclic voltammetry. Increasing the delay time between consecutive readings, will produce an I-V characteristic where the negative and positive phases 'pinch' closer together.

In all instances, the fingerprints of memristive devices are observed in specimens taken from nature. It can be expressed that memristance is indeed not a binary feature, however it exists more of a continuum [0,1] - 0 representing pure resistance, 1 representing the ideal memristor — each device can then be assigned a number on the scale [0,1] to characterise its 'degree of memristance'.

More generally mem-fractance which is a general paradigm linking memristive, mem-capacitive and mem-inductive property of electric elements, should be the adequate frame for the mathematical modelling all plants and fungi. The use of fractional derivatives to analyse the mem-fractance, is obvious if one considers that fractional derivatives have memory, which allow a perfect modelling of memristive elements. Their handling is however delicate if one wants to avoid any flaw. In Section 4, the case of onion is analysed. Increasing the frequency of sampling of the current intensity and changing the range of voltage leads to slightly different mem-fractance. With low frequency and higher voltage, the onion has properties which is a combination of memristor, mem-capacitor and second order memristor. In the case of high frequency, and low voltage, the onion is merely more a mix of resistor, capacitor and memristor, showing less memory effect!

Additionally, current oscillations during the cyclic voltammetry are produced by all sample specimens. Typically, the oscillatory effect can be observed only on one phase of the voltammetry for a given voltage range which is, again, a behaviour that can be associated to a device whose resistance is a function of its previous resistance. Although, it is worth stating that some samples do produce overlapping oscillatory effects (both phases of voltammetry) for certain conditions — however this can be controlled through careful selection of voltammetry conditions. This spiking activity is typical of a device that exhibits memristive behaviours as having been previously observed in experiments with the electrochemical devices with a graphite reference electrodes [10], in experiments with electrode metal on solution-processed

flexible titanium dioxide memristors [13], see also analysis in [12]. The spiking properties of the meristive devices can be utilized in the field of neurmorphic systems [27, 16, 26, 24, 21, 17].

Acknowledgement

This project has received funding from the European Union's Horizon 2020 research and innovation programme FET OPEN "Challenging current thinking" under grant agreement No 858132.

With special thanks to Neil Phillips and Andrew Geary (UWE, Bristol, UK) for providing the data on tap water.

References

[1] M.-S. Abdelouahab, R. Lozi, and L. Chua. Memfractance: a mathematical paradigm for circuit elements with memory. *International Journal of Bifurcation and Chaos*, 24(9):1430023, 2014.

[2] Nariman A.Khalil, Lobna A.Said, Ahmed G.Radwan, and Ahmed M.Solimane. General fractional order mem-elements mutators. *International Journal of Bifurcation and Chaos*, 90:211–221, 2019.

[3] Julien Borghetti, Zhiyong Li, Joseph Straznicky, Xuema Li, Douglas AA Ohlberg, Wei Wu, Duncan R Stewart, and R Stanley Williams. A hybrid nanomemristor/transistor logic circuit capable of self-programming. *Proceedings of the National Academy of Sciences*, 106(6):1699–1703, 2009.

[4] Julien Borghetti, Gregory S Snider, Philip J Kuekes, J Joshua Yang, Duncan R Stewart, and R Stanley Williams. 'memristive'switches enable 'stateful' logic operations via material implication. *Nature*, 464(7290):873–876, 2010.

[5] Alessandro Chiolerio, Thomas C Draper, Richard Mayne, and Andrew Adamatzky. On resistance switching and oscillations in tubulin microtubule droplets. *Journal of colloid and interface science*, 560:589–595, 2020.

[6] L. Chua. Memristor-the missing circuit element. *IEEE Transactions on Circuit Theory*, 18(5):507–519, Sep. 1971.

[7] Leon Chua. If it's pinched it's a memristor. *Semiconductor Science and Technology*, 29(10):104001, 2014.

[8] María del Rocío Cantero, Paula L Perez, Noelia Scarinci, and Horacio F Cantiello. Two-dimensional brain microtubule structures behave as memristive devices. *Scientific reports*, 9(1):1–10, 2019.

[9] Victor Erokhin, Tatiana Berzina, and Marco P Fontana. Hybrid electronic device based on polyaniline-polyethyleneoxide junction. *Journal of applied physics*, 97(6):064501, 2005.

[10] Victor Erokhin and Marco P Fontana. Electrochemically controlled polymeric device: a memristor (and more) found two years ago. *arXiv preprint arXiv:0807.0333*, 2008.

[11] Ella Gale, Andrew Adamatzky, and Ben de Lacy Costello. Slime mould memristors. *BioNanoScience*, 5(1):1–8, 2015.

[12] Ella Gale, Ben de Lacy Costello, and Andrew Adamatzky. Emergent spiking in non-ideal memristor networks. *Microelectronics Journal*, 45(11):1401–1415, 2014.

[13] Ella Gale, David Pearson, Steve Kitson, Andrew Adamatzky, and Ben de Lacy Costello. The effect of changing electrode metal on solution-processed flexible titanium dioxide memristors. *Materials Chemistry and Physics*, 162:20–30, 2015.

[14] Yenpo Ho, Garng M Huang, and Peng Li. Nonvolatile memristor memory: device characteristics and design implications. In *Proceedings of the 2009 International Conference on Computer-Aided Design*, pages 485–490, 2009.

[15] Thang Hoang. Memristor model. `https://www.mathworks.com/matlabcentral/fileexchange/25082-memristor-model`, 2020. MATLAB Central File Exchange. Retrieved January 13, 2020.

[16] Giacomo Indiveri, Bernabé Linares-Barranco, Robert Legenstein, George Deligeorgis, and Themistoklis Prodromakis. Integration of nanoscale memristor synapses in neuromorphic computing architectures. *Nanotechnology*, 24(38):384010, 2013.

[17] Giacomo Indiveri and Shih-Chii Liu. Memory and information processing in neuromorphic systems. *Proceedings of the IEEE*, 103(8):1379–1397, 2015.

[18] Shiv Prasad Kosta, Yogesh P Kosta, Mukta Bhatele, YM Dubey, Avinash Gaur, Shakti Kosta, Jyoti Gupta, Amit Patel, and Bhavin Patel. Human blood liquid memristor. *International Journal of Medical Engineering and Informatics*, 3(1):16–29, 2011.

[19] Shahar Kvatinsky, Dmitry Belousov, Slavik Liman, Guy Satat, Nimrod Wald, Eby G Friedman, Avinoam Kolodny, and Uri C Weiser. Magic—memristor-aided logic. *IEEE Transactions on Circuits and Systems II: Express Briefs*, 61(11):895–899, 2014.

[20] Shahar Kvatinsky, Guy Satat, Nimrod Wald, Eby G Friedman, Avinoam Kolodny, and Uri C Weiser. Memristor-based material implication (imply) logic: Design principles and methodologies. *IEEE Transactions on Very Large Scale Integration (VLSI) Systems*, 22(10):2054–2066, 2013.

[21] Bernabe Linares-Barranco, Teresa Serrano-Gotarredona, Luis A Camuñas-Mesa, Jose A Perez-Carrasco, Carlos Zamarreño-Ramos, and Timothee Masquelier. On spike-timing-dependent-plasticity, memristive devices, and building a self-learning visual cortex. *Frontiers in neuroscience*, 5:26, 2011.

[22] Eike Linn, R Rosezin, Stefan Tappertzhofen, U Böttger, and Rainer Waser. Beyond von neumann—logic operations in passive crossbar arrays alongside memory operations. *Nanotechnology*, 23(30):305205, 2012.

[23] Ø G Martinsen, S Grimnes, CA Lütken, and GK Johnsen. Memristance in human skin. *Journal of Physics: Conference Series*, 224(1):012071, 2010.

[24] Matthew D Pickett, Gilberto Medeiros-Ribeiro, and R Stanley Williams. A scalable neuristor built with mott memristors. *Nature materials*, 12(2):114–117, 2013.

[25] I. Podlubny. *Fractional Differential Equations*. Academic Press, San Diego, 1999.

[26] Mirko Prezioso, Y Zhong, D Gavrilov, Farnood Merrikh-Bayat, Brian Hoskins, G Adam, K Likharev, and D Strukov. Spiking neuromorphic networks with metal-oxide memristors. In *2016 IEEE International Symposium on Circuits and Systems (ISCAS)*, pages 177–180. IEEE, 2016.

[27] Teresa Serrano-Gotarredona, Themistoklis Prodromakis, and Bernabe Linares-Barranco. A proposal for hybrid memristor-CMOS spiking neuromorphic learning systems. *IEEE cIrcuIts and systEms magazInE*, 13(2):74–88, 2013.

[28] Dmitri B. Strukov, Gregory S. Snider, Duncan R. Stewart, and R. Stanley Williams. The missing memristor found. *Nature*, 453(7191):80–83, May 2008.

[29] A G. Volkov and V S. Markin. Electrochemistry of gala apples: Memristors in vivo. *Russian Journal of Electrochemistry*, 53(9):1011–1018, Sept. 2017.

[30] Alexander G Volkov, Clayton Tucket, Jada Reedus, Maya I Volkova, Vladislav S Markin, and Leon Chua. Memristors in plants. *Plant signaling & behavior*, 9(3):e28152, 2014.

6 Appendix

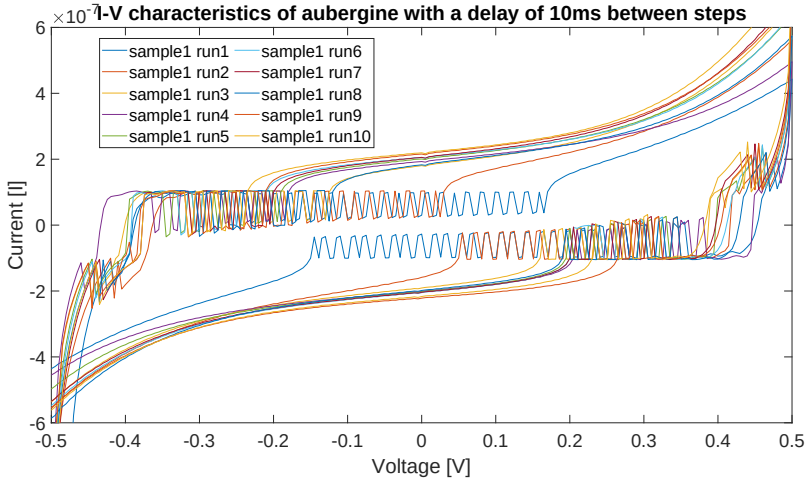

(a)

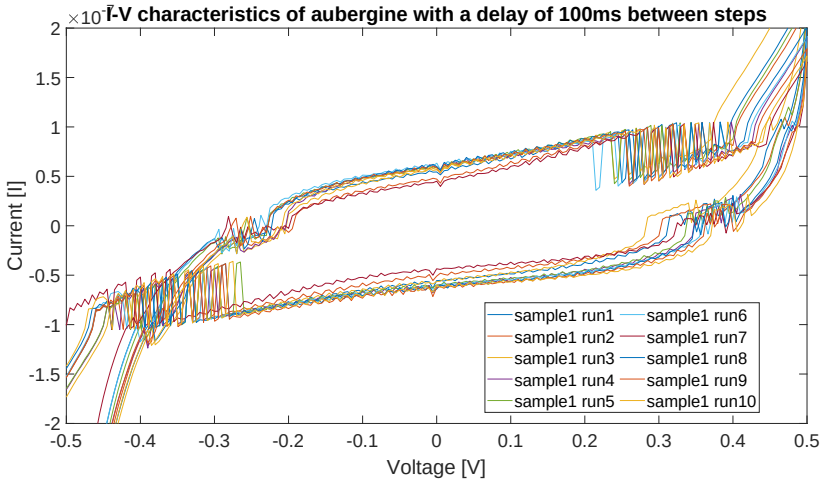

(b)

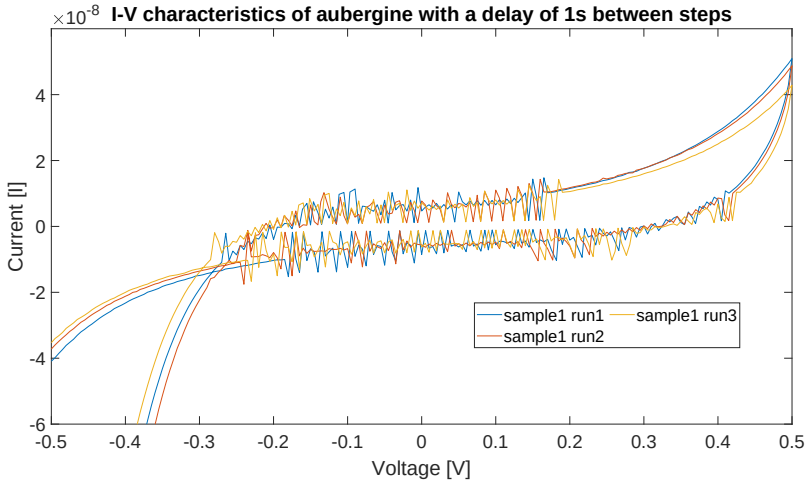

(c)

Figure 35: Cyclic voltammetry (-0V5 to 0V5) of aubergine. (a) delay time between settings is 10ms, (b) delay time between settings is 100ms, (c) delay time between settings is 1000ms

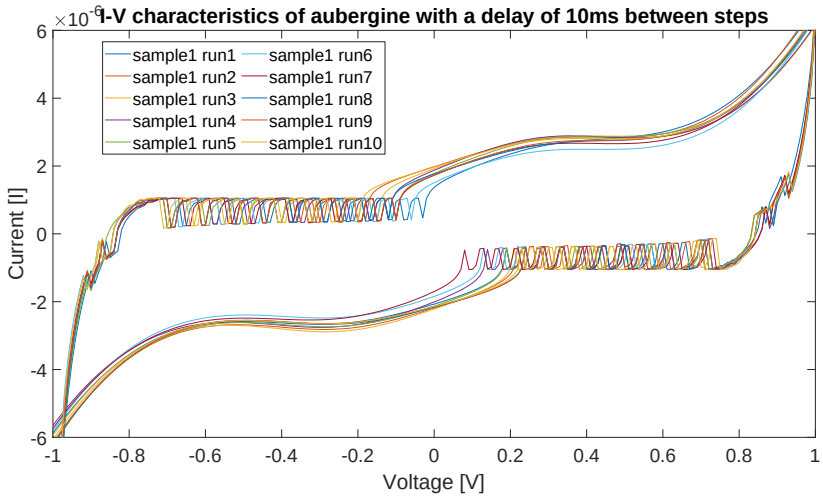

(a)

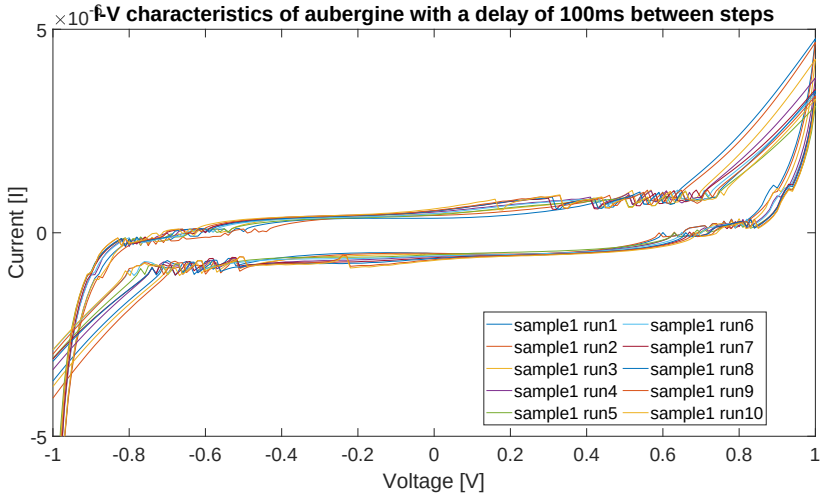

(b)

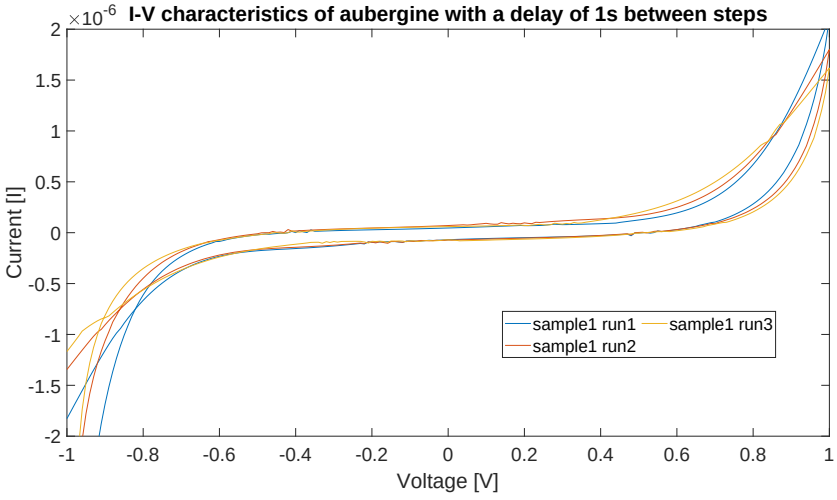

(c)

Figure 36: Cyclic voltammetry (-1V to 1V) of aubergine. (a) delay time between settings is 10ms, (b) delay time between settings is 100ms, (c) delay time between settings is 1000ms

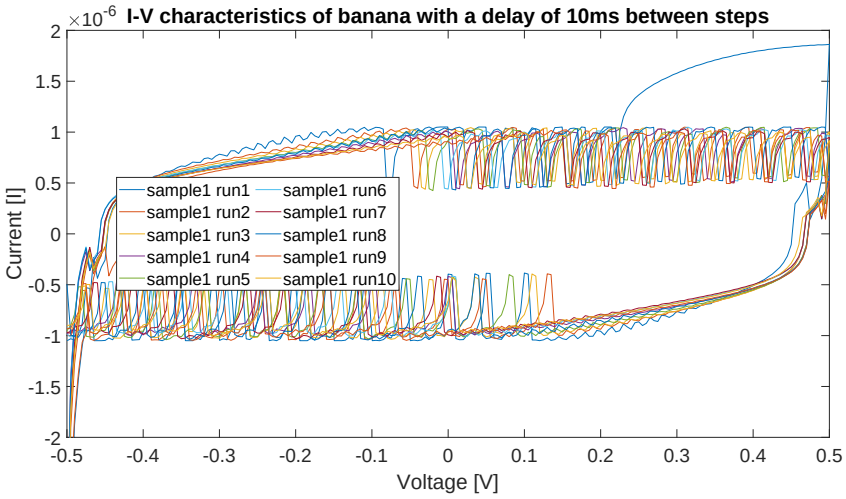

(a)

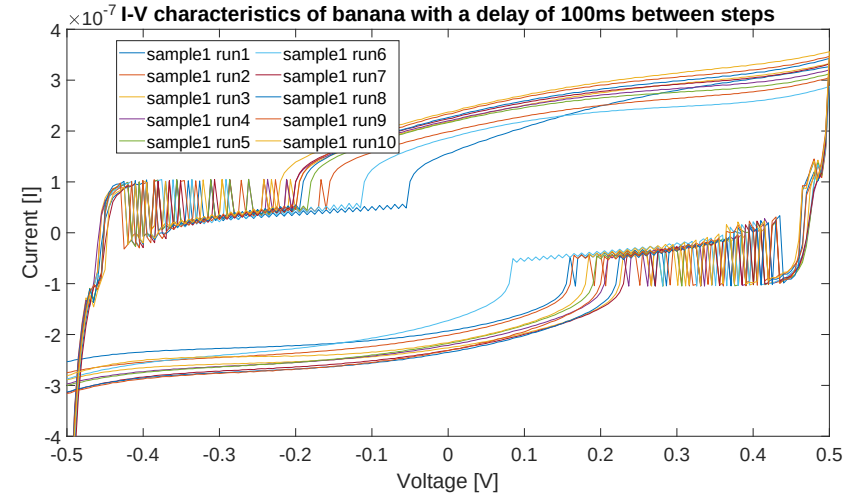

(b)

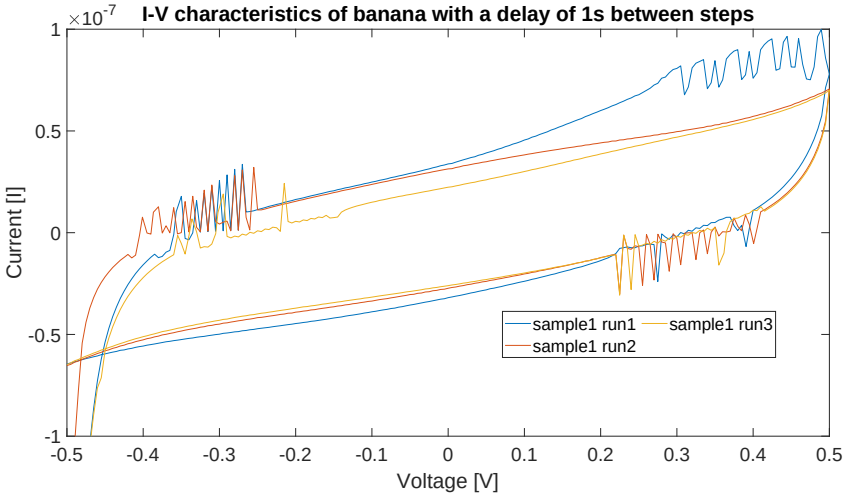

(c)

Figure 37: Cyclic voltammetry (-0V5 to 0V5) of banana. (a) delay time between settings is 10ms, (b) delay time between settings is 100ms, (c) delay time between settings is 1000ms

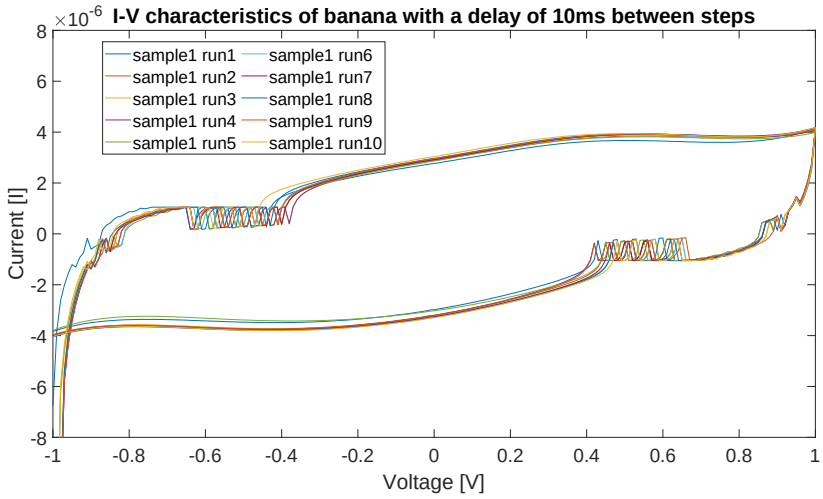

(a)

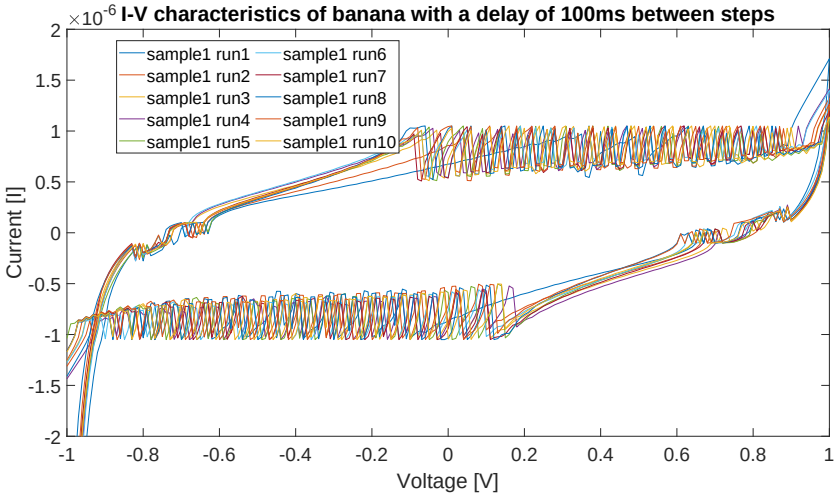

(b)

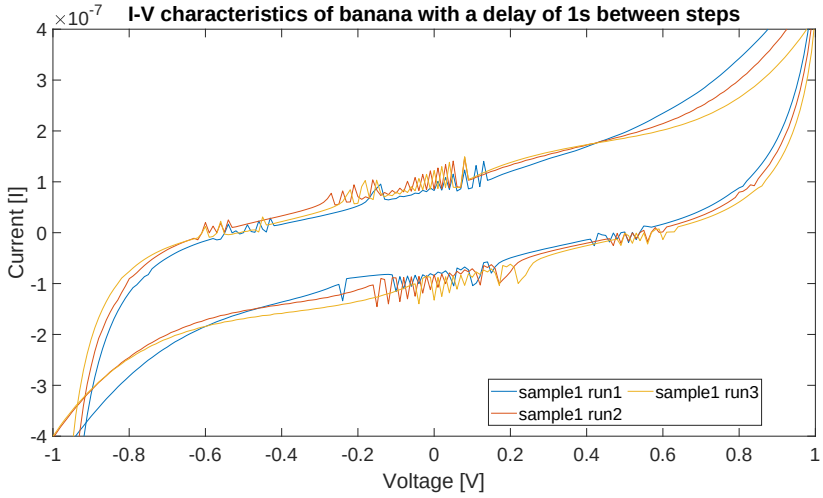

(c)

Figure 38: Cyclic voltammetry (-1V to 1V) of banana. (a) delay time between settings is 10ms, (b) delay time between settings is 100ms, (c) delay time between settings is 1000ms

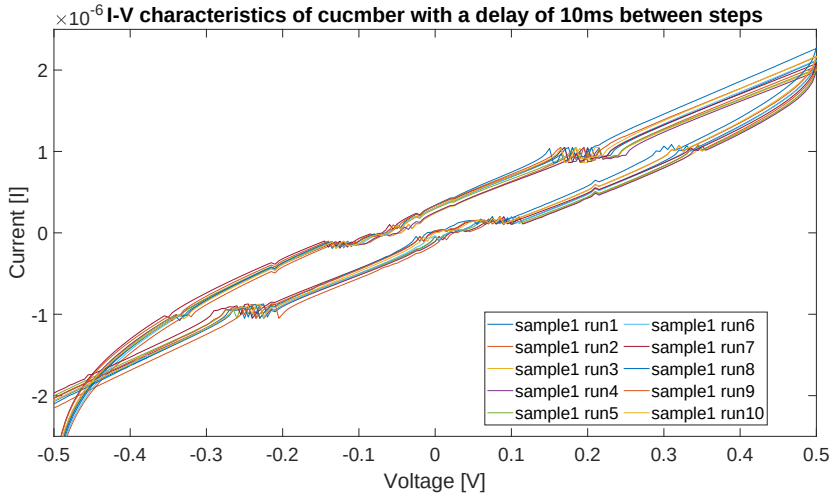

(a)

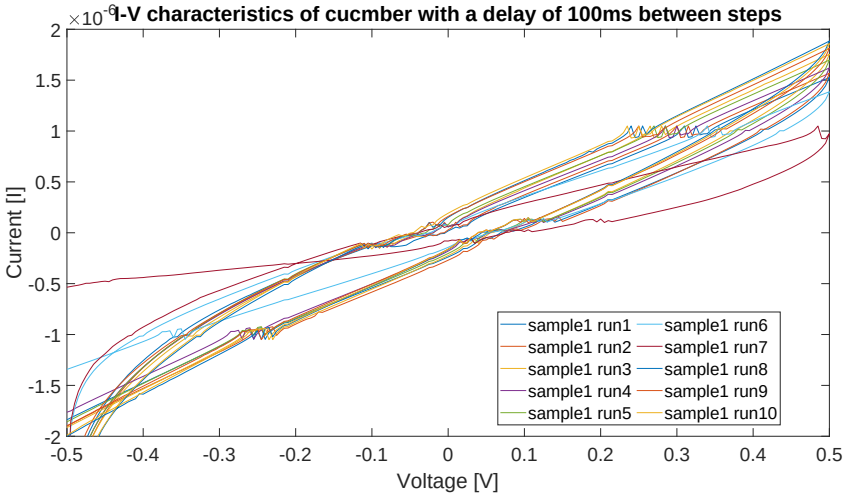

(b)

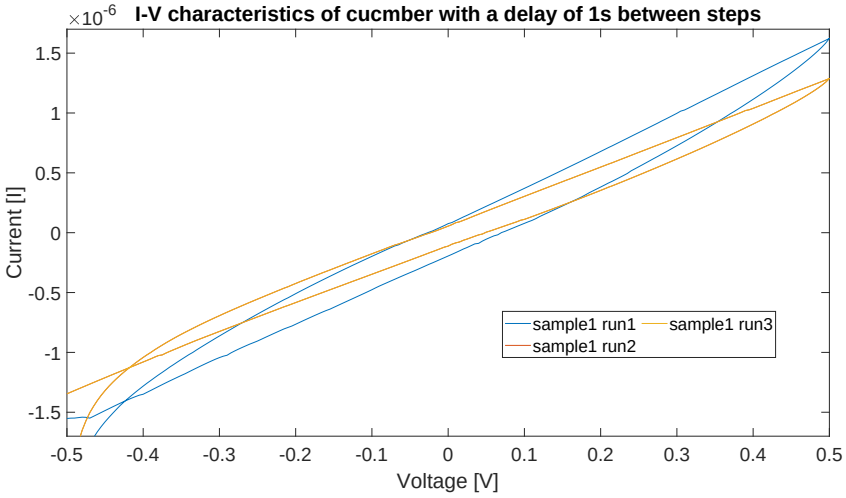

(c)

Figure 39: Cyclic voltammetry (-0V5 to 0V5) of cucumber. (a) delay time between settings is 10ms, (b) delay time between settings is 100ms, (c) delay time between settings is 1000ms

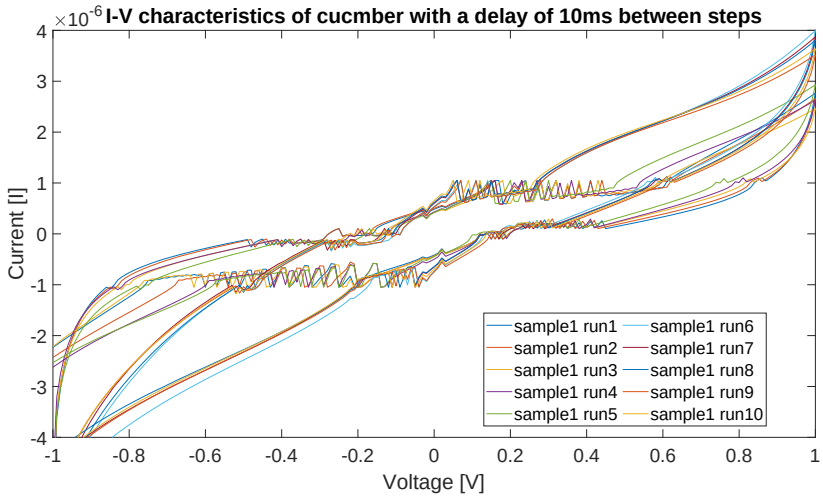

(a)

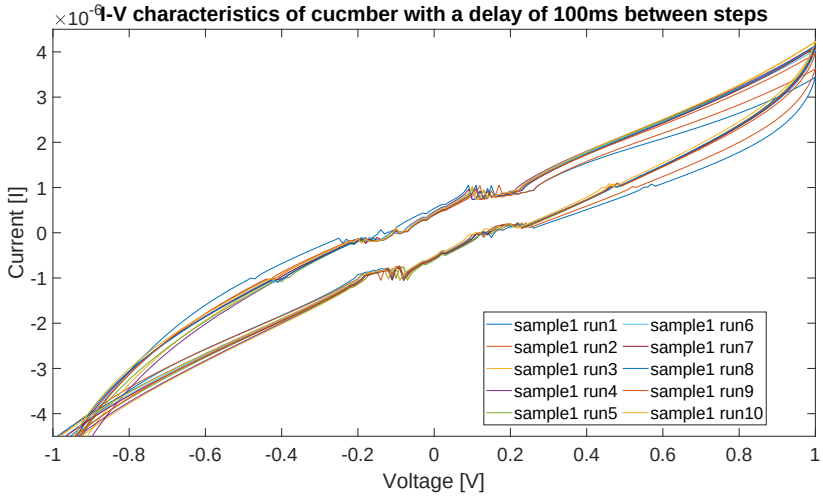

(b)

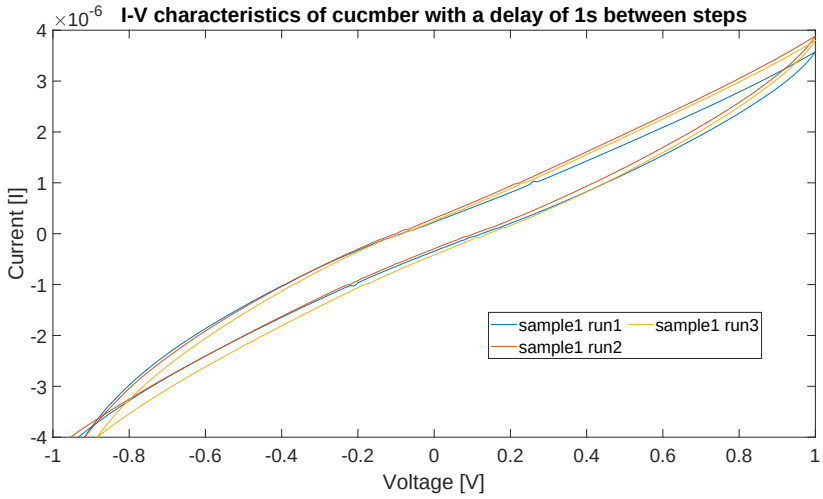

(c)

Figure 40: Cyclic voltammetry (-1V to 1V) of cucumber. (a) delay time between settings is 10ms, (b) delay time between settings is 100ms, (c) delay time between settings is 1000ms

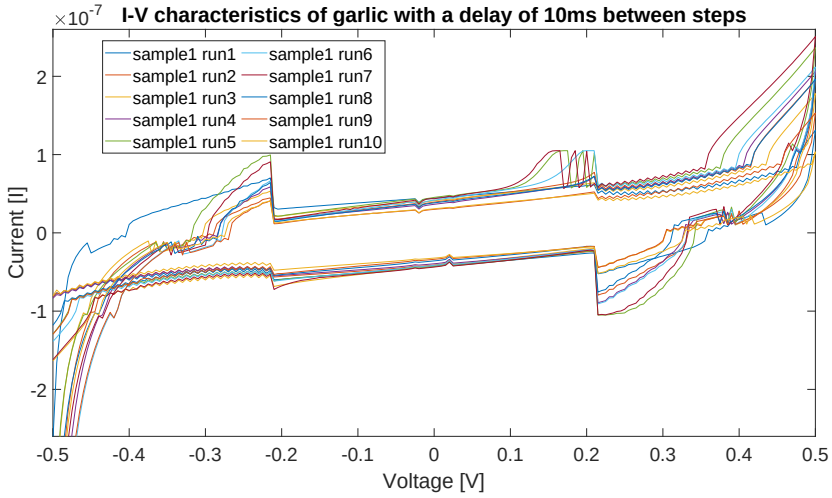

(a)

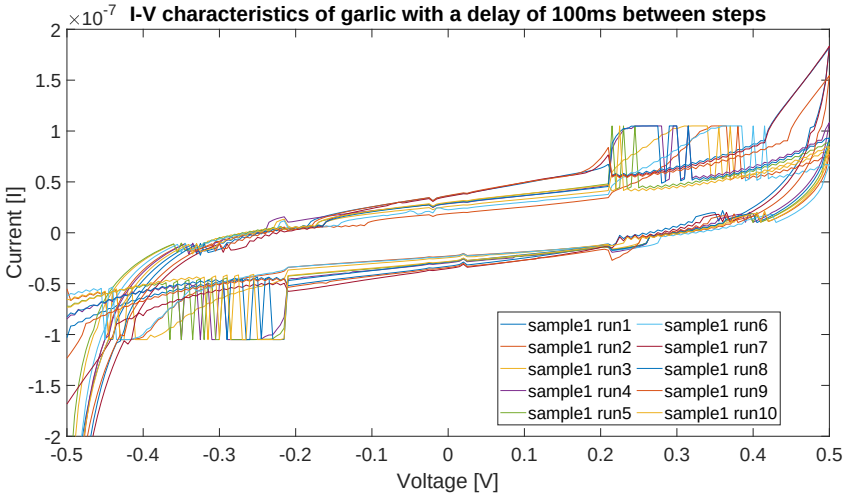

(b)

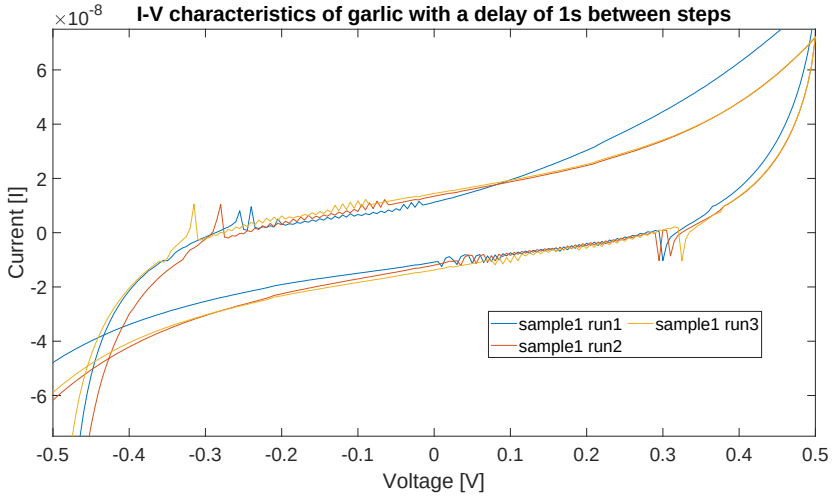

(c)

Figure 41: Cyclic voltammetry (-0V5 to 0V5) of garlic. (a) delay time between settings is 10ms, (b) delay time between settings is 100ms, (c) delay time between settings is 1000ms

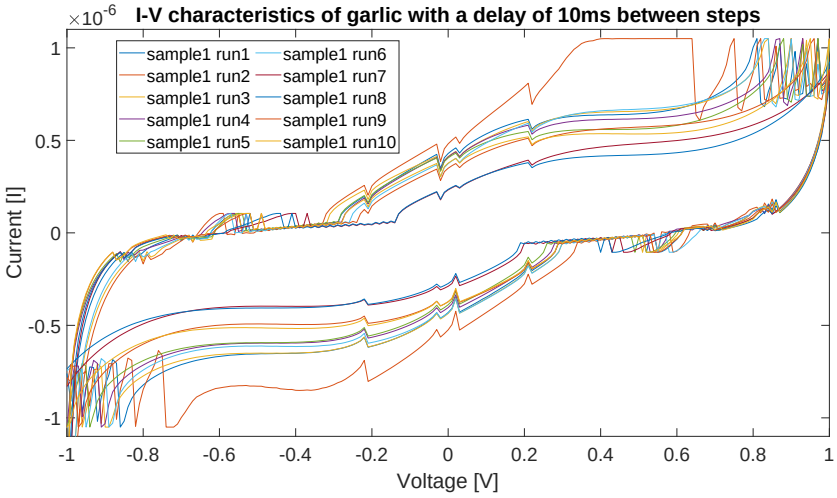

(a)

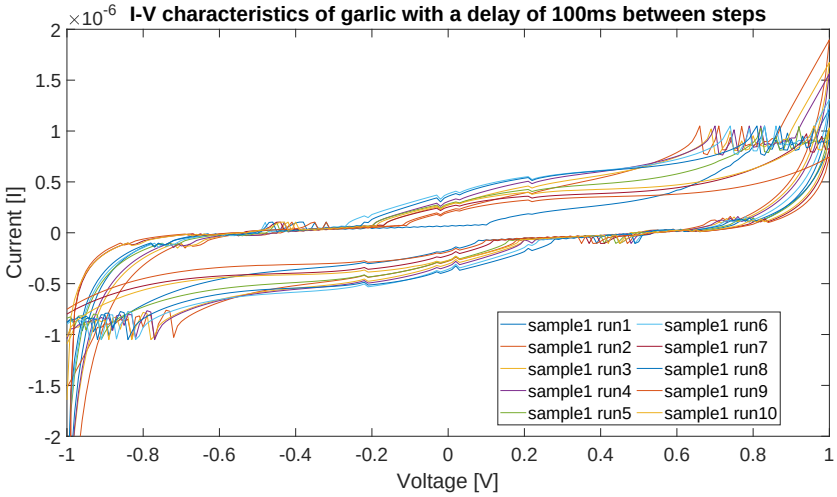

(b)

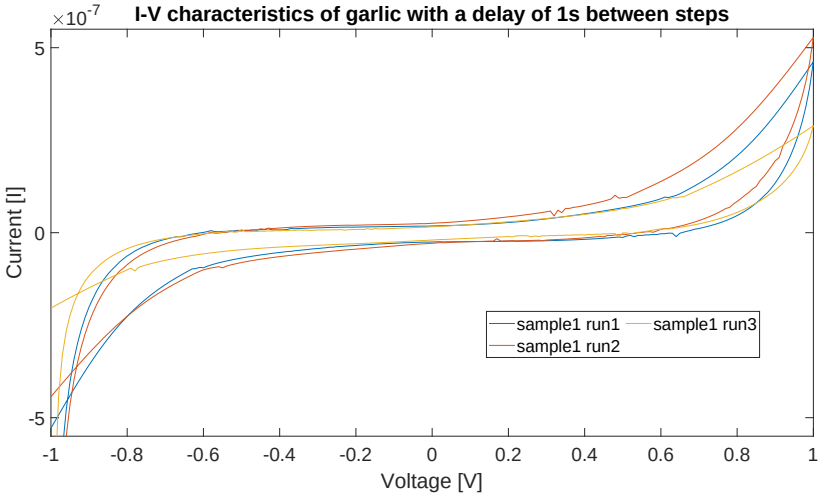

(c)

Figure 42: Cyclic voltammetry (-1V to 1V) of garlic. (a) delay time between settings is 10ms, (b) delay time between settings is 100ms, (c) delay time between settings is 1000ms

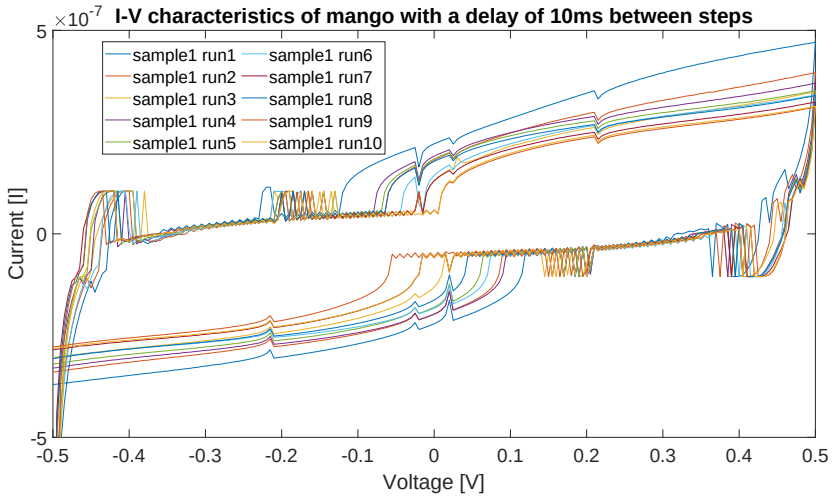

(a)

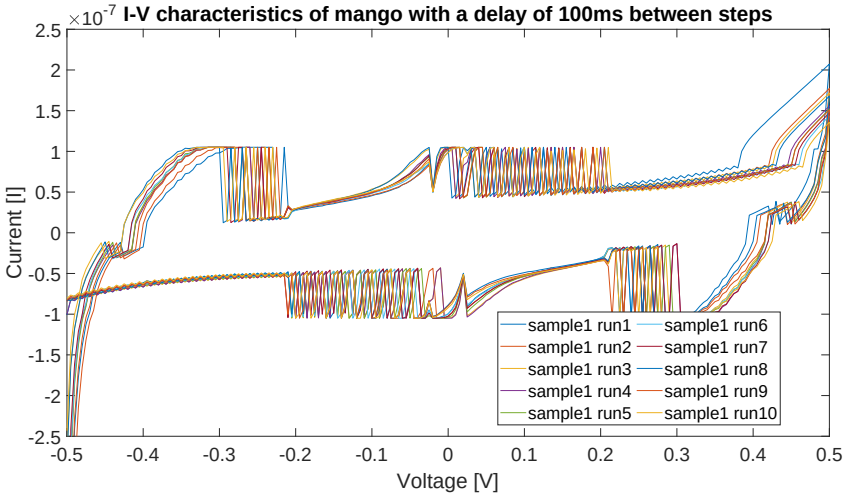

(b)

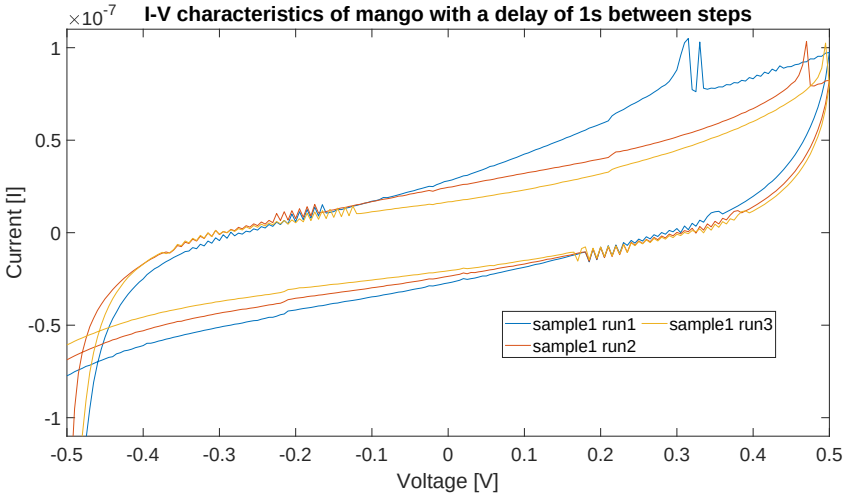

(c)

Figure 43: Cyclic voltammetry (-0V5 to 0V5) of mango. (a) delay time between settings is 10ms, (b) delay time between settings is 100ms, (c) delay time between settings is 1000ms

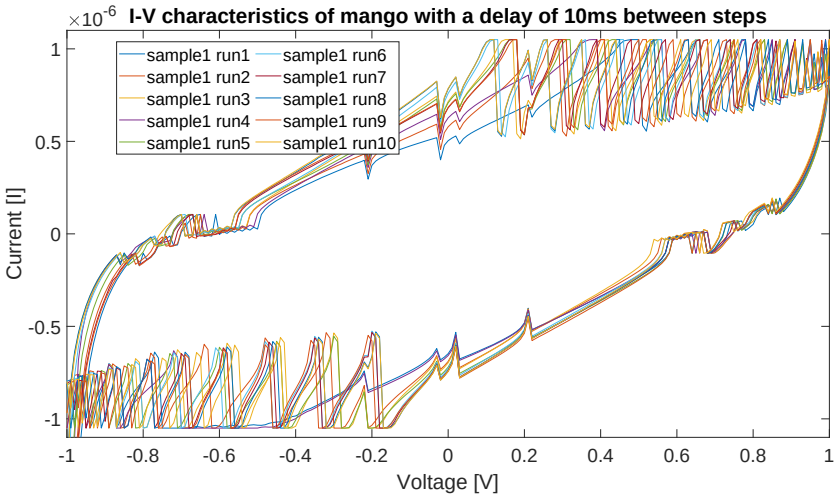

(a)

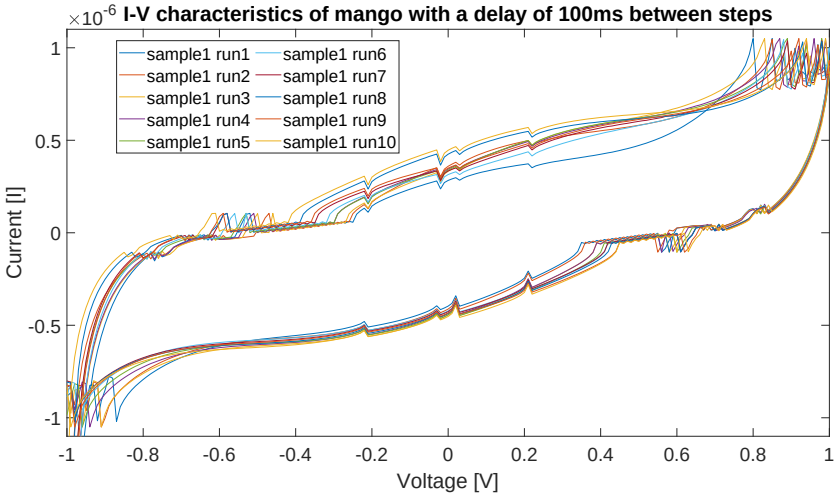

(b)

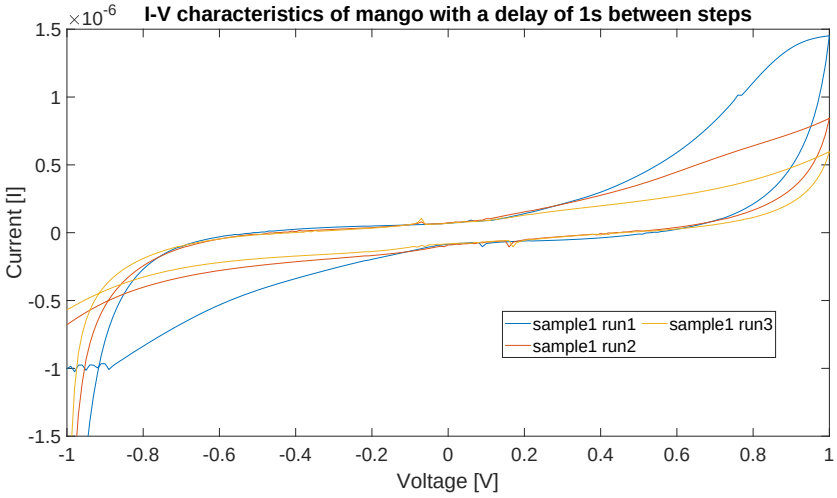

(c)

Figure 44: Cyclic voltammetry (-1V to 1V) of mango. (a) delay time between settings is 10ms, (b) delay time between settings is 100ms, (c) delay time between settings is 1000ms

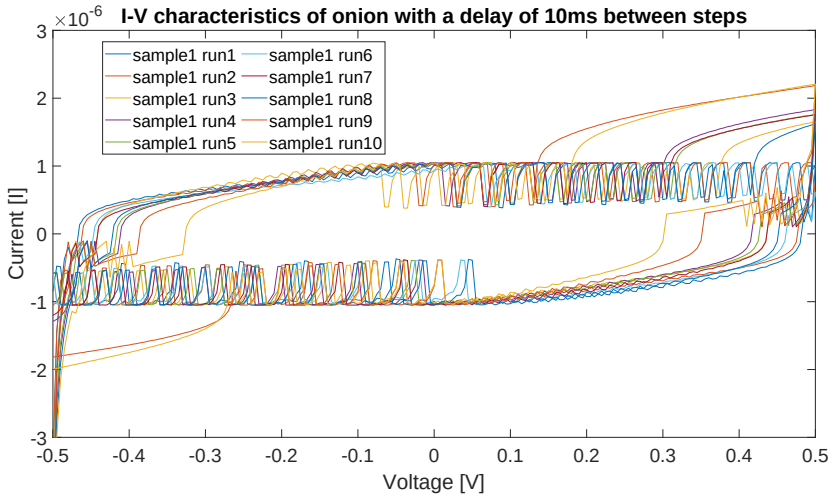

(a)

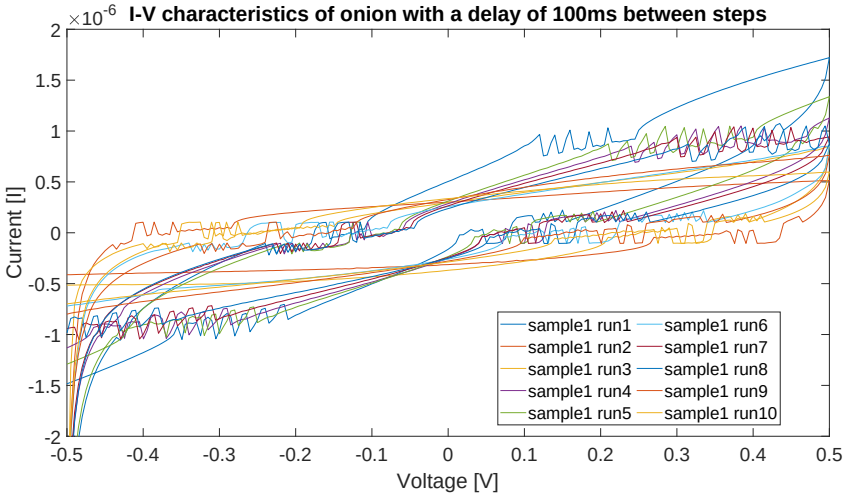

(b)

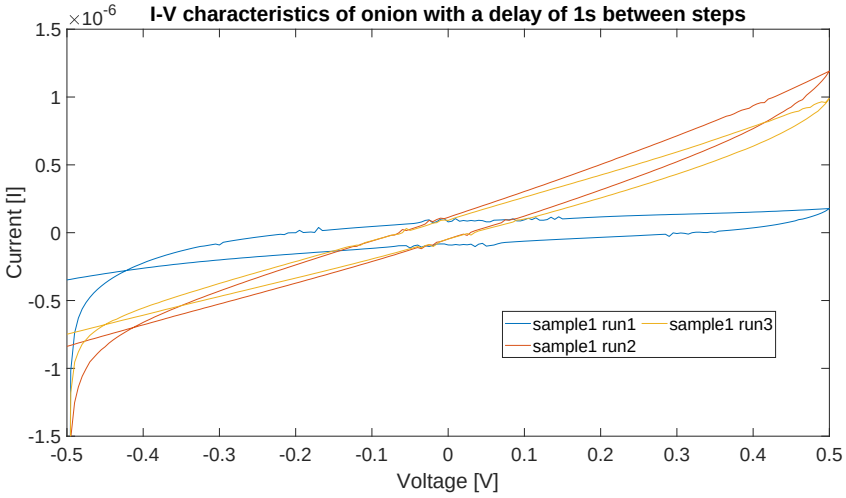

(c)

Figure 45: Cyclic voltammetry (-0V5 to 0V5) of onion. (a) delay time between settings is 10ms, (b) delay time between settings is 100ms, (c) delay time between settings is 1000ms

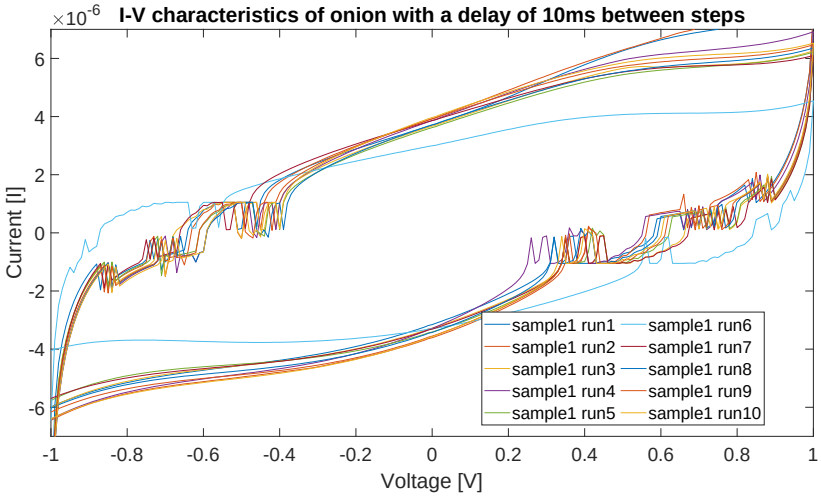

(a)

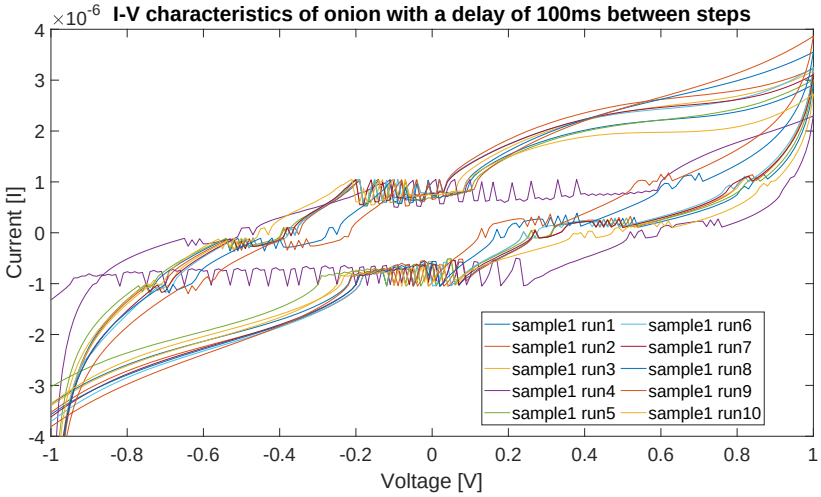

(b)

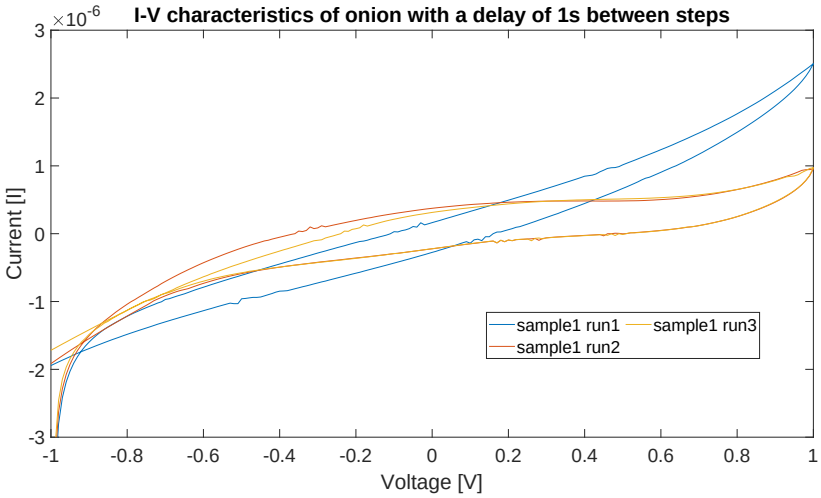

(c)

Figure 46: Cyclic voltammetry (-1V to 1V) of onion. (a) delay time between settings is 10ms, (b) delay time between settings is 100ms, (c) delay time between settings is 1000ms

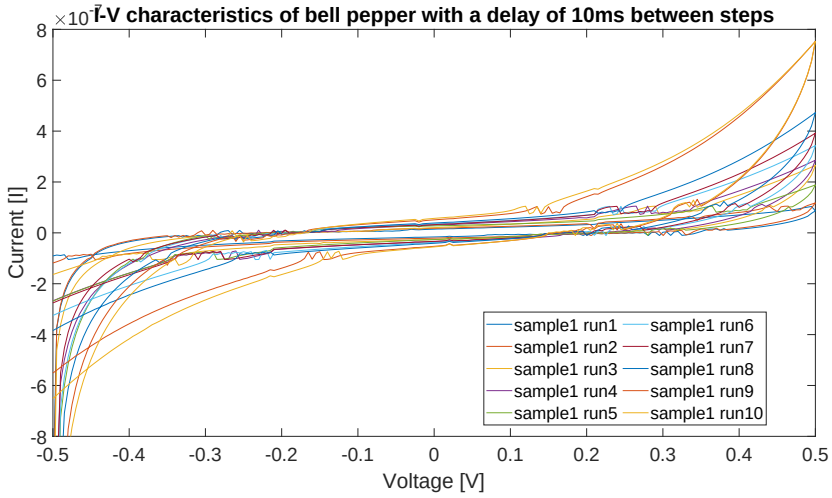

(a)

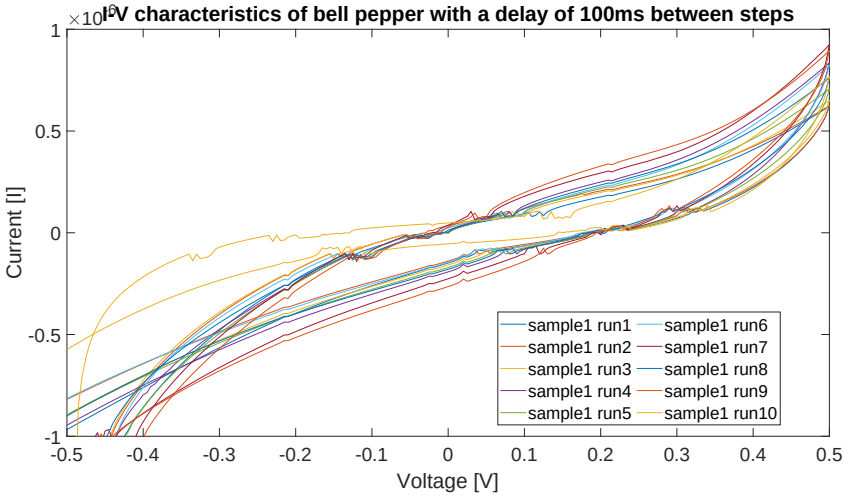

(b)

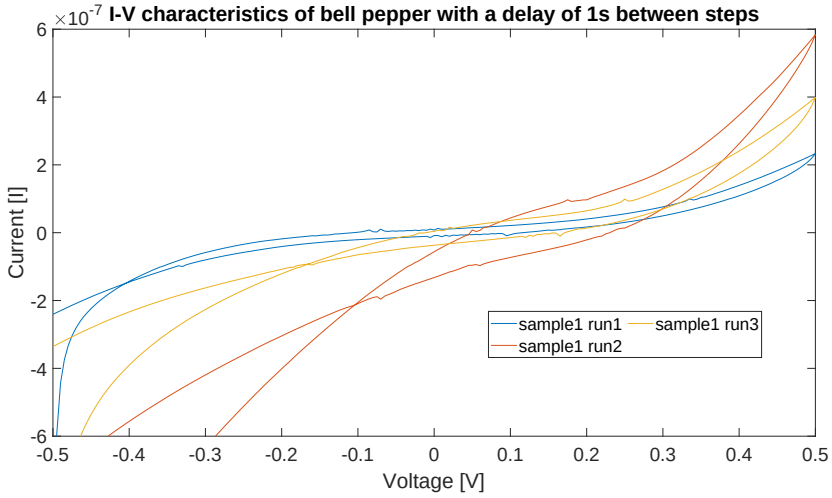

(c)

Figure 47: Cyclic voltammetry (-0V5 to 0V5) of pepper. (a) delay time between settings is 10ms, (b) delay time between settings is 100ms, (c) delay time between settings is 1000ms

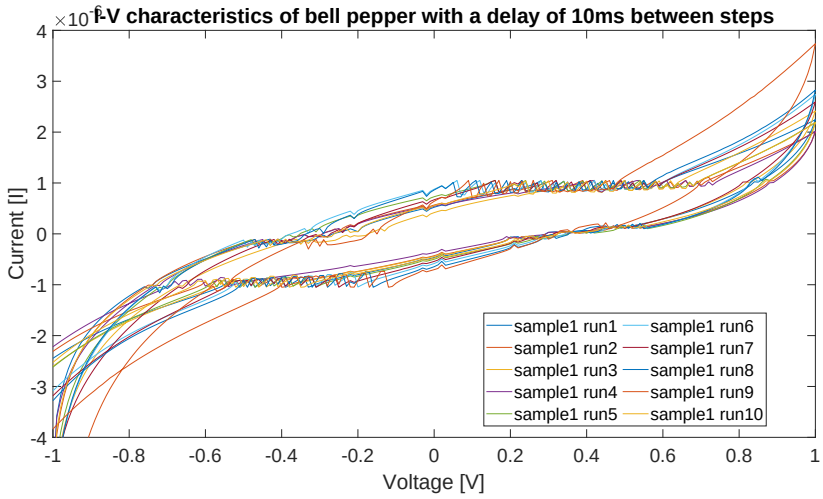

(a)

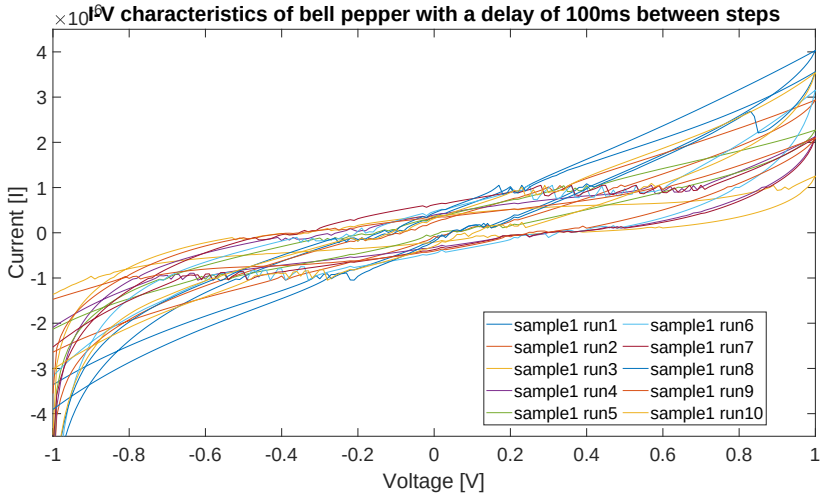

(b)

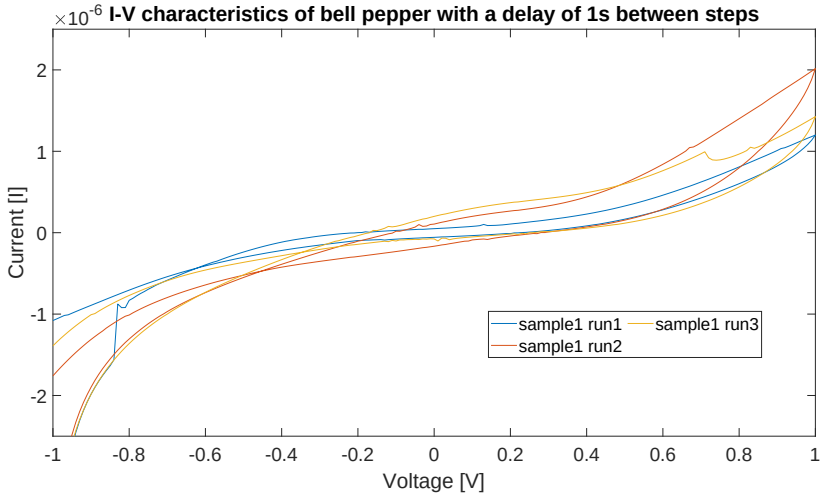

(c)

Figure 48: Cyclic voltammetry (-1V to 1V) of pepper. (a) delay time between settings is 10ms, (b) delay time between settings is 100ms, (c) delay time between settings is 1000ms

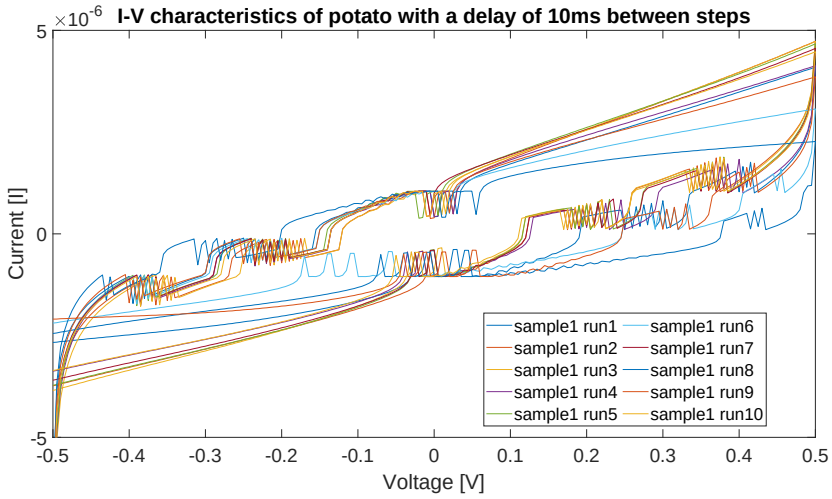

(a)

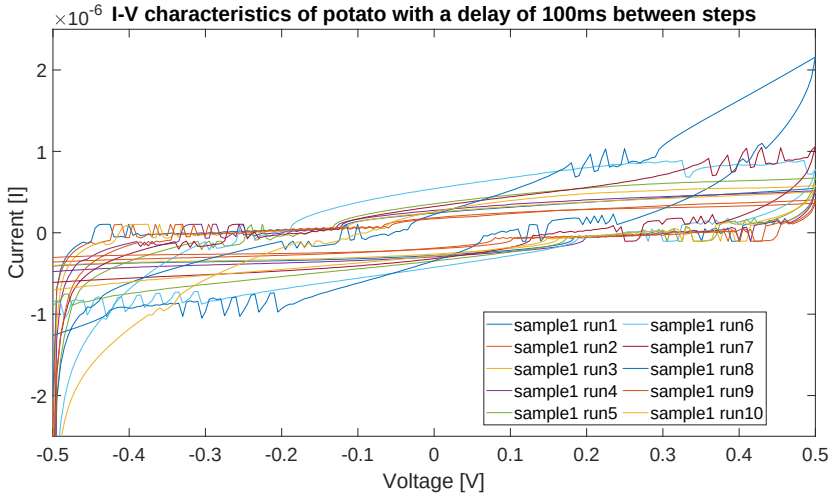

(b)

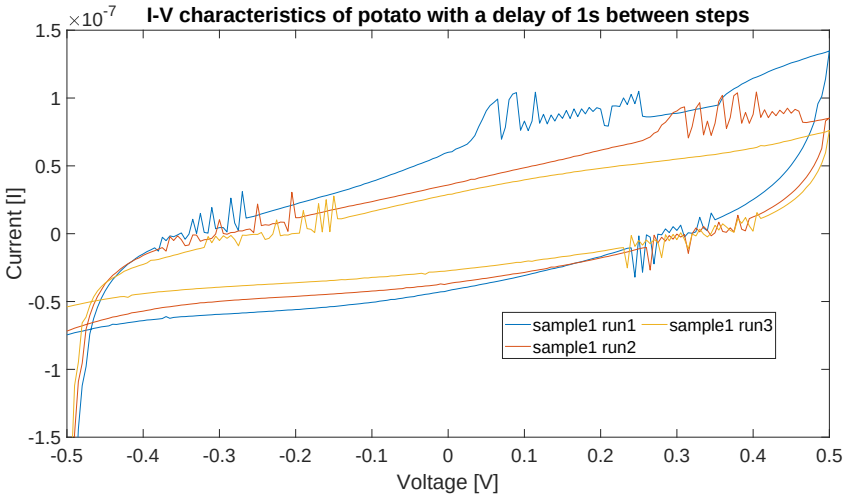

(c)

Figure 49: Cyclic voltammetry (-0V5 to 0V5) of potato. (a) delay time between settings is 10ms, (b) delay time between settings is 100ms, (c) delay time between settings is 1000ms

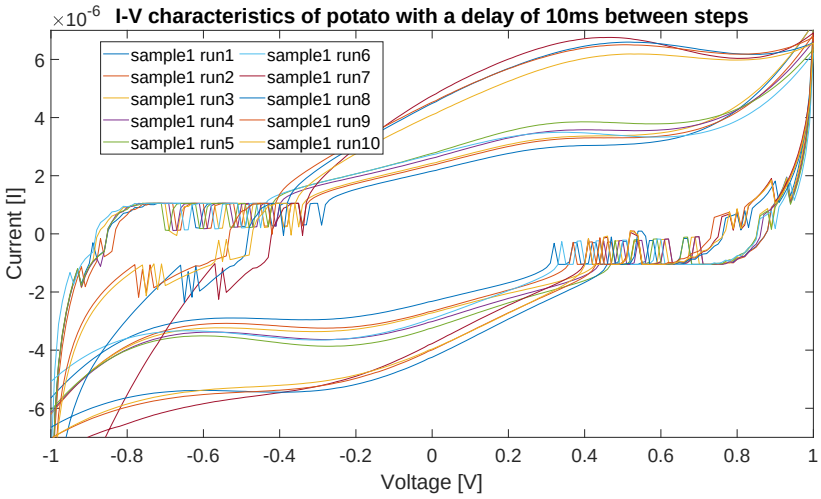

(a)

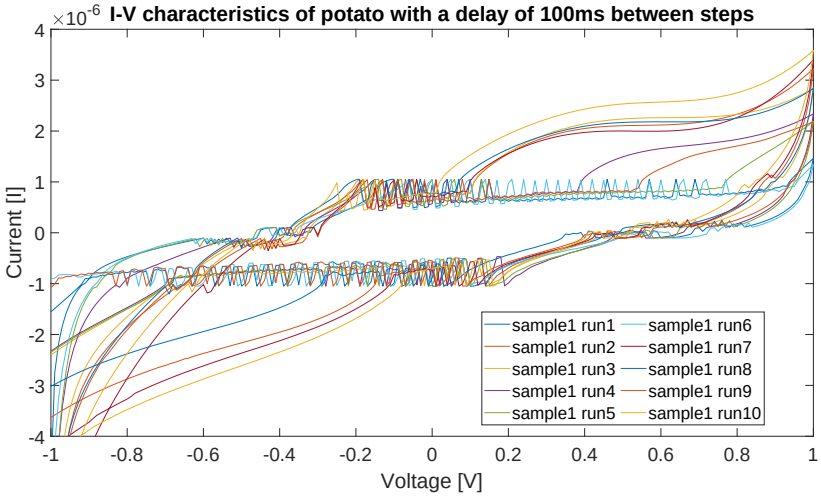

(b)

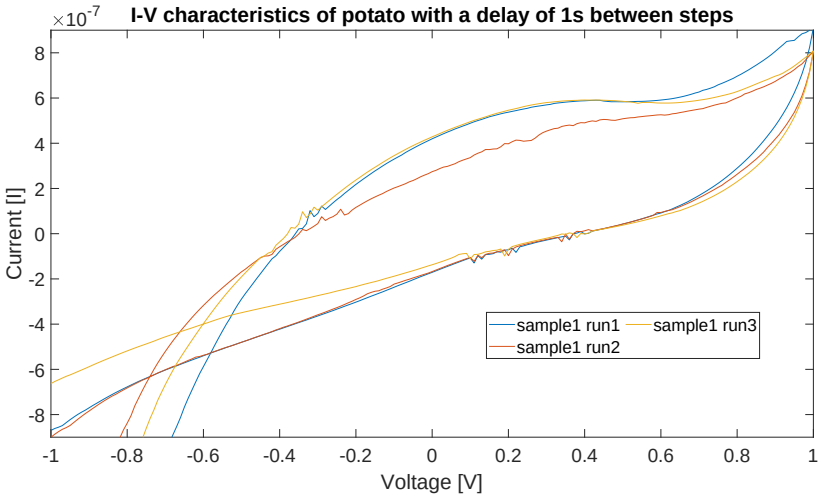

(c)

Figure 50: Cyclic voltammetry (-1V to 1V) of potato. (a) delay time between settings is 10ms, (b) delay time between settings is 100ms, (c) delay time between settings is 1000ms

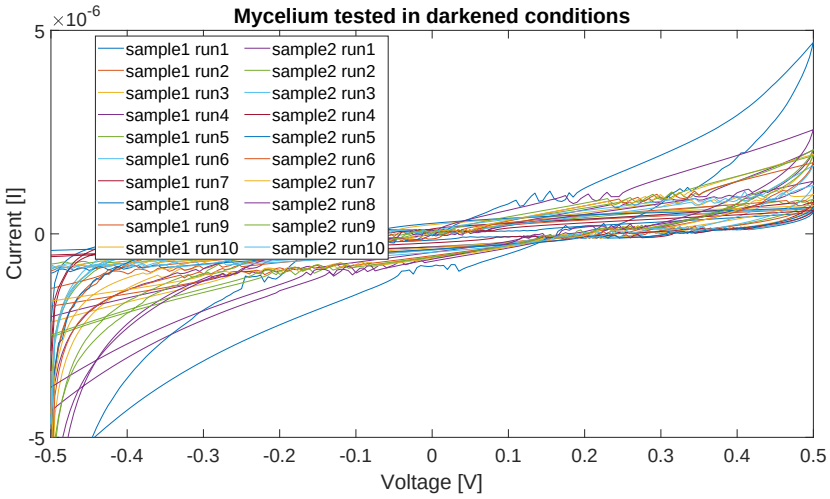

(a)

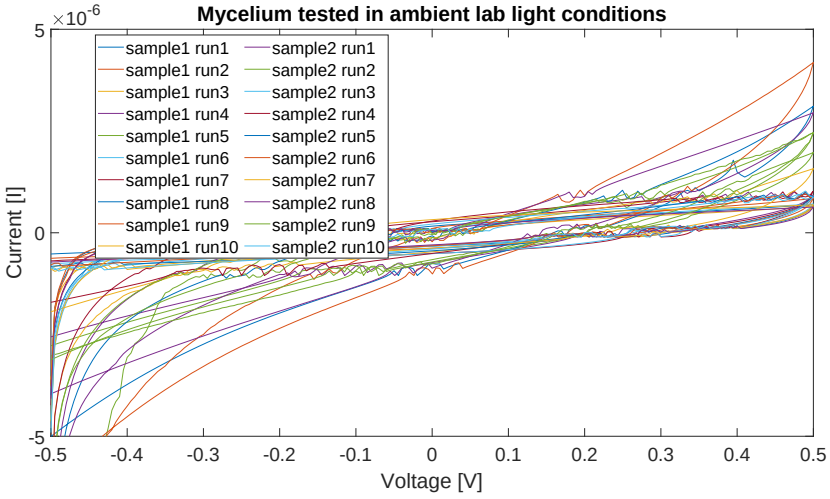

(b)

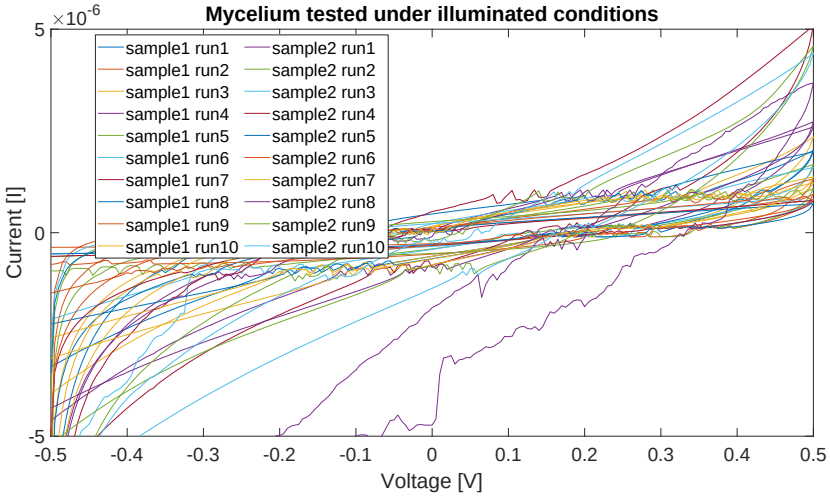

(c)

Figure 51: Cyclic voltammetry (-0V5 to 0V5) of mycelium substrate cultivated on damp wood shavings with three different light levels. (a) covered, (b) ambient lab light (965 Lux), (c) illuminated (1500 Lux).

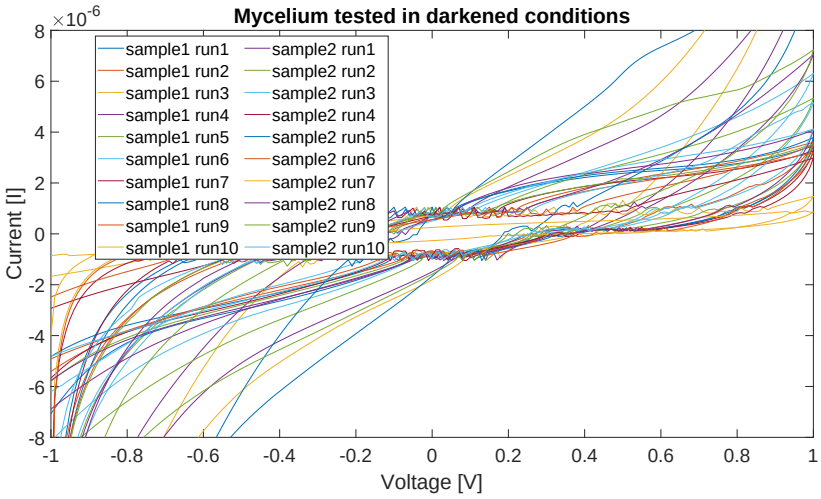

(a)

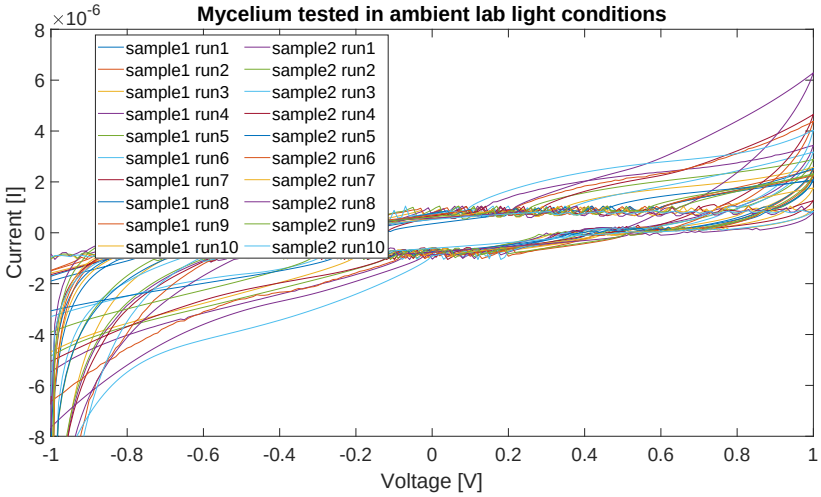

(b)

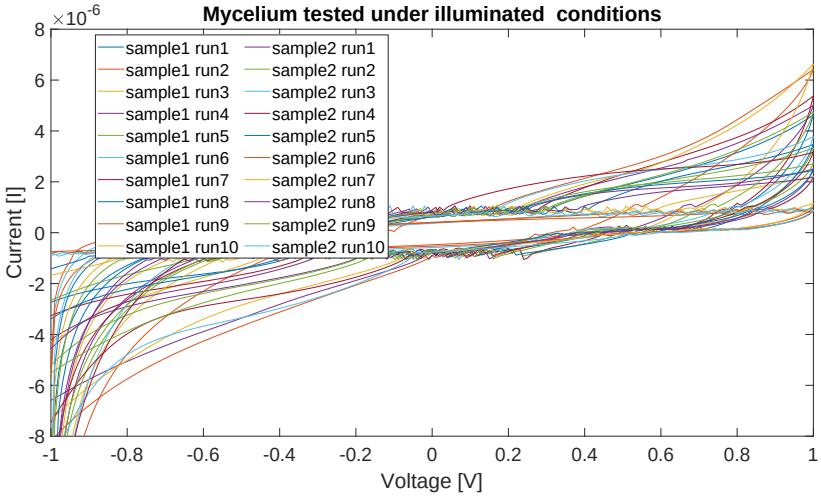

(c)

Figure 52: Cyclic voltammetry (-1v to 1v) of mycelium substrate cultivated on damp wood shavings with three different light levels. (a) covered, (b) ambient lab light (965 Lux), (c) illuminated (1500 Lux).

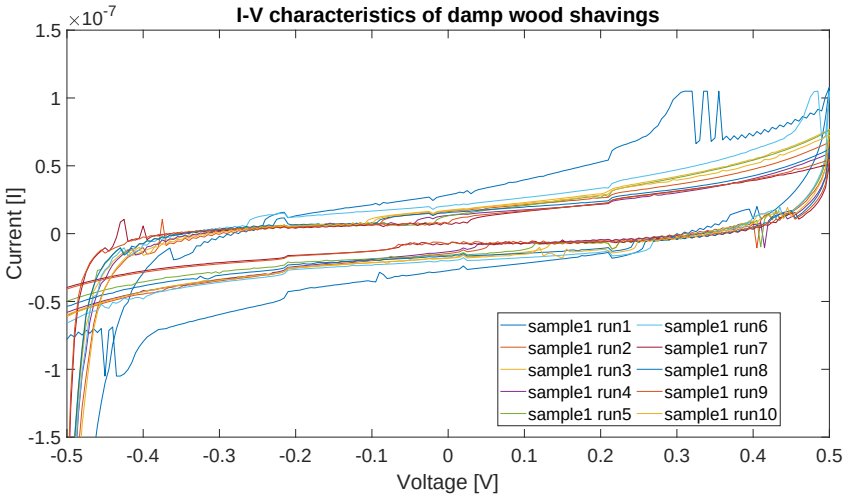

(a)

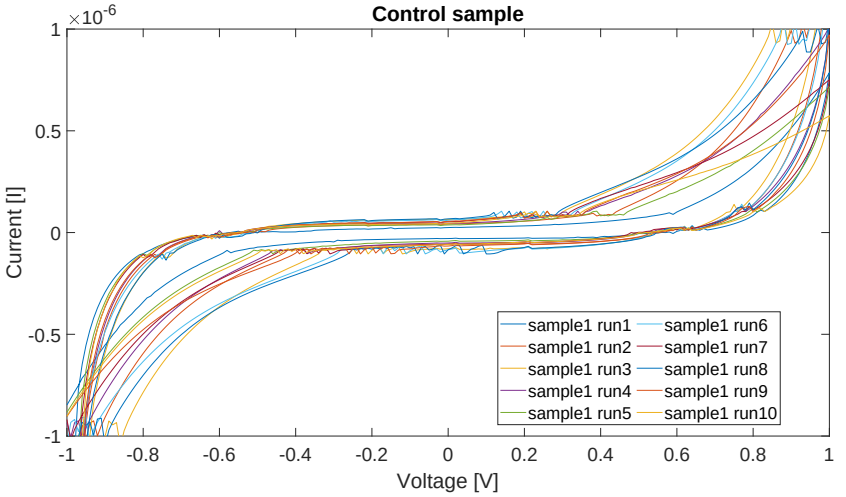

(b)

Figure 53: Cyclic voltammetry of damp wood shavings used as a control for mycelium tests. (a) -0V5 to 0V5, (b) -1V to 1V

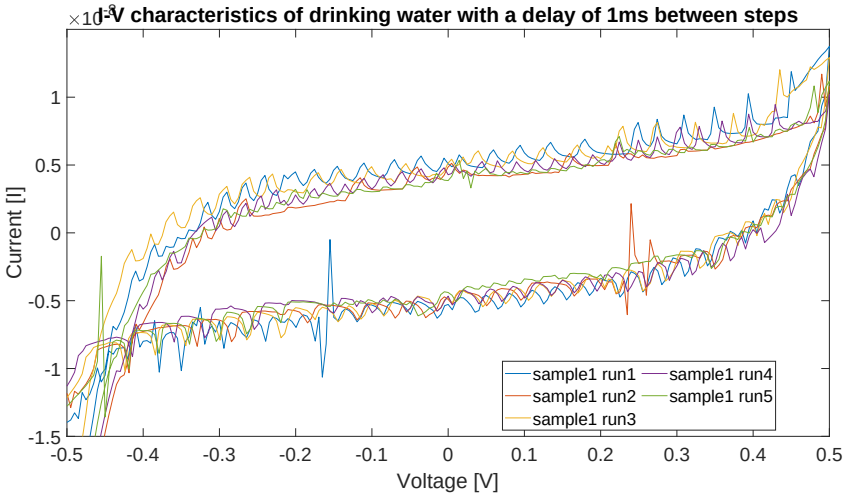

(a)

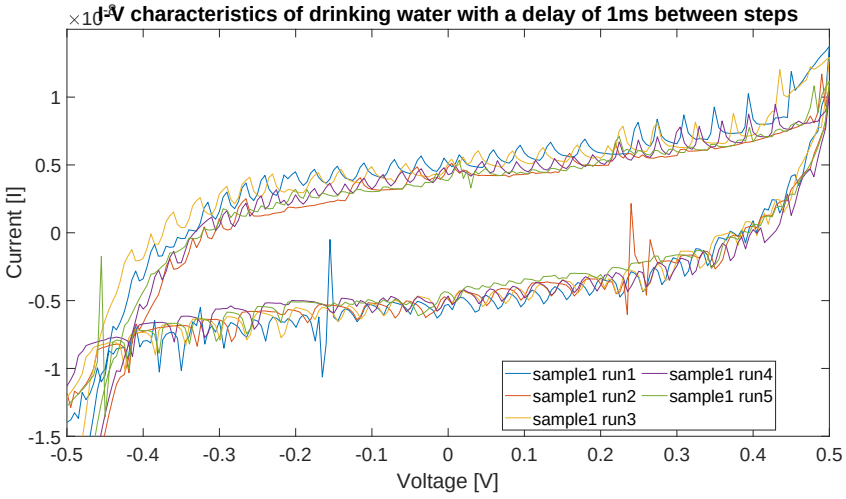

(b)

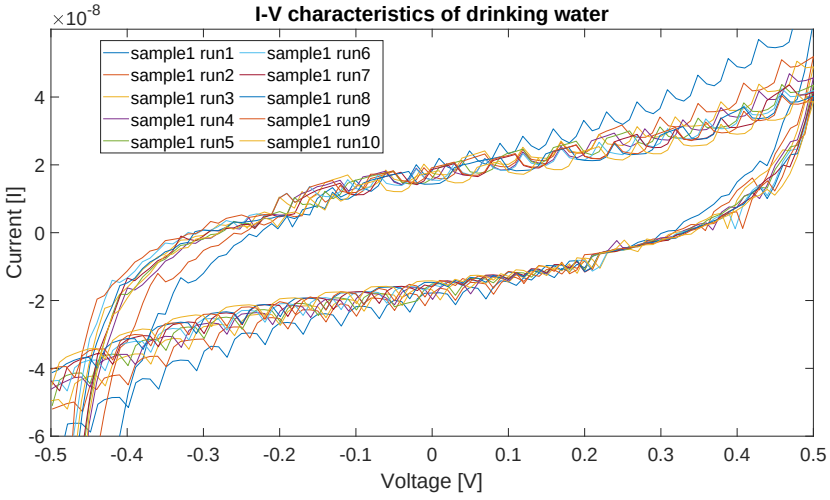

(c)

Figure 54: Cyclic voltammetry (-0V5 to 0V5) of drinking water used as a control for mycelium tests. (a) delay between voltage steps is 1ms, (b) delay between voltage steps is 10ms, (c) delay between voltage steps is 100ms

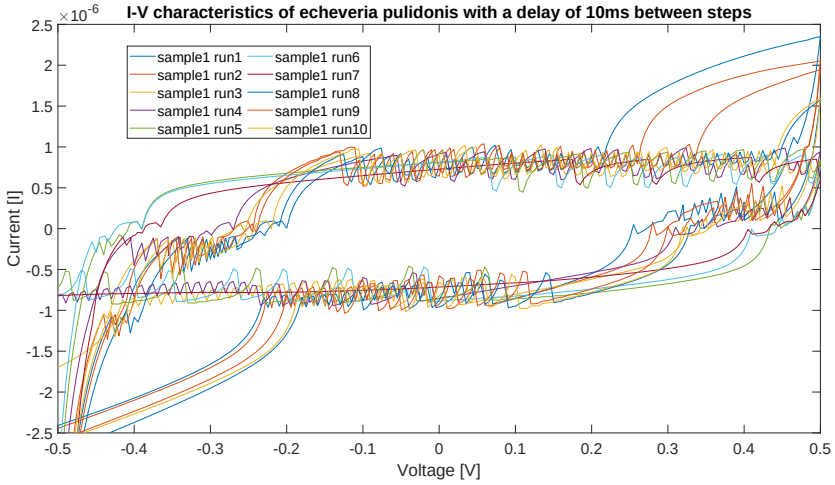

(a)

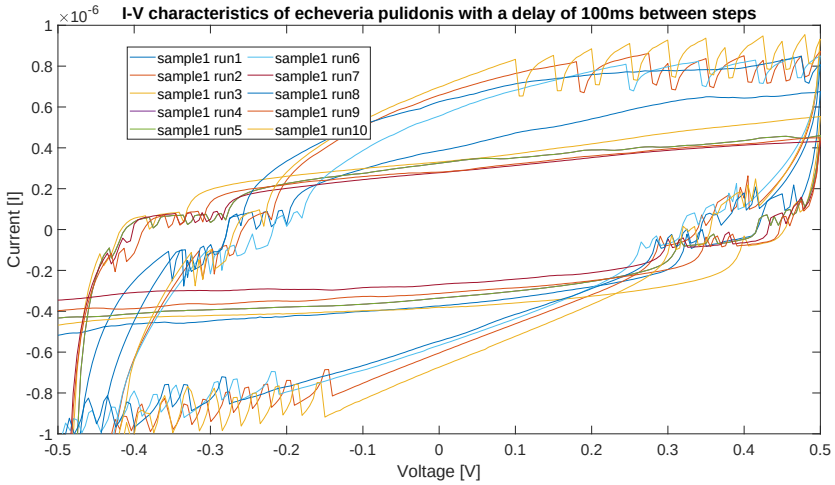

(b)

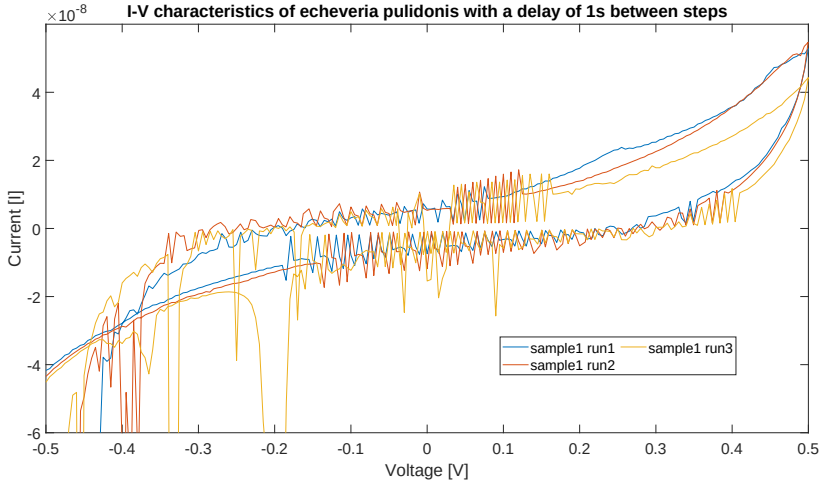

(c)

Figure 55: Cyclic voltammetry (-0V5 to 0V5) of echeveria pulidonis. (a) delay time between settings is 10ms, (b) delay time between settings is 100ms, (c) delay time between settings is 1000ms

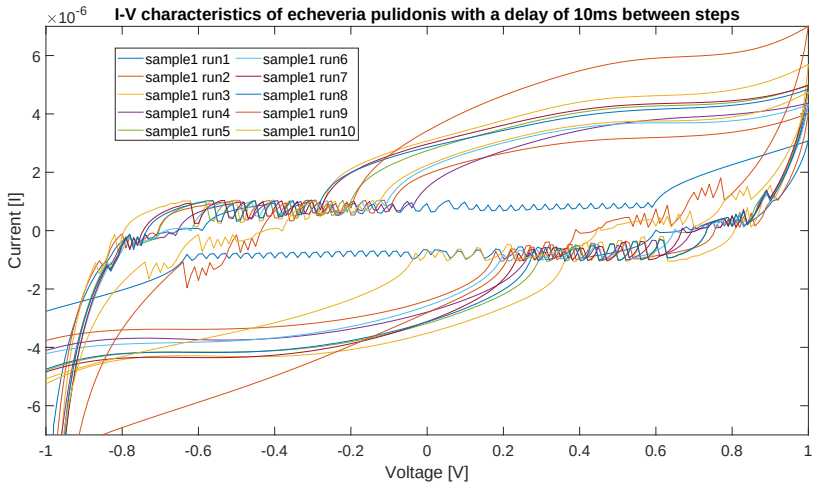

(a)

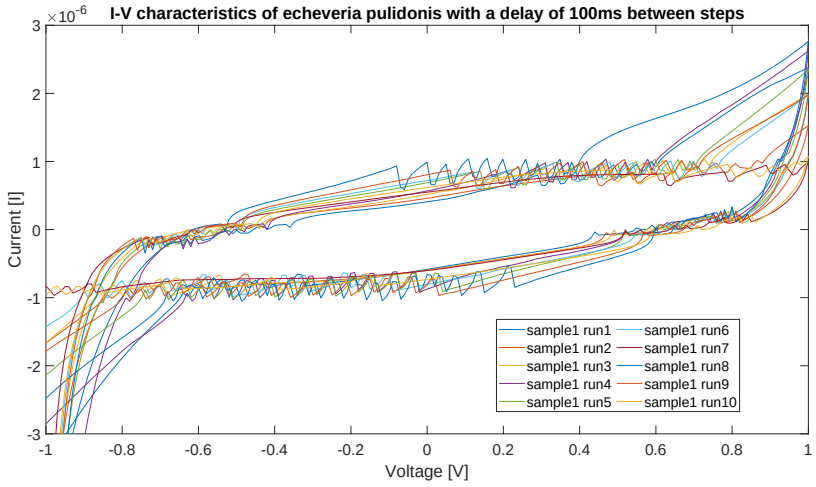

(b)

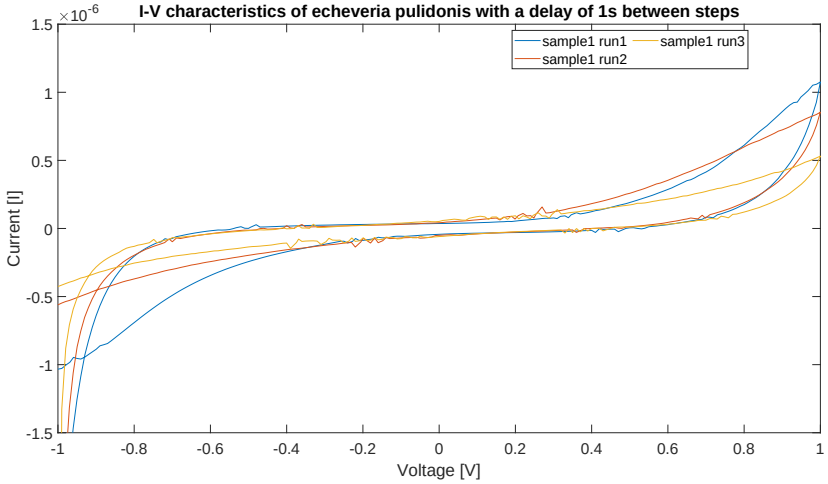

(c)

Figure 56: Cyclic voltammetry (-1V to 1V) of echeveria pulidonis. (a) delay time between settings is 10ms, (b) delay time between settings is 100ms, (c) delay time between settings is 1000ms

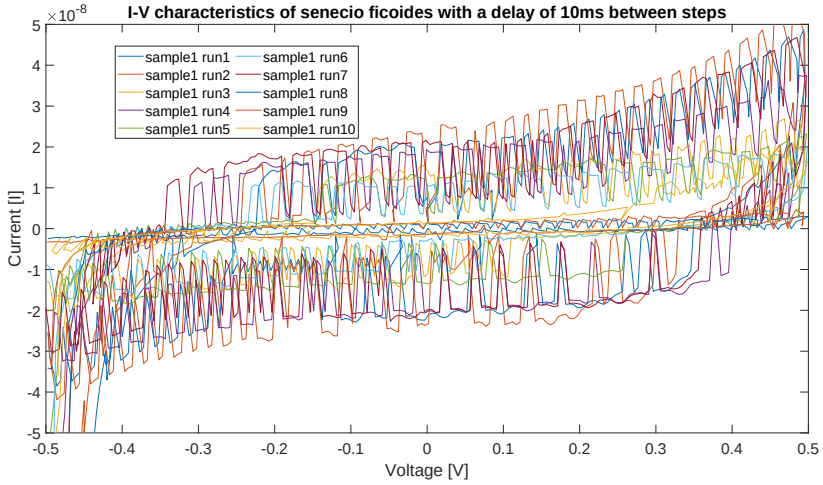

(a)

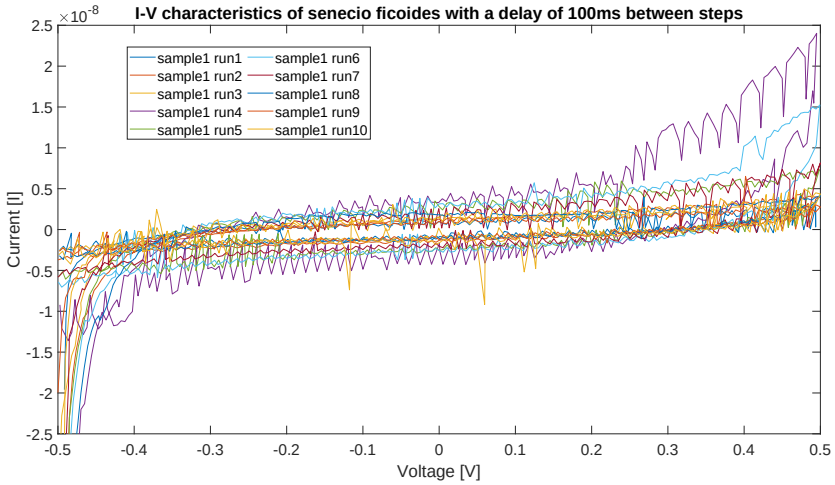

(b)

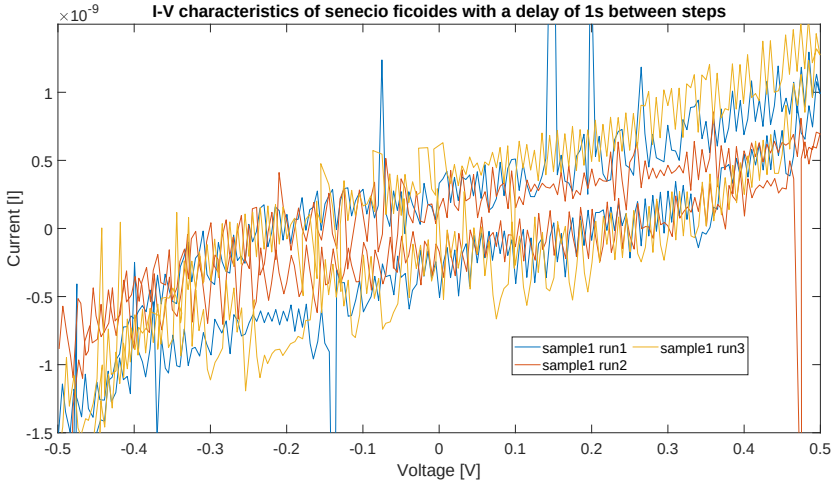

(c)

Figure 57: Cyclic voltammetry (-0V5 to 0V5) of senecio ficoides. (a) delay time between settings is 10ms, (b) delay time between settings is 100ms, (c) delay time between settings is 1000ms

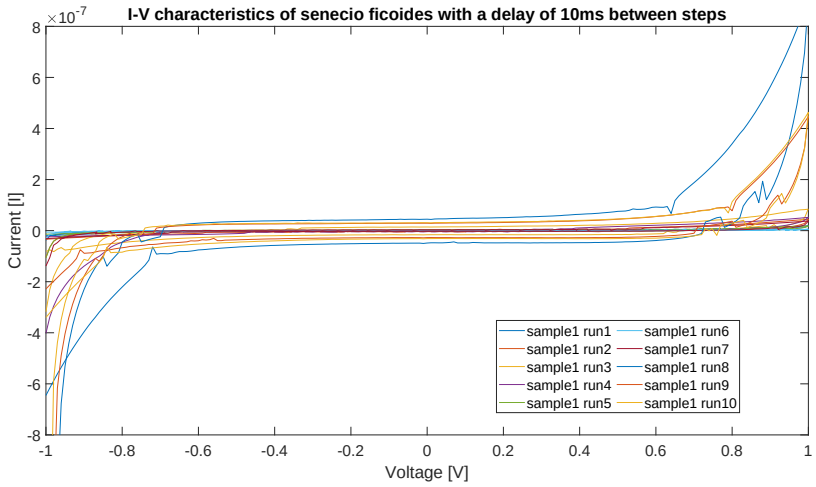

(a)

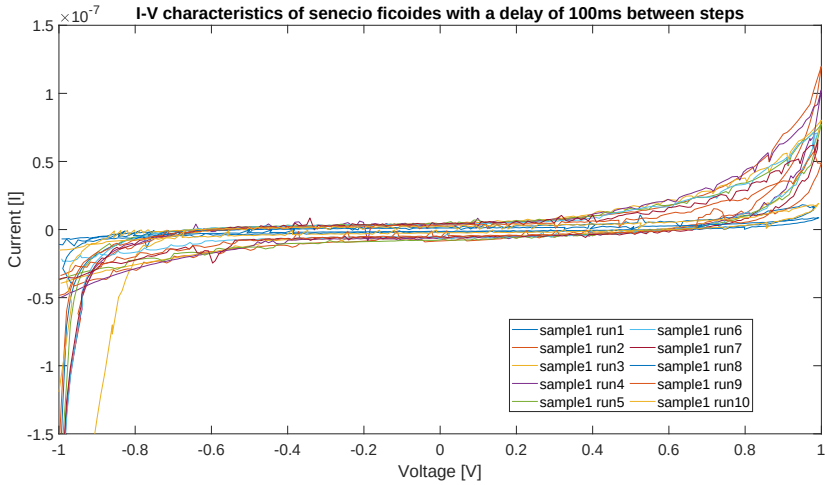

(b)

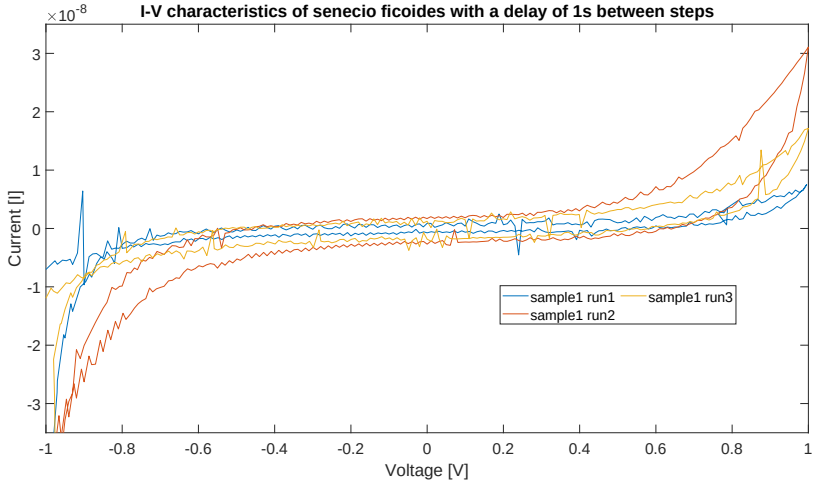

(c)

Figure 58: Cyclic voltammetry (-1V to 1V) of senecio ficoides. (a) delay time between settings is 10ms, (b) delay time between settings is 100ms, (c) delay time between settings is 1000ms